1-1-2013

Parsing the Effects of Physical Microenvironmental Cues on Stem Cell Adhesion and Lineage Specification

Greg M. Harris
University of South Carolina - Columbia

PARSING THE EFFECTS OF PHYSICAL MICROENVIRONMENTAL CUES ON STEM CELL ADHESION AND LINEAGE SPECIFICATION

by

Greg M. Harris

Bachelor of Science
Iowa State University, 2008

Submitted in Partial Fulfillment of the Requirements

For the Degree of Doctor of Philosophy in

Chemical Engineering

College of Engineering and Computing

University of South Carolina

2013

Accepted by:

Ehsan Jabbarzadeh, Major Professor

Tarek Shazly, Committee Member

Melissa Moss, Committee Member

James Blanchette, Committee Member

John Weidner, Committee Member

Lacy Ford, Vice Provost and Dean of Graduate Studies

Dedication

This dissertation is lovingly dedicated to my wife Haley. Her support, encouragement, and constant love have guided me throughout this process.

Acknowledgements

I am very grateful to the members of my committee, Dr. Tarek Shazly, Dr. Melissa Moss, Dr. James Blanchette, and Dr. John Weidner for their time, encouragement, and knowledge helping me throughout my studies and projects. I would like to give a special thanks to my advisor Dr. Ehsan Jabbarzadeh for his guidance and persistence throughout my Ph.D. and helping to lead me to become an independent researcher. I would also like to thank Dr. Marina Pryzkhova for her immense help in mentoring and training me in cell biology and lab practices. Dr. Mathew Skiles, Dr. Suchit Sahai, and Dr. Blanchette also provided me much help with the use of their inverted microscope as well as knowledge on hydrogel systems.

I would like to thank my wife Haley for all of her support and love throughout my studies and know that I couldn't have made it through without her. I would also like to give a special thank you to my parents for pushing me to be successful throughout my years of school and their support and encouragement. I would like to thank my parents-in-law John and Pennie for their support as well as thanking all of my friends and family in both South Carolina and Iowa. Dr. Will Reed, Kerry O'Connell, and J.C. Rotchford also provided much needed relief in passing through graduate school by always being willing to grab a beer for an impromptu happy hour.

This also couldn't have been possible without my lab group at South Carolina in Dr. Jabbarzadeh's lab. Special thanks to Qingsu Cheng for all his valuable insight into

my projects and to all my undergraduate students who helped run experiments for me including Ray Cormany, Marc-Olivier Blais, Jason Lauer, Kim Gillens, Richard Doe, and Maria Piroli.

Abstract

Tissue engineering is a broad field geared toward improving or replacing biological material and comprises an immense collection of biological nuances to consider before strategies for clinical applications can be fully realized. Physical and biochemical signals are responsible for making up a cell's microenvironment to guide morphology and function through cell-extracellular matrix signaling, cell-cell signaling, and soluble signaling. In particular, a deeper understanding of these cell-extra cellular matrix factors guiding stem cell adhesion, spreading, and differentiation is crucial to harnessing the potential to develop tissue for regenerative purposes. Mounting evidence suggests that physical cues are a key to understanding the potential of stem cells and significant efforts have been made to begin to parse the effects of cell-matrix interactions, yet little is known about the interplay in guiding cell signaling. The work presented here focuses on utilizing novel methods and materials to deconstruct individual cell-matrix interactions and gain a deeper understanding of the cooperative signaling behaviors for mesenchymal and embryonic stem cells.

Micropatterning studies utilizing dip pen nanolithography showed that physical signals in the microenvironment are vital to regulating mesenchymal stem cell adhesion. Matrix elasticity, ligand density, and adhesion topography were individually altered to observe single cell adhesion and spreading with matrix elasticity proving to regulate the

adhesion and spreading of the cells. Photolithography based studies detailing cell spreading and matrix elasticity showed that when confining single cells into different geometric shapes and sizes on a matrix of tunable elasticity, cell shape and size ultimately became responsible for stem cell lineage commitment over matrix elasticity. Signaling pathway inhibition experiments utilizing nocodazole and Y-27632 suggested that RhoA is a key regulator of cell response to the cooperative effect of these tunable substrate variables. Embryonic stem cells were then micropatterned on novel UV/ozone modified polystyrene to detail and observe the physical effects on single embryonic stem cells. Micropatterned cells were able to be cultured for up to 48 hours on patterns while forming stress fibers and focal adhesions similar to somatic cells, thereby demonstrating their responsiveness to extracellular matrix cues while maintaining expression of pluripotency transcription factor Oct4. The results from this work validate the immense importance of physical signaling and the effects on mesenchymal and embryonic stem cells. By understanding the effects of physical signaling in conjunction with biochemical signaling in controlling cell spreading and lineage commitment, tissue engineering is able to draw one step closer to potential applications for repairing and replacing biological function.

Table of Contents

List of Tables

List of Figures

List of Symbols

°	Degrees
μ	Micro
ρ	Density
v	Poisson's Ratio
E	Elastic Modulus

List of Abbreviation

2D.....Two Dimensional

3D.....Three Dimensional

AFM.....Atomic Force Microscope

ALP.....Alkaline Phosphatase

BSA.....Bovine Serum Albumin

CN.....Charge Neutralizer

DAPI.....4’-6-diamidino-2-phenylindole

DI.....Deionized

DMEM.....Dulbecco’s Modified Eagle Medium

DMSO.....Dimethyl Sulfoxide

EC.....Endothelial Cell

ECM.....Extracellular Matrix

FBS.....Fetal Bovine Serum

FGF.....Fibroblast Growth Factor

FN.....Fibronectin

hESC.....Human Embryonic Stem Cell

hiPSC.....Human Induced Pluripotent Stem Cell

hrFGF.....Human Recombinant Fibroblast Growth Factor

hPSC.....Human Pluripotent Stem Cell

LGN.....G-protein-signaling Modulator 2

MEF.....Mouse Embryonic Fibroblast

MSC ..... Mesenchymal Stem Cell

MW ..... Molecular Weight

PEG ..... Poly(ethylene) Glycol

PEG-DA ..... Poly(ethylene) Glycol Diacrylate

PEG-SH ..... Poly(ethylene) Glycol Thiol

PDMS ..... Polydimethyl Siloxane

PLGA ..... Poly(lactic-co-glycolide)

PS ..... Polystyrene

PVA ..... Polyvinyl Alcohol

PVC ..... Polyvinyl Chloride

ROCK ..... Rho-associated Kinase

RT ..... Room Temperature

RPM ..... Rotations Per Minute

SAM ..... Self-assembled Monolayer

SEM ..... Scanning Electron Microscope

UV ..... Ultraviolet

VEGF ..... Vascular Endothelial Growth Factor

CHAPTER 1: Tissue Engineering

1.1 Introduction

Transplantation of organs such as hearts, livers, or even bone is a key and necessary therapy for otherwise inoperable illnesses and has come to the forefront of medicine in recent years [1-4]. However, the need for transplant donors far exceeds the supply with many potential transplant candidates dying while waiting for a donor each year [5-7]. In seeking to correct this dire need for transplant donors, researchers have begun looking at alternative measures and solutions to the problem, including tissue engineering. Tissue engineering is a diverse field encompassing the study of cells, engineered biomaterials, and biochemical factors to enhance or replace natural biological functions. The ultimate goal of these engineering principles is to develop fully functional tissue for implantation into the donor utilizing the donor's own cells, thus reducing the chance of immunorejection in the patient [8, 9].

Tissue engineering is a broad concept that seeks to integrate cells into an engineered synthetic scaffold to provide the framework for which these cells can proliferate and develop into the desired tissue aided by the use of biochemical factors in the scaffold as seen in Figure 1.1 [1, 5, 10-13]. A scaffold is able to provide the initial structure and adhesion points for cells until a suitable ECM has been deposited, at which point the scaffold is degraded or metabolized. Among the many advantages to using an

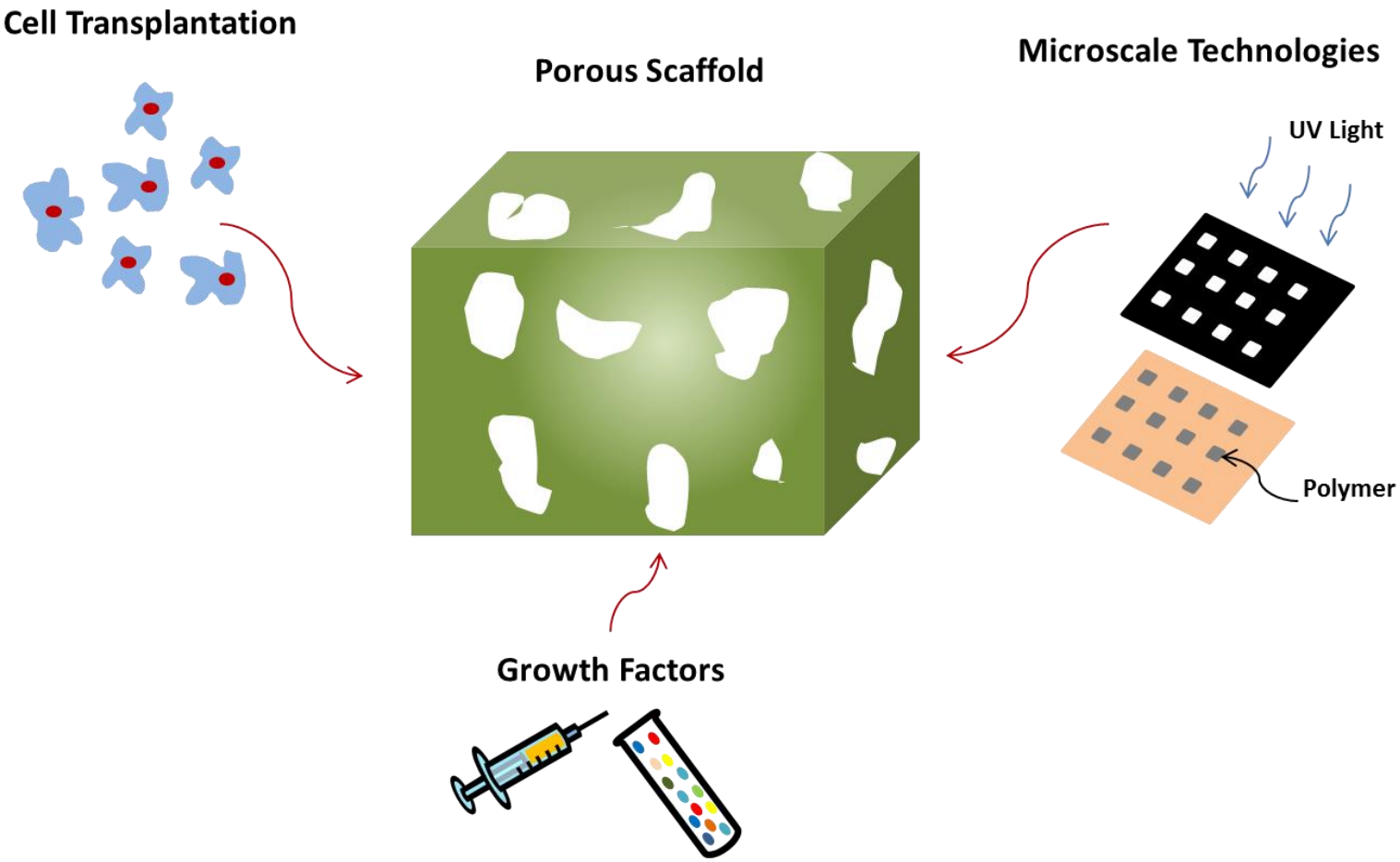

Figure 1.1: Schematic drawing of growth factor delivery, cell transplantation, and microscale patterning strategies to induce tissue growth in porous biomaterials for tissue engineering applications.

engineered, degradable scaffold are the elimination of disease transmission, a greatly reduced risk of infection, fewer surgical procedures, and the wide availability of synthetic polymers to create scaffolds. Synthetic scaffolds have rigorous requirements with the first and foremost being the ability to be shaped into the appropriate structure for implantation. Other substantial factors to consider when designing material include its biocompatibility, ability to host biological function long term, and degradation properties. The engineering of scaffolds along with the combination of cells and biochemical factors are key elements to fully realizing the potential for clinical applications of tissue engineering.

In particular, the ability to engineer anatomically correct portions of functional human tissue for critically sized defects stemming from incidents such as cancer resections or trauma is of the utmost importance [14]. In dealing with engineered bone scaffolds in particular, the ability of the cellular source to secrete the correct tissue-specific proteins onto this mechanically apt scaffold and subsequent degradation of the scaffold is paramount to a functional tissue [15-17]. The secretion of proteins from cells in combination with scaffold properties is a key factor shown to greatly influence cell function and phenotype [18-20]. This has also delved into its own wide-ranging field to study the effects of ECM factors on regulating the morphology and function of the cell, and thus tissue depending on the makeup of this cell microenvironment.

1.2 Cell-extra Cellular Matrix Physiology

The ECM in tissue is composed of large amounts of biochemically differing components such as proteins, glycoproteins, proteoglycans, and polysaccharides with vastly different physical and biochemical properties [21, 22]. For instance, the protein

composition of a 3D gel matrix affects the ligand density, matrix stiffness, and pore size of the tissue under surveillance and will greatly affect the migration, adhesion, and differentiation of the cells [23-26]. Cell-ECM and cell-cell signaling is governed by transmembrane proteins, mostly integrins, but also cadherins, cell adhesion molecules, and selectins, that are able to link the cell to the proteins of the ECM and other cells [27, 28].

Generally the physical properties of the ECM refer to its rigidity (elasticity), porosity, insolubility, spatial arrangement, and orientation (topography) to determine specific properties and its role as a scaffold to support a tissue. These traits in the ECM can ultimately play a positive or negative role in cell adhesion and migration by acting as an anchorage point or barrier for cell movement. Cell migration in 3D environments during tumor formation [29, 30], immune response [31, 32], and tissue repair [33, 34] have large deformations of cells during penetration of interstitial tissues where the pore size varies from a few microns to hundreds of microns, and also include remodeling of the ECM in terms of matrix stiffness and topography [35-37]. Cells are able to use these signals from the ECM to reorganize the cytoskeletal network in a "real time" fashion while the ECM is being modified during adhesion and migration.

There are thought to be two regimes of ECM sensing from cells which include "outside-in" sensing that involves the cell responding to a force exerted upon it like shear stress, and "inside-out" sensing where the internal forces of the cells sense and measure ECM properties such as elasticity, topography, and ligand density through the focal adhesions, cytoskeleton, and integrins [38]. These factors combine to tell us the ECM plays a crucial role in cell adhesion, migration, and differentiation in cells while the

interplay between cells and ECM cues are highly intertwined and vital to cell function.

1.3 Physical Microenvironment Signaling

Tissue is fundamentally different across the many ECM microenvironments and plays a pivotal role in cell signaling [39-42]. The ECM microenvironment can be as varied and diverse as brain, fat, or bone progenitor cells, which influence cell dynamics in a number of ways. Cells are able to sense these topographical and physical forces through cell-matrix adhesion molecules called integrin receptors [43-45]. These differences in microenvironmental signals lead to conflicting signals with limited studies shown interpreting the dynamics of multiple cues and the cooperative effects on each other. Thus, it appears that microenvironments are an important piece of stem cell lineage specification, but it has shown difficult to adequately control and decouple conflicting signals.

Cells are constantly exposed to mechanical stimuli in the body from a variety of sources including muscle forces, blood flow, and gravity among many other factors [46-50]. Even as early as the early 1900s, scientists were able to determine the mechanical environment is highly influential to embryonic development. Historic tests were able to show that cultured chick rudiments under static compression following displacement of the periosteum and perichondrium resulted in cartilaginous tissue formation but tensile stresses led to bone formation [51]. To take these mechanical experiments further, ECM topography has shown to be a major factor in cellular organization and past work has shown that size and geometry of available surface area alter cell shape, traction forces, and spreading [19, 52-59]. The cell morphology is crucial in determining final stem cell

lineage as cell shape has been previously shown to be rounded for adipocytes [60, 61] and polygonal in the case of osteoblasts [62, 63]. Micropatterning of proteins has become a useful tool in studying the mechanisms of cell shape by precisely controlling areas available for cell attachment and migration. In single cell studies, smaller ECM islands cells generally take on a rounded morphology where the cell is constricted in its placement, but larger islands with less or no constriction are able to flatten and spread similar to 2D cultures [53]. With this approach in mind, it has enabled groups to differentiate hMSCs to adipogenic and osteoblastic phenotype by controlling cell placement and spreading [19]. This recent study was able to microcontact print 10,000 μm^2 versus 1,024 μm^2 protein areas and observed single cell spreading directly led to osteoblast differentiation on 10,000 μm^2 spots as opposed to adipogenic differentiation on 1,024 μm^2 spots showing cell spreading and shape have a direct influence on stem cell fate.

It has also been shown that ECM elasticity has the ability to drastically influence cell processes such as cell morphology, traction force exerted on substrate, cell motility, and differentiation [18, 20, 64-69]. Varying the matrix elasticity for previously differentiated adult somatic cells has been shown to alter the existing cytoskeletal organization as well as the focal adhesion structure [41, 70-72]. By varying matrix elasticity on previously differentiated cells the traction force the cell exerts is altered, and the cell is able to decipher these new biophysical programming cues. A recent study was able to utilize polyacrylamide gels to mimic tissue elasticity from 1 kPa up to 40 kPa to differentiate stem cells into distinct lineages by solely altering ECM elasticity [18]. This difference in matrix elasticity was shown to directly control hMSC differentiation into a

variety of lineages including neural, myogenic, and osteogenic and can potentially play a significant role for the development of scaffolds in tissue engineering [18].

CHAPTER 2: Stem Cell Sources for Tissue Engineering Applications

2.1 Introduction

A key component to regenerative therapies and tissue engineering is cells to generate or repair tissue. Tissue engineering in the original sense called for the usage of organ-specific cells for use in seeding a scaffold *ex-vivo*. In modern tissue engineering, stem cells have become popular as they have the ability to perpetuate themselves through self-renewal while also retaining the ability to differentiate into tissue specific cells [5, 73-79]. In utilizing stem cells for tissue engineering, it provides the opportunity to guide differentiation of cells on scaffolds into specific 3D tissues [80]. This strategy is superior to using differentiated cells alone for a multitude of reasons including the ease of culturing large numbers of stem cells for depositing on scaffolds and the potential ability to create a fully functional tissue with multiple cell types. These cells hold incredible promise to being able to fully recreate any tissue in the body with the right combination of scaffold and microenvironmental factors.

Stem cells hold different potential for creating all of the cell types in the body depending on cell age and site of extraction. Pluripotent stem cells are capable of differentiating to all types of cells in the body, multipotent cells are capable of differentiating to a few cell types, and unipotent cells are terminally differented cells. These cells can come from a variety of sources including adult tissue and an embryo. Embryonic stem cells are pluripotent cells derived from the inner cell mass of a

blastocyst, which is an early stage embryo. Adult stem cells are found in tissue in the body after development and replenish themselves by cell division to maintain stem cells in the body as well as regenerate wounded tissue. Induced pluripotent stem cells are adult somatic cells that are induced into a pluripotent state by reprogramming certain genes to make the cell capable of differentiating to all types of cells. iPSCs are similar to ESCs but the exact relationship is still being investigated.

2.2 Adult Stem Cells

Adult stem cells such as mesenchymal stem cells (MSCs) are multipotent cells that can differentiate into connective tissue such as bone, fat, and cartilage [76] as seen in Figure 2.1 with MSCs differentiated to a mixed population of osteoblasts and adipocytes. MSCs are found in adult bone marrow and are generally characterized by a small cell body with long processes as shown in Figure 2.2. Adult tissue contains populations of stem cells for renewal of tissue after trauma, disease, or aging and may be found in the tissue or in other tissue that serves as a stem cell "pool" [81-86]. MSCs are generally characterized by their ability to differentiate into osteoblasts, chondrocytes, and adipocytes as well as the expression of CD73, CD90, and CD105 while lacking expression of CD11b, CD14, CD19, CD34, CD45, CD79a, and HLA-DR surface markers [87].

In a recent study, MSCs have also been shown to possess the ability to differentiate into endothelial cells *in vitro* and these endothelial cells were observed to

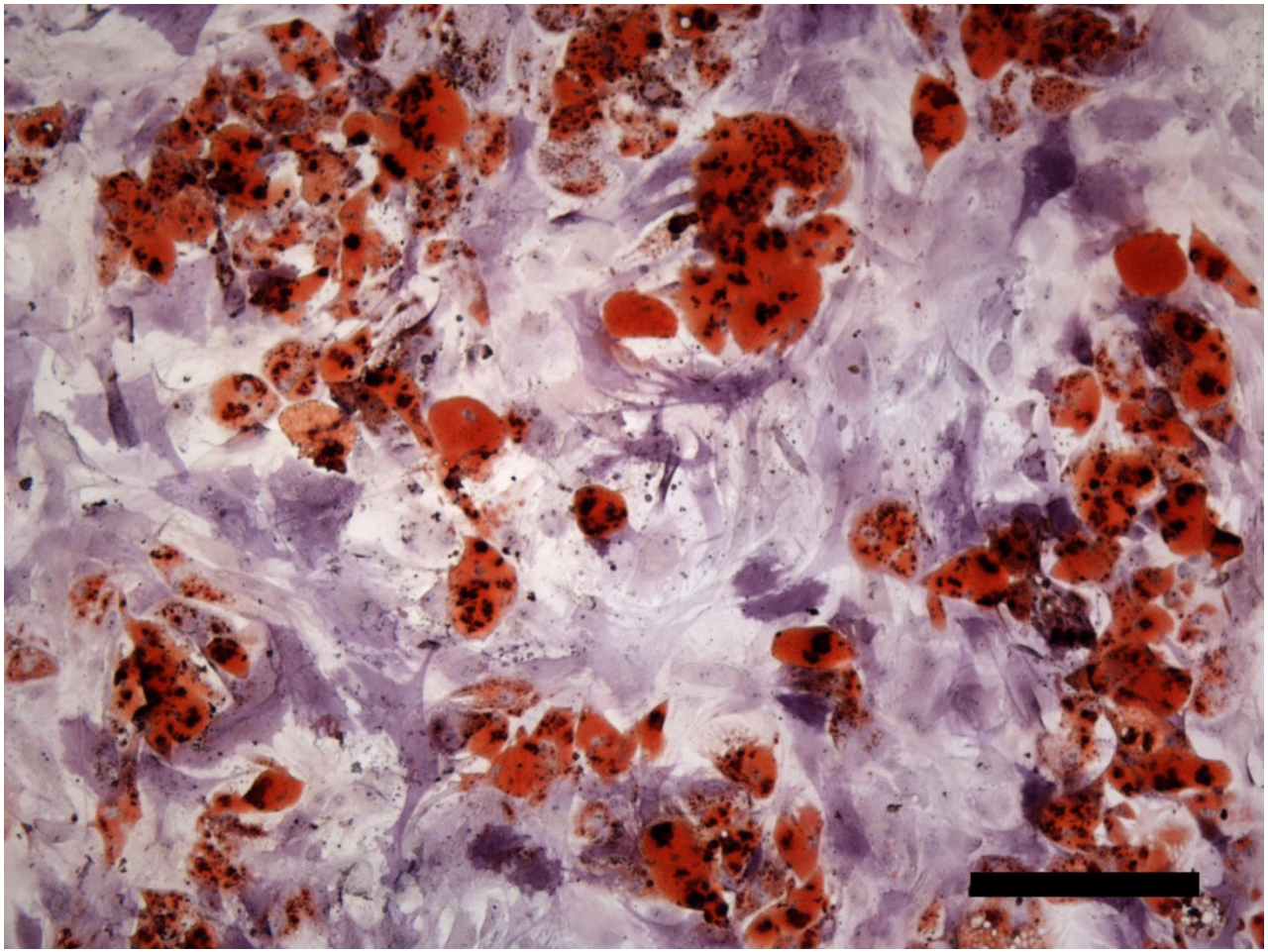

Figure 2.1: Mesenchymal stem cells cultured for 14 days in a 50:50 mixture of adipogenic and osteogenic differentiation medium. Oil Red O staining (red) for adipogenic differentiation and alkaline phosphatase staining (purple) for osteoblast differentiation. Scale bar is 200 μm.

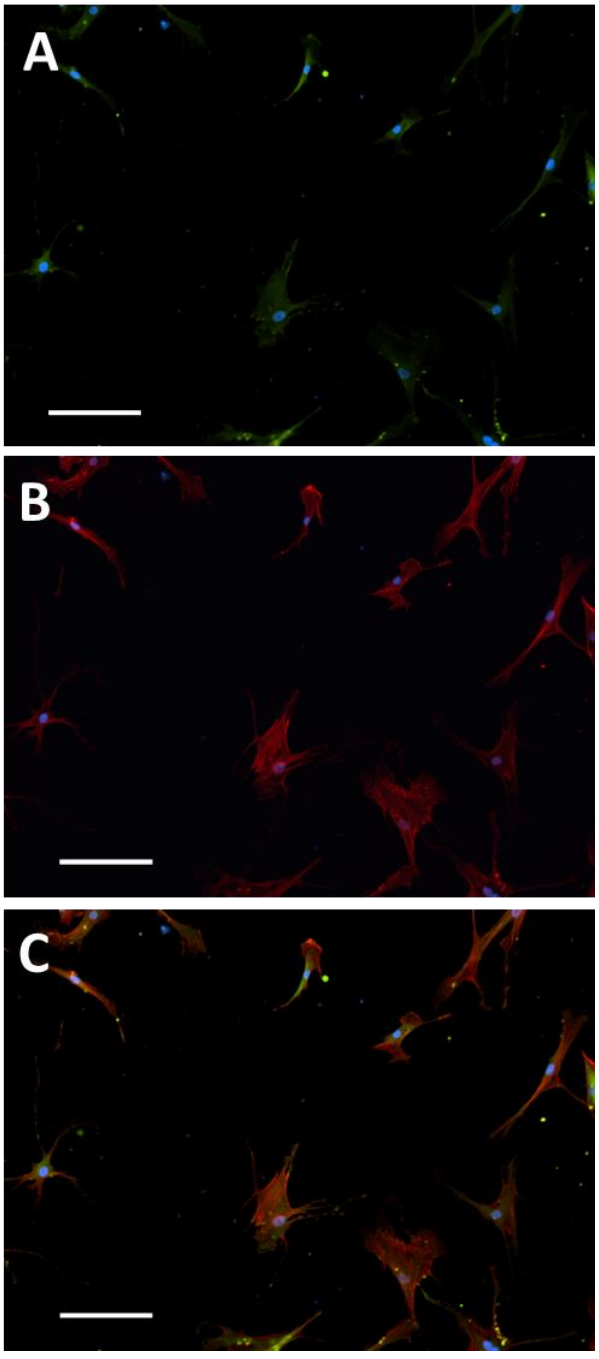

Figure 2.2: Adult stem cells are capable of differentiating to several lineages. Mesenchymal stem cells shown here are extracted from bone marrow and have a small cell body with long processes. (A) MSCs stained for DAPI (blue) and vinculin (green) to show focal adhesion structure. (B) MSCs stained for DAPI (blue) and F-Actin (red) to show cytoskeletal structure. (C) Merged image. Scale bars are 200 µm

then organize into capillary-like structures [88]. This demonstrates the potential to use MSCs for inducing angiogenesis in tissue grown on scaffolds as well as connective tissue. Furthermore, MSCs seeded onto scaffolds containing angiogenic and osteogenic growth factors can form new blood vessels and bone in a manner similar to bone development in an embryo, and this can further be enhanced by co-culturing of MSCs with endothelial cells on scaffolds [89]. These studies demonstrate the importance of building vascular architecture in conjunction with forming new tissue when using stem cells for engineering [90].

MSCs have also become very crucial in patterning studies to help understand and delineate ECM factors regulating stem cell fate and function. A key study showed that by micro contact printing islands of fibronectin they could control MSC lineage commitment. This study showed MSCs on small 1,024 μm^2 islands cells displayed adipogenic differentiation while on 10,000 μm^2 islands cells displayed osteogenic differentiation and was regulated strictly by switching the mechanical environment influencing cell shape and RhoA activity [19]. These studies further show the untapped potential of MSCs in tissue engineering in addition to the ease of culture and limited restrictions placed on them for use in therapies.

2.3 Embryonic Stem Cells

Embryonic stem cells are pluripotent cells with the ability to differentiate into all of the three germ layers [78, 91-94]. ESCs are derived from the inner cell mass of a blastocyst, which is an early stage embryo [79, 95, 96]. The two distinctive properties of

ESCs are the ability to self-renew indefinitely and their pluripotency. Since ESCs are capable of renewing themselves perpetually, sources for these cell lines are generally pre-existing lines for researchers due to government limitations. Other sources include spare embryos from fertility clinics as well as custom made embryos from somatic cell nuclear transfer [97].

Studies have shown ESCs to be an incredibly versatile cell capable of differentiation into vascular endothelial cells (ESC-EC) in embryoid bodies [98] and 2D culture conditions [99], osteogenic cells [100], adipose cells [101], and cardiomyocytes [102] among the rest of the cells in the body. These studies show the incredible potential to implant ESCs into scaffolds while using growth factors and other stimuli to direct differentiation into cells that compose the tissue itself as well as the blood vessels required to vascularize the newly formed tissue. To fully understand the potential of ESCs, studies will need to be completed on controlling differentiation while parsing out the ECM cues necessary to stem cell fate. To begin to address this interplay, recent advances have made embryonic stem cells (ESCs) culture possible in single cells as well as the traditional colony methods as seen in Figure 2.3 [103-105].

Preliminary studies have begun to utilize single cell culture techniques to show individual ESC characteristics by micropatterning restrictive cell attachment points for colonies and single cells [106, 107]. Although. it has proven exceedingly difficult to adequately characterize ESCs as single cells for long periods of time due to apoptosis without the presence of cell-cell contact. A recent study aimed to differentiate ESCs into pancreatic cells by patterning them into differing colony sizes to achieve optimum

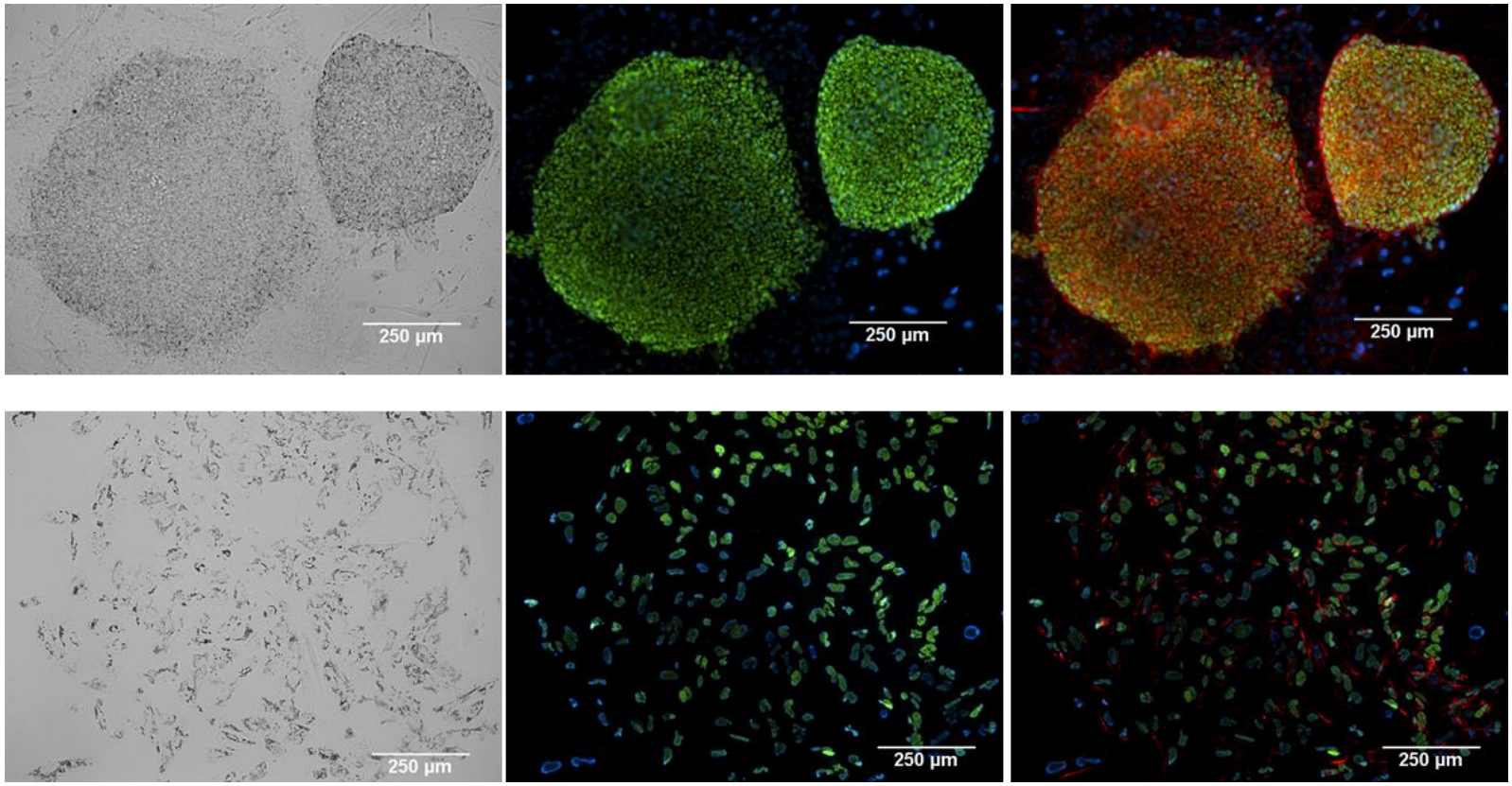

Figure 2.2: Top images showing H9 embryonic stem cell colonies with brightfield image, pluripotency marker Oct4 with DAPI, and merged image showing cytoskeletal marker F-actin, DAPI, and OCT4 (right to left). Bottom images showing single cell culture of embryonic stem cells with brightfield image, pluripotency marker Oct4 with DAPI, and merged image showing cytoskeletal marker F-actin, DAPI, and OCT4 (right to left).

nutrient and oxygen levels [107]. The study controlled colony size on glass cover slips by patterning laminin in circular patches of 120 μm diameter. This was able to control ESCs to express PDX1 and NKX6 factors to efficiently produce pancreatic endocrine precursors *in vitro*.

However, even as ESCs are able to differentiate to any cell type in the body, ethical and medical concerns have arisen from their use. Unless the transplantation is autologous, the patient receiving the transplanted cells will contain different genetic information, so the risk of immunorejection remains high. There is also the potential for teratoma formation after transplantation and the risks remain high with limited knowledge of the mechanisms of ESCs *in vivo*.

2.4 Induced Pluripotent Stem Cells

Induced pluripotent stem cells, like ESCs, are pluripotent cells created by reprogramming adult somatic cells to return to the potential to differentiate into any of the three germ layers [108-110]. This was first accomplished by inducing forced expression of the transcription factors Oct4, Sox2, Nanog, and lin28 through a lentiviral system [110]. Further studies have shown that the key genes to inducing pluripotency are Oct-3/4, Sox2, Klf4, and c-Myc while the others are extra or unnecessary for pluripotency [111]. With the ability to regain pluripotency in adult cells, researchers are presented with attractive options for engineering complete tissues from easily found cell sources such as dermal cells.

In a recent study, human induced pluripotent stem cells were differentiated into endothelial cells and then injected into immunodeficient mice with ischemic limbs. The amount of capillaries increased by 60% and perfusion improved by 30% demonstrating the potential to introduce iPSCs to scaffolds lacking vasculature in order to form blood vessels [112, 113]. Another recent study used iPSC derived fetal liver kinase-1 positive cells and transplanted them into mice with ischemic hind legs, increasing blood flow by inducing angiogenesis and the expression of VEGF [114]. iPSCs have also demonstrated the ability to differentiate into cardiac cells, smooth muscle cells, and endothelial cells when directly injected into the limb of a mouse containing few blood vessels [115]. These breakthroughs are establishing new techniques in using iPSCs to generate blood vessels in scaffolds for a variety of tissue engineering applications. iPS cells have also recently begun to be used in micropatterning techniques to characterize cell-ECM interactions as well [47, 116]. A recent study used elastomeric membranes to control cell position by plasma polymerization of allylamine on PDMS. Airbrushing techniques were used to deposit the ECM protein such as matrigel and fibronectin with resolution up to micron scale precision.

Although iPSCs are extremely promising to scientists because they contain identical genetic information as the patient, concerns about viral reprogramming methods must be addressed to avoid the risk of tumor formation and introducing vector DNA into the host. Other concerns include the fact that iPS proliferation rates are lower than ESC rates and cell death is higher when cells are differentiated *in vitro*.

CHAPTER 3: Microscale Technologies

3.1 Introduction

Cellular interactions with the ECM are generally a function of mechanical, chemical, and topographical properties of the environment. The ECM is generally regarded as the insoluble proteins that exist in tissues. Tissues are composed of multiple cell types with differing ECM components secreted for the specific function of the tissue that regulates cell behavior. Endothelial cells in particular are known for their migratory ability and are constantly restructuring and renewing the ECM by synthesis of new ECM proteins through interactions with the microenvironment. By altering the ECM physical properties, cell behavior can be controlled through a variety of means such as cell-cell contact, cell morphology, and cell orientation [117-119].

Surface roughness is one of the key ECM characteristics that have an important effect on the adhesion, proliferation, and migratory ability of the cells [120]. As an example, it has been shown that cells can sense the nanoscale surface grooves and are able to adhere and adapt to the geometry of the structure [121]. Recent reports utilizing control of topography by spatial patterning of the ECM have demonstrated that endothelial cells can be organized into tubes with lumens within 24-48 hours of seeding. In this example, collagen gels were micromolded into tubular structures up to 1 cm in length and could be controlled by varying collagen concentration and tube widths [122]. Other studies have further delved into regulating cell positioning by controlling

angiogenesis through polarizing micropatterns, varying ligand density and size of micropatterns, as well as presenting conflicting cues to direct cell behavior [123-125]. This area of research has shown to be promising in hopes of recreating and mimicking the native *in vivo* environment and show the importance of surface topography in regulation of cell-ECM interactions.

While different ECM models can clearly have differing chemical characteristics and alter cellular behavior, the mechanical make up of these microenvironments differ with varying composition [126] and chemical bonds [127, 128]. In the design of ECM microenvironments, the mechanical properties need to be engineered to withstand cell contractile forces [65, 129]. Cellular behavior has previously been shown to be heavily influenced by ECM stiffness *in vitro* [3, 18, 20] with cells showing reduced spreading and organization of the cytoskeleton on soft substrates [72]. As a result of the lower cytoskeletal tension, cells tend to show less migratory ability. In contrast, on stiffer substrates, cells show the ability to spread and migrate throughout the scaffold. Interestingly, ECs show a distinct change in spreading at 3 kPa stiffness where actin stress fibers begin appearing [130]. This study goes on to demonstrate the morphological changes that ECs undergo with varied elasticity of polyacrylamide gels on which cells were rounded at 180 Pa and well spread at 16 kPa. The ability of ECs to form tubular networks decreases with higher substrate stiffness [127, 131]. A recent report showed the formation of a network of tubes on compliant substrates (0.2 – 1 kPa) and a monolayer of ECs on stiffer substrates (10 kPa) [132].

In creating tissue, micro-fabrication of vascular networks for scaffolds is generally achieved using methods such as photolithography and soft lithography [13, 25,

122, 133-139]. These methods are all meant to allow oxygen and other nutrients into the deeper portions of the tissue to be created. Soft lithography can specifically be used for a variety of microfluidic channel applications. Branched networks replicating vasculature can be connected to perfusion systems for fluid flow [12] and micro-contact printing can be used to create microscale features [140] for capillary formation. Microcontact printing generally uses a binding chemical interaction between gold substrates and thiol containing moieties to micropattern different molecules [55]. Layer by layer microfluidic approaches have also been used successfully in generating 3D vascularized tissue scaffolds [139, 141, 142]. Polymers such as polydimethylsiloxane (PDMS), poly(lactide-co-glycolide) (PLGA), and poly(glycerol sebacate) have been used as microfluidics channels that are then seeded with ECs [133, 143, 144]. These methods have been shown to be precise techniques to regulate the formation of vascular cells in a preset, methodical fashion. A recent study was able to use soft lithography techniques to mimic early events of angiogenesis while using a co-culture of human MSCs and human vein ECs. This was done by forming non-adherent agarose templates to build tissues with micrometer and millimeter scale precision and study the mechanical impact of angiogenesis along with the VEGF expression of these patterned tissues [140].

Microscale technologies are exciting, enabling technologies to study *in vitro* characteristics of cell-ECM interactions in tissue engineering. Whether as a tool for understanding cellular behavior and biology or by altering implantable constructs for tissue regeneration, these methods are vital for the future. Challenges to *in vivo* research remains such as proper scaffold degradation rates, biomaterials, and precise mechanical properties for implanted tissue. The knowledge gained from these technologies will

undoubtedly prove invaluable to directing cell fate and incorporating cells into scaffolds through the joint effort of engineering, medicine, materials, and biology as clinical trials come to fruition.

3.2 Dip Pen Nanolithography

Dip Pen Nanolithography is a technique to printing proteins or hydrogels that utilizes an atomic force microscope (AFM) tip to transfer molecules to the substrate. Generally this technique is used to transfer alkane thiolates to a gold surface, but advancements have made deposition of molecules to many surfaces possible [145-148]. This technique is a direct contact writing style where the AFM cantilever is used as a pen, dipped in the material, and put into contact to write on the substrate. Recent advances with DPN have made it possible to pattern molecules from 50 nm up to 10 μm while using parallel array tips with up to 55,000 tips per pen. This technique has been utilized in tissue engineering to deposit proteins and hydrogels in highly specific arrays at subcellular resolution.

The DPN Nscriptor system by NanoInk was utilized for micropatterning as shown in Figure 3.1. All micropatterning experiments done with the system were encased in a glove box to control humidity and temperature. To micropattern thiols, “A” pen tips containing 1 pen per cantilever and “M” tips containing 12 pens per cantilever were purchased from Nanoink. The basic patterning process consists of two key steps, the first

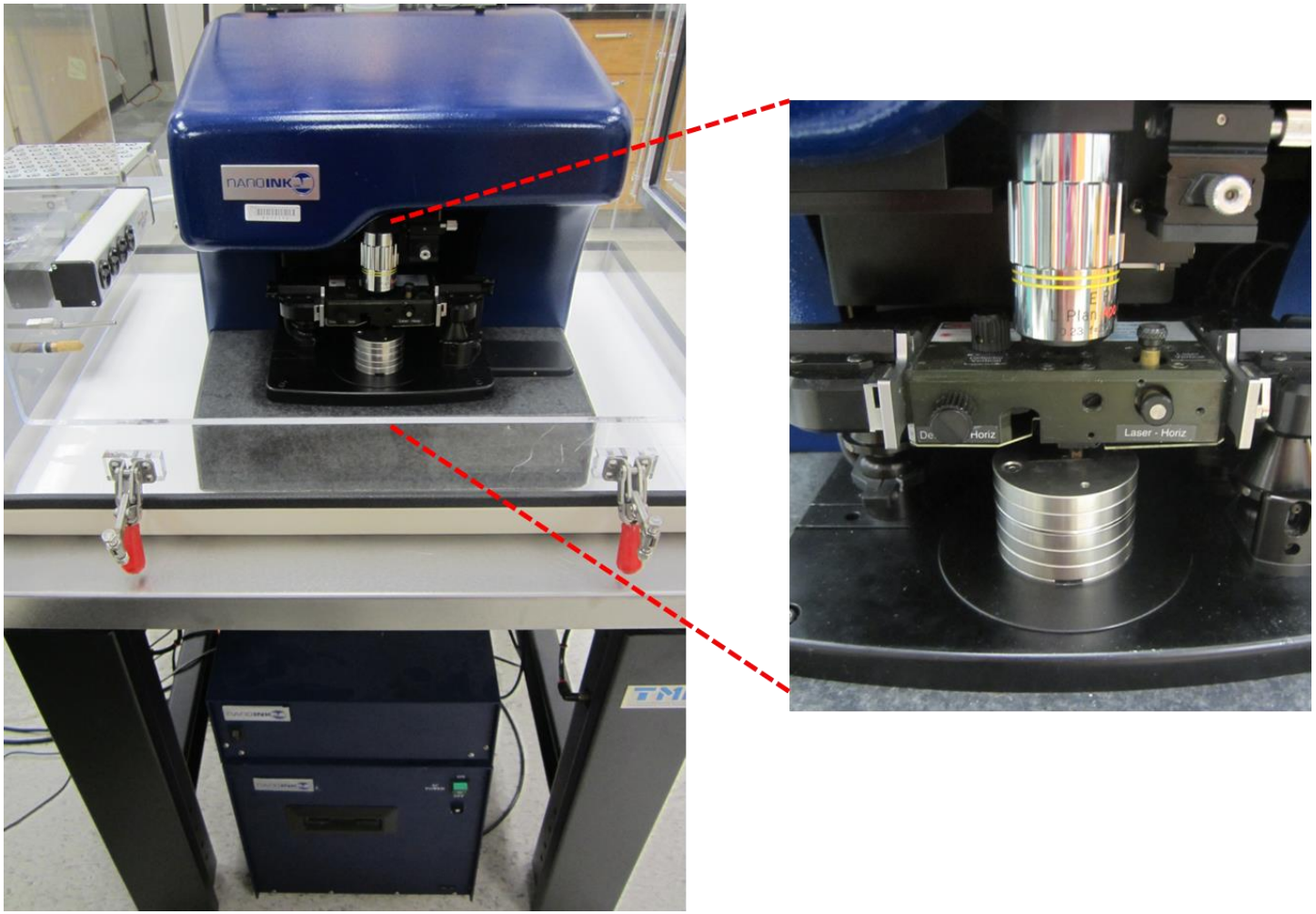

Figure 3.1: NanoInk Nscriptor functionalized AFM system capable of writing inks at subcellular levels onto substrates. This is a fully integrated hardware and software system optimized for dip pen nanolithography.

of which is the molecular transport from the tip to the substrate of the "ink" to be deposited and the second being the actual adsorption of the ink to the substrate as shown in Figure 3.2. This includes a natural water meniscus that forms between the tip and substrate, but the actual transport of molecules is highly dependent on variables such as temperature, humidity, writing speed, tip-substrate contact force, and the physiochemical properties of the ink [56, 146, 149, 150]. To pattern thiols, commonly used 16-mercaptohexadecanoic acid (MHA) was patterned onto a gold surface to in which the ink was adsorbed onto the surface into a self –assembled monolayer shown in Figure 3.3 [151, 152]. This is accomplished with the terminal sulfur ion binding to the gold while leaving the carboxylic acid end groups to be left free to potentially bind to proteins. Pen tips were first cleaned in ozone cleaner (Bioforce Nanoscience, Ames, IA) to remove any materials from cantilever. MHA-coated tips were prepared by dipping tips into MHA saturated solution for 1 minute and loaded onto DPN for patterning. All writing and imaging with DPN was done in contact mode at differing frequencies.

DPN is a highly important microscale patterning tool due to the ease of creating high resolution, tunable printing for the studying of cell-ECM interactions. Studies have shown DPN capable of depositing thiols and proteins at subcellular levels to facilitate cell adhesion with high precision and placement as examples are shown in Figure 3.3 of MHA onto gold [150]. DPN is also capable of writing with liquid hydrogels such as PEG in its precursor form to form subcellular hydrogel structures. Hydrogel precursor DPN protocols are discussed in detail in Chapter 4. This ability to write hydrogels gives DPN the capability of writing varying concentrations of PEG hydrogels for a tunable elastic matrix attachment point for cells. These studies further go on to utilize DPN to control

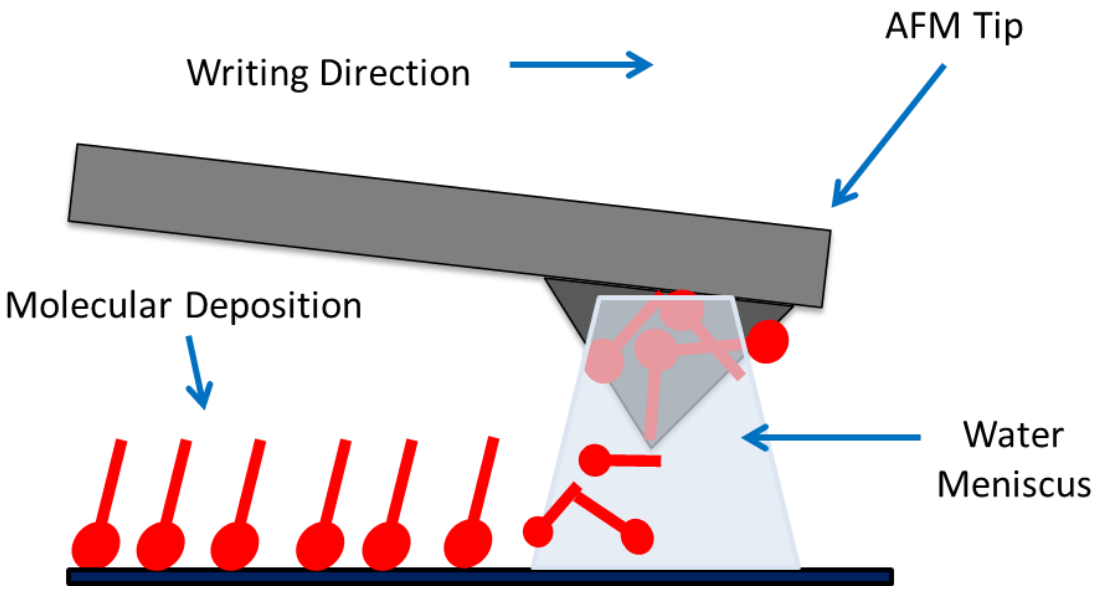

Figure 3.2: Schematic of DPN process. A single DPN tip coated with molecules deposits the “ink” via a water meniscus onto the surface in a nanopatterned array.

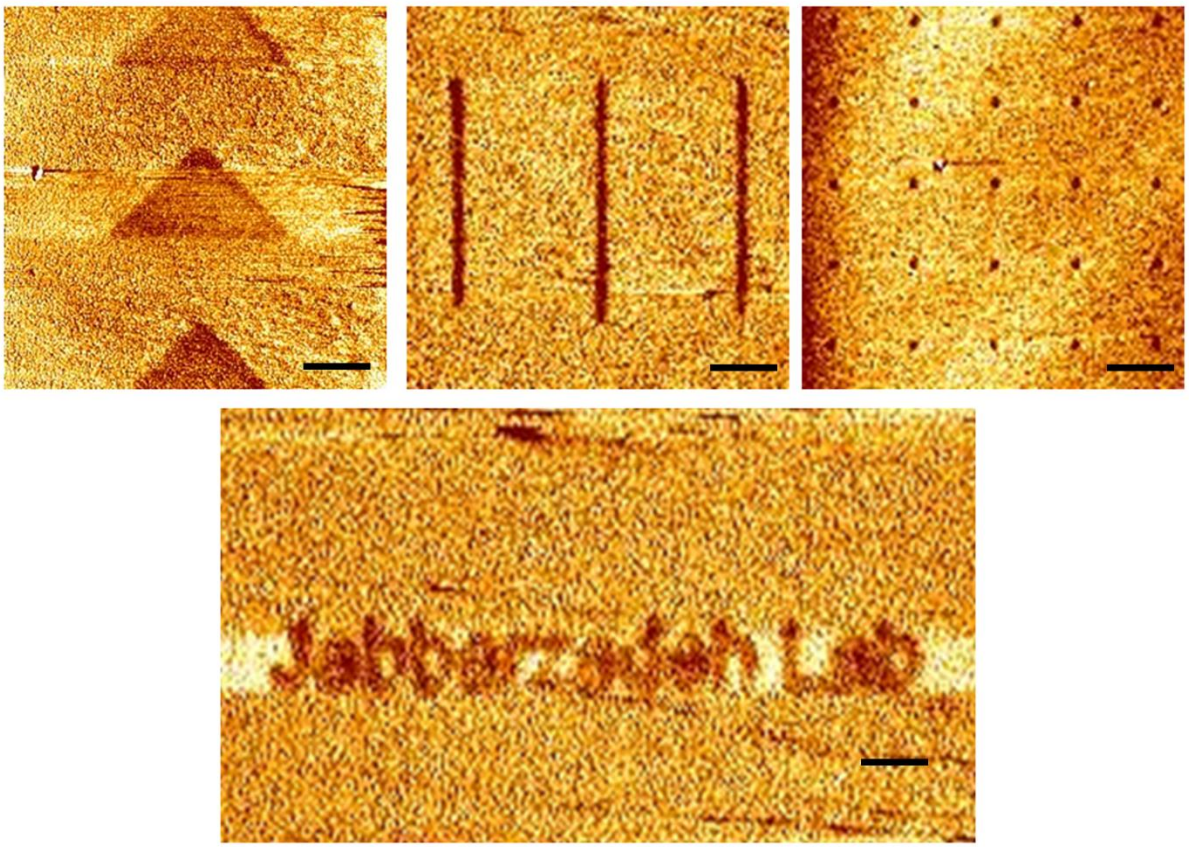

Figure 3.3: Dip Pen Nanolithography is a scanning probe lithography used to deposit substances onto a surface through an atomic force microscope tip. Shown here is alkane thiols printed onto a gold surface. (A)-(C) Triangles, lines, and circles respectively and (D) “Jabbarzadeh Lab” printed out in alkane thiols. Scale bars are 500 nm.

physical characteristics of the microenvironment to regulate stem cell behavior as detailed in Chapter 4.

3.3 UV Lithography using Hydrogels

A common approach to tissue engineering is through the use of photolithography to create micro-patterned scaffolds using a photomask. A photomask is generally an opaque plate or transparency sheet that allows light to pass through in specially designed patterns while restricting light from passing elsewhere [153-157]. Generally polymers that crosslink when exposed to light, especially UV, are used with photomask technology due to the ease of crosslinking the features in the design of the mask. Therefore, only pre-polymer resting below the transparent regions is crosslinked and polymerized through light exposure. To achieve this method of micro-patterning the components necessary are a prepolymer, a photomask, and a photoinitiator. The propolymer must be capable of polymerization by free radicals and the photoinitiator is necessary to facilitate the reaction quickly while optimally remaining nontoxic to cell function. This has been successful with a number of hydrogels in tissue engineering including poly(ethylene) glycol [123, 158-160], methacrylated hyaluronic acid [161-164], and gelatin methacrylate [165, 166] as seen in Figure 3.4 with micropatterned PEG bound with fluorescent protein. Detailed methods for this hydrogel micropatterning can be found in Chapter 5.

In a recent study [123], endothelial cells were regulated on functionalized bio-active PEGDA hydrogels by altering the adhesive ligand RGD in differing concentrations

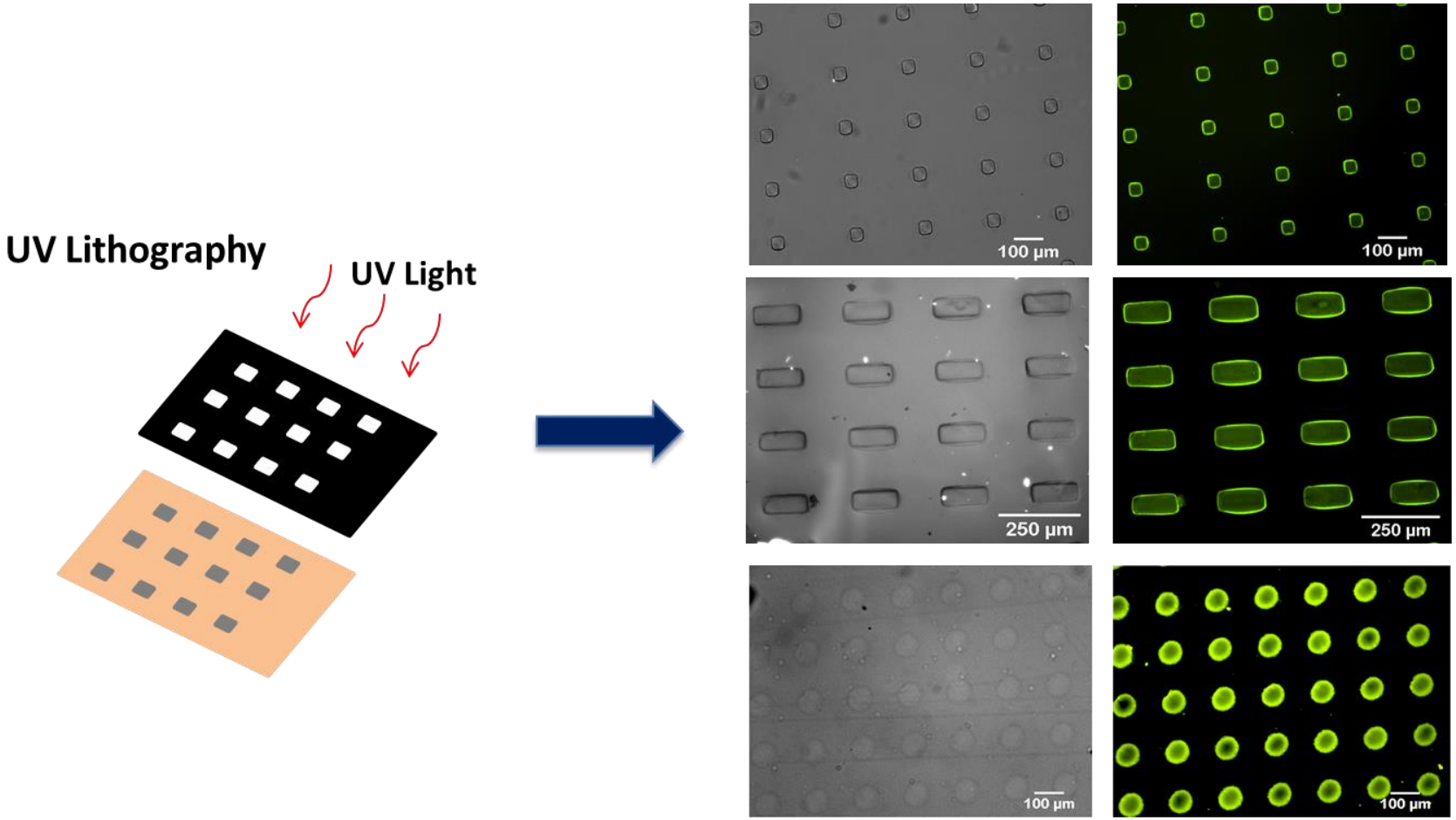

Figure 3.4: UV lithography can be used to pattern hydrogels by selectively allowing UV light to pass through a photomask crosslinking only the exposed hydrogel precursor. This schematic shows using UV light to create patterns such as squares, rectangles, and circles and attaching protein to the hydrogels. Fluorescent BSA was used as a model protein and attached to the hydrogels shown in green.

and geometries. It was shown that ECs formed cords resembling capillaries on 50 µm wide strips, but not larger, and also cord formation was stimulated at a concentration of 20 µg/cm^2 but inhibited at higher concentrations. Another recent study also used UV lithography to micropattern poly(vinyl alcohol) (PVA) onto polystyrene cell-culture plates to examine ECM effects on cell function [167]. This study patterned 5 geometries including squares, triangles, circles, hexagons, and pentagons at equal areas to determine adipogenic differentiation capabilities using MSCs. This study showed adipogenic differentiation capabilities were similar regardless of the pattern shape with these equal area shapes. The use of photolithography to regulate cell-ECM interactions is a simple method capable of studying cellular behavior with micro-scale structures. This area of research is capable of rapidly expanding with more polymers and is an exciting tool for tissue engineering research.

3.4 UV Lithography using Plastics

UV lithography can also be applied to materials capable of being "activated" by UV light such as polystyrene. The UV light is able to promote oxygen group adhesion to the surface rendering it open for cell adhesion. Figure 3.5 shows an MSC on an umbrella shaped pattern on an activated polystyrene coverslip. This method has proved excellent for cell-ECM studies by making micrometer sized patterns aimed at protein adsorption on the surface [168-171]. Instead of utilizing a hydrogel to crosslink, UV light is used to change the surface characteristics of a plastic or thin film on a plastic [167, 168]. This technique of micropatterning uses UV light to pass through a photomask allowing the flat surface underneath to be exposed in geometric shapes and treated. This high precision

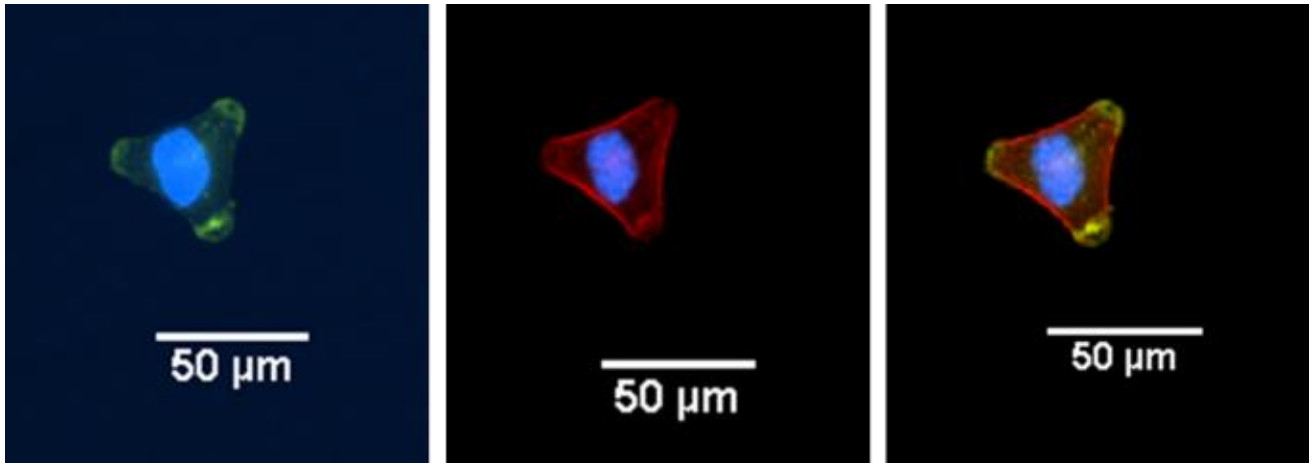

Figure 3.5: MSC showing vinculin and DAPI staining, F-actin and DAPI staining, and merged images from right to left respectively. This cell was adhered to a UV treated polystyrene coverslip with 2.5 minutes of UV treatment and vitronectin bound to the surface and stretched across an umbrella shaped pattern showing distinct stress fibers.

procedure requires a flat substrate to micropattern and works best when creating 2D images. This method is generally applied when there is a need to control cell shape or cell geometry *in vitro* for cell assays.

The UV lithographic method used here is adapted from Azioune et al. and was applied to mesenchymal and embryonic stem cells [168]. A photomask was first designed using AutoCAD with the appropriate features to be studied and printed on a quartz plate with feature sizes down to 1 micrometer. 22x22 mm glass coverslips were used and were initially washed in ethanol for 1 minute and dried with absorbant paper. Coverslips were then illuminated under deep UV light (Bioforce Nanosciences, Ames, IA) for 5 minutes. Polylysine-grafted-poly(ethylene) glycol (PLL-PEG) was diluted to 0.1 mg/ml in 10 mM HEPES buffer of pH 7.4 and a droplet of 50 µl was placed onto activated side of coverslip. Coverslip with droplet was sandwiched with parafilm to ensure PLL-PEG coverage of entire area and incubated for 1 hour at room temperature. Coverslips were then washed in PBS and dried. Photomask was washed with 70% isopropanol and placed under deep UVs for 5 minutes to render mask hydrophilic. Coverslip with pegylated side was placed in contact with photomask using a 5 µl droplet of sterile, DI water to ensure better contact between photomask and coverslip. Coverslip was exposed to deep UVs for 5 minutes for MSCs and ESCs and 1 ml sterile, DI water was placed around coverslip until it was suspended from photomask and removed. Coverslip was then incubated with 25 µg/ml fibronectin solution diluted with 100 mM sodium bicarbonate solution at pH 8.5 for 1 hour. Cells were then seeded onto coverslips at 5,000 cells/cm^2 and allowed 1 hour for initial attachment to patterns. Medium was then gently changed and cells were allowed overnight to fully attach and spread over patterns.

A key use for this type of UV lithography is detailing cell behavior in highly defined conditions. An example of this is looking into how physical characteristics affect properties such as cell shape, adhesive characteristics, and lineage commitment. By regulating the amount of adhesive area micropatterned and the shape, it's possible to control the cell's adhesion and cytoskeletal arrangement. The cells cytoskeleton is a highly complex network made up of a series of biological materials that make up the structural basis that supports cell shape regulation [170, 172-175]. As shown in Figure 3.6 and 3.7 it is possible to constrain and control cell adhesion in distinct shapes such as umbrellas, circles, squares, and Y shapes in a 2D setting. By regulating cell shape, it gives the opportunity to look at distinct cell properties such as polarity and focal adhesion structure.

Cell polarity is generally referred to as the shape and structure of the cells with asymmetrical shape being linked to asymmetric divisions of the cell which are responsible for tissue creation in embryo development [176-179]. In Figure 3.6, polarity protein LGN was stained and observed to be centrally localized in both Y and circle patterns while being located primarily at the apex of the cell in the umbrella shaped pattern. By controlling the cell polarity and shape through UV lithography, it can provide insight into the early stages of development in morphogenesis.

The focal adhesion structure is also able to be controlled and studied through UV lithographic patterns. Focal adhesions are cell-matrix adhesions that involve multiple proteins and serve as the mechanical linkage between the cell's cytoskeleton and the underlying ECM [45, 54, 70, 71, 180]. Figure 3.7 shows hESCs on circles, umbrella, I, and Y shaped patterns showing distinct vinculin expression. Vinculin is one of the

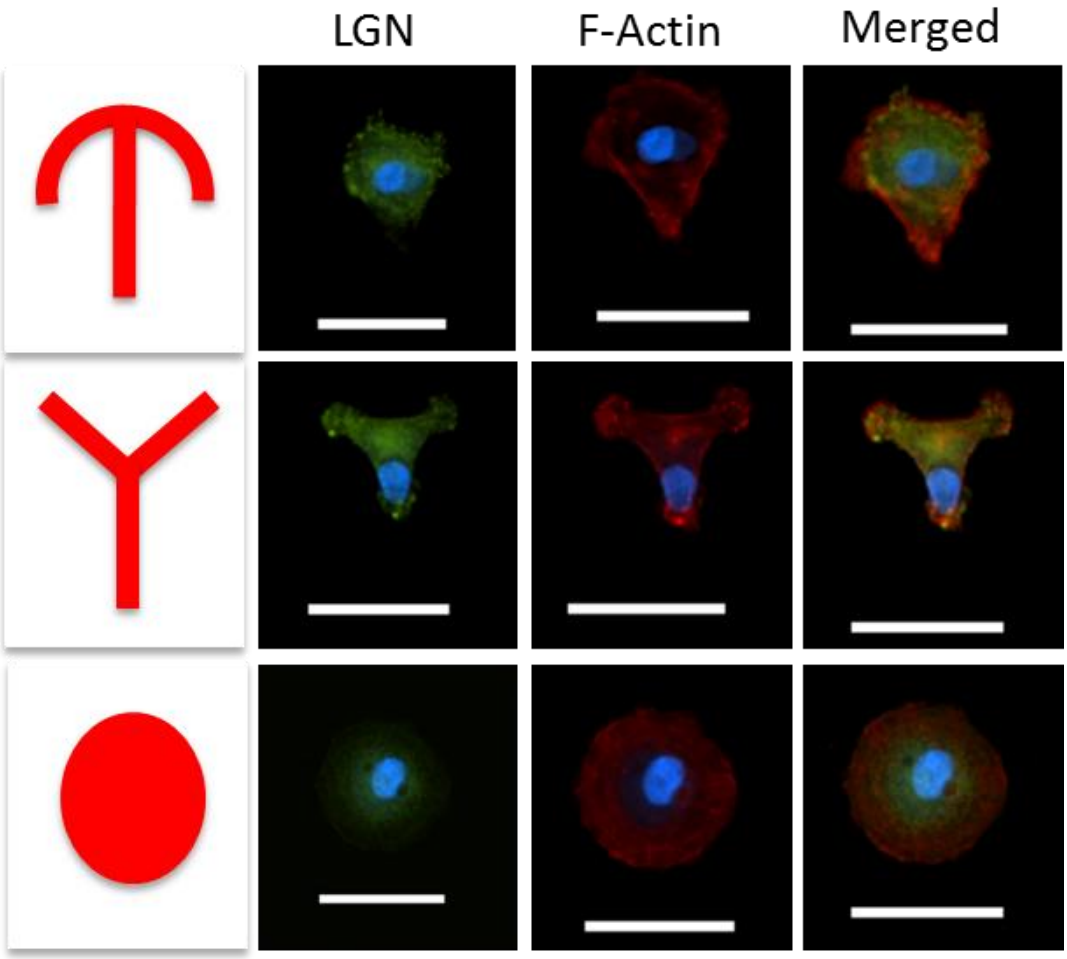

Figure 3.6: MSCs adhered to patterned fibronectin shapes through UV lithography. Shown are umbrella, Y, and circle shapes with LGN (green) and DAPI (blue), F-Actin (red) and DAPI (blue), and merged image respectively. LGN functions as a conformational switch that links Gα and NuMA proteins and is used to determine spindle orientation and cell polarity in human cells [181-183]. As shown, Y and circle patterns show symmetrical distribution of LGN while umbrella shaped pattern shows LGN centered at the top of the umbrella. Scale bars are 50 μm.

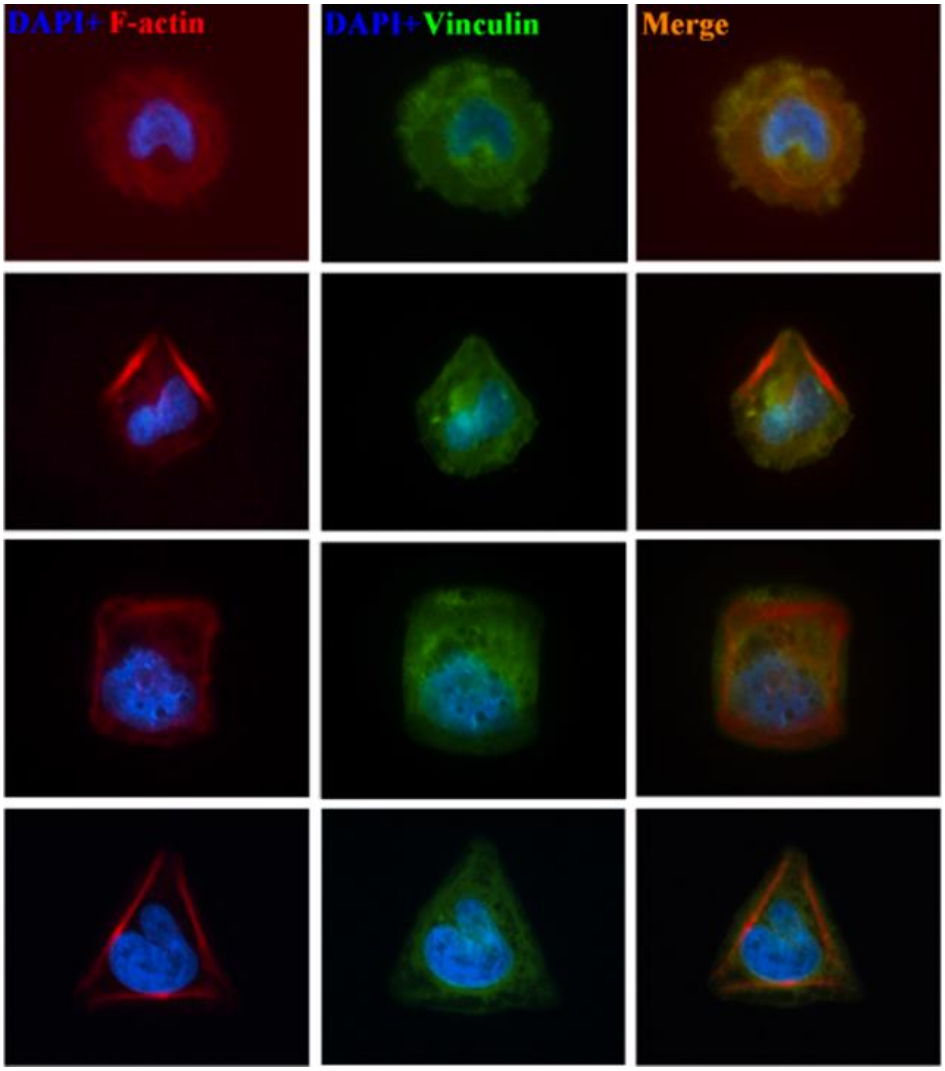

Figure 3.7: Embryonic stem cells are able to be patterned into distinct shapes through UV lithography. Circles, umbrellas, I's, and Y's were seeded onto patterns generated on polystyrene and coated with fibronectin from top to bottom respectively. DAPI (blue) and F-actin (red) are shown in the first column denoting cytoskeletal structure, DAPI and vinculin (green) are shown in the 2nd column denoting focal adhesion structure, and merged images are shown in the 3rd column. Cells are shown at 40x magnification.

proteins that make up focal adhesions along with talin, focal adhesion kinase, and paxillin among many others [45, 67, 180, 184, 185]. By studying focal adhesions and their structure, it is possible to gain an understanding into cell-matrix signaling in relation to characteristics such as cell geometry and matrix elasticity and how they cooperatively tune cell function.

3.5 Soft Lithography

Soft lithography has shown to be a valuable tool in the study of stem cells with capabilities for replicating micrometer to nanometer structures using stamps, molds, and photomasks. Soft lithography can also be specifically used for a variety of microfluidic channel applications consisting of networks of channels for cell culture while being connected to perfusion systems for fluid flow [12], micro-contact printing microscale features [140], and deciphering physical stresses placed on cell behavior due to shear from the fluid flow [63].

The process used to develop microfluidic channels is shown in Figure 3.8. To start, silicon wafers (Silicon, Inc., Boise, ID) were piranha treated (4:1 mixture of sulfuric acid and hydrogen peroxide) for one hour on a hotplate. Wafers were then rinsed thoroughly in DI water and placed in oven at 150 degrees Celsius for 30 minutes to dry. The wafers were then spincoated with SU8 photoresist (Microchem, Newton, MA) to desired thickness according to protocol as shown in Figure 3.9. Wafers were prebaked at 90 degrees Celsius for 20 minutes, let cool until photoresist hardened, and exposed to UV light through photomask with microfeatures for 15 seconds under Blak Ray (UVP,

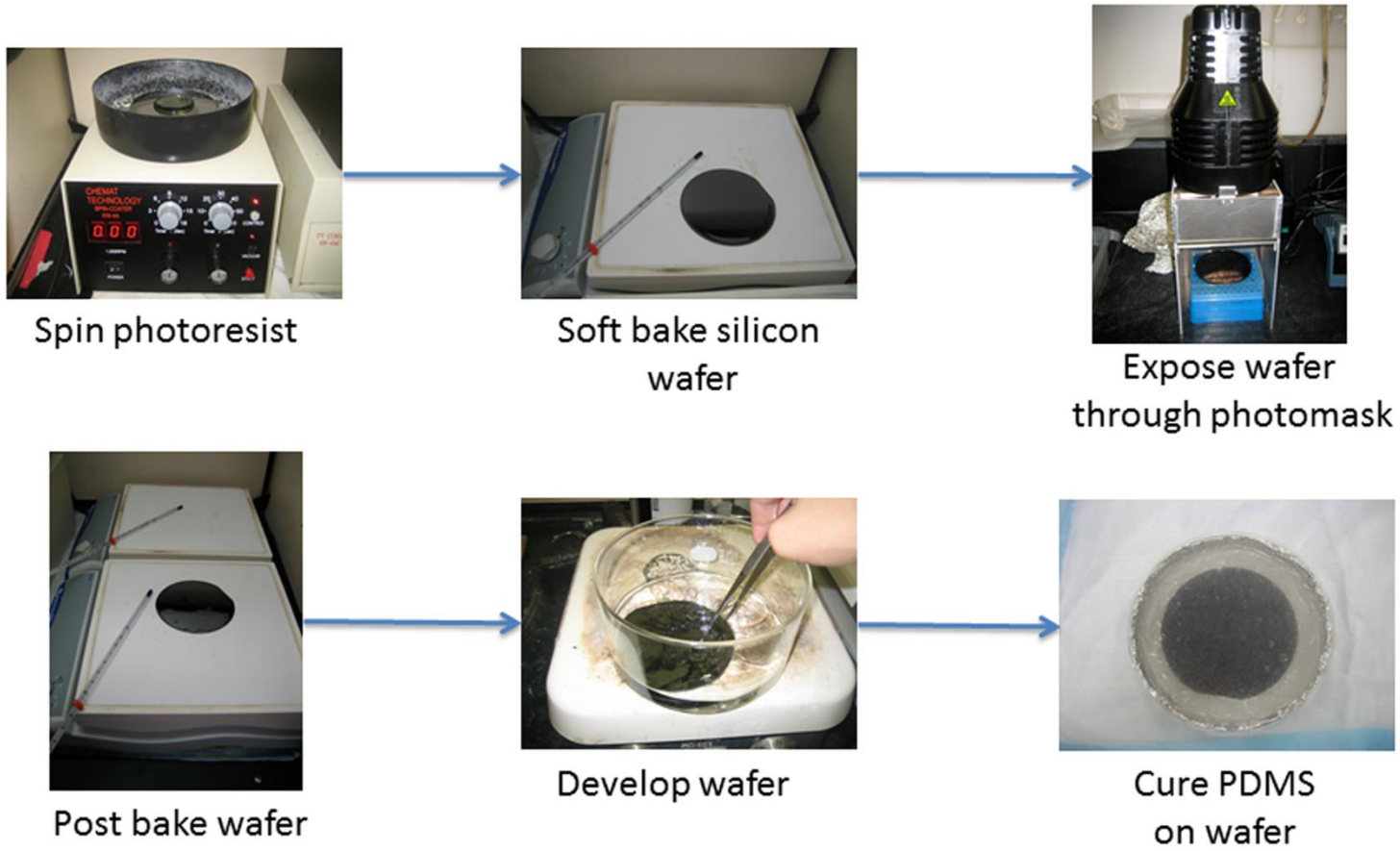

Figure 3.8: Schematic showing the procedure for development of microfluics channels. First photoresist is spincoated onto silicon wafer at desired thickness and wafer is soft baked for recommended time. Wafer is then exposed to UV light through a photomask to pattern desired features into photoresist and post baked. Wafer is then developed to remove uncured photoresist and PDMS is coated onto developed wafer to make microfluidic channels.

Recommended Program

(1) Dispense 1ml of resist for each inch(25mm) of substrate diameter
(2) Spin at 500 rpm for 5-10 sec with acceleration of 100 rpm/second
(3) Spin at 3000 rpm for 30 sec with acceleration of 300 rpm/second

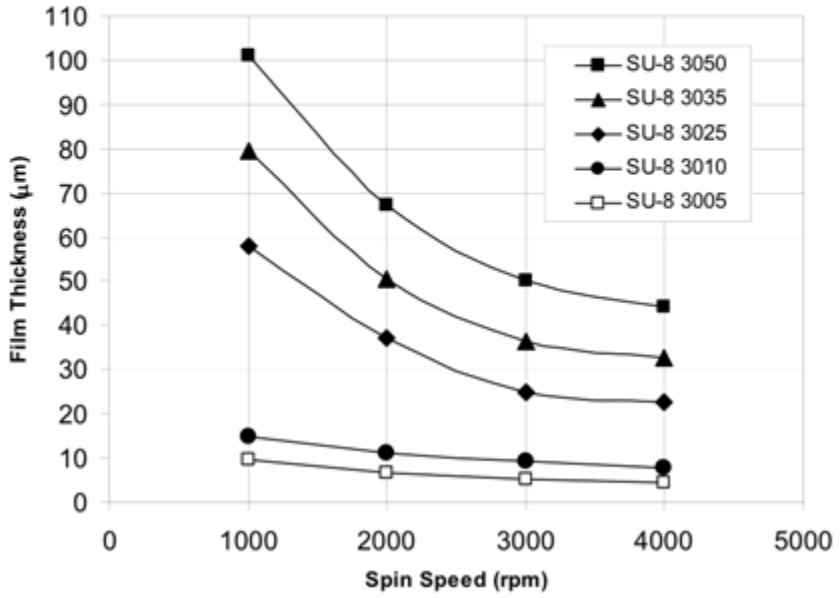

Figure 3.9: Spin speed versus thickness for SU8 3000 photoresists at 21 degrees Celsius

Upland, CA) UV light source. Wafer was then postbaked on hot plates for 5 minutes at 60° C followed by 5 minutes at 90°C. Photoresist was cooled until it hardened and then put into dish filled with photoresist developer (Microchem, Newton, MA) to wash uncrosslinked photoresist from wafer. Wafers were let dry and placed inside a 15 cm petri dish. Sylgard 184 silicone elastomer base and Sylgard 184 silicone elastomer curing agent were mixed vigorously in a 10:1 ratio in a plastic cup to create polydimethyl siloxane, dessicated for 5 minutes, and poured on top of wafer in petri dish until fully covering wafer. Dish was left for 48 hours for polydimethyl siloxane to cure and then patterns were carefully cut off the top of silicon wafer using a razor blade. Individual PDMS channels and 22x22 mm glass coverslip were ozone treated (Bioforce Nanoscience, Ames, IA) and adhered together. Ethanol was run through channels initially, followed by PBS, and finally cells were added in medium to channels and let sit for 8 hours to adhere for culture as shown in Figure 3.10.

Soft lithographic applications for microcontact printing generally utilize a binding chemical interaction between gold substrates and thiol containing moieties to micropattern different molecules [55]. Layer by layer microfluidic approaches have also been used successfully in generating 3D vascularized scaffolds [139, 141, 142]. Polymers such as PDMS, PLGA, and PGS have been used as microfluidics channels that are then seeded with cells [133, 143, 144]. These approaches have been shown to be a precise technique to regulate other cell behaviors such as formation of vascular cells in a preset, methodical fashion. A recent study was able to use soft lithography techniques to mimic early events of angiogenesis while using a co-culture of human MSCs and human vein endothelial cells. This was done by forming non-adherent agarose templates and

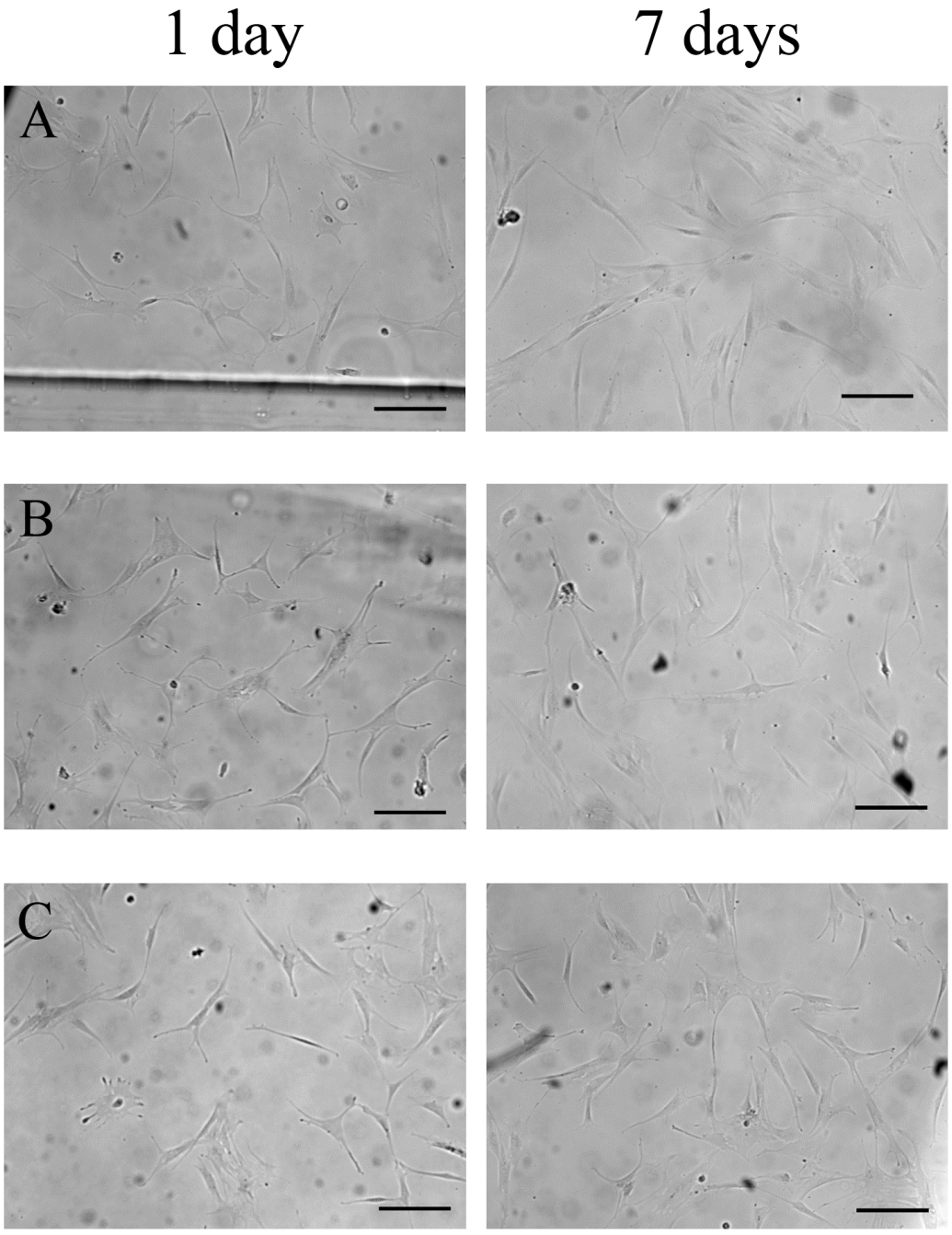

Figure 3.10: Microfluidic chambers were developed to culture stem cells over long periods. (A) 2 mm wide channel showing MSCs after 1 day and 7 days in culture. (B) 4 mm wide microfluidics channel showing MSCs after 1 day and 7 days in culture. (C) 6 mm wide microfluidics channel showing MSCs after 1 day and 7 days in culture. Scale bars are 100 μm.

using these templates to build tissues with micrometer and millimeter scale precision to study the mechanical impact of angiogenesis along with the VEGF expression of these patterned tissues [140]. Other studies done involving soft lithographic principles include utilizing microfluidics channels for shear stress to simulate interstitial fluid flow on cells. A recent study developed a method to generate chemical concentration and mechanical shear stress gradients in a single microfluidics chip [186]. This system was able to expose L929 mouse fibroblasts to mechanical and chemical gradients and affect cell alignment, migratory velocity, and cell attachment while able to sustain long term culture of cells in physically relevant conditions. This is an emerging field of research capable of providing *in vivo* conditions to cells while also versatile enough to construct features on the micrometer to nanometer scale.

CHAPTER 4: Deciphering the Combinatorial Roles of Geometric, Mechanical, and Adhesion Cues in Regulation of Stem Cell Spreading

4.1 Introduction

Human mesenchymal stem cells (hMSCs) are uniquely positioned as a highly promising cell source for tissue engineering and cell transplant strategies due to their unique capability of self-renewal and capability to differentiate into many diverse cell types [109, 187-190]. However, their use as a therapy thus far is hampered due to the limited understanding of mechanisms by which cells integrate environmental stimuli. In the regeneration process, the temporary extracellular matrix (ECM) provides multiple signals to the migrating cells to guide the process of new matrix formation. Major advances have been made in the identification of these biochemical and biophysical regulators of stem cell fate [3, 18, 48, 52, 191-197]. It has been proposed that many of these signals are intertwined, yet definitive studies have been unable to identify the correlation between biological signaling pathways and how cells receive these signals to develop and repair tissue.

Tissue is fundamentally diverse across ECM environments and plays a major role in cell signaling [39-42]. The ECM is composed of large amounts of biochemical components including proteins, glycoproteins, proteoglycans, and polysaccharides with vastly different physical and biochemical properties [21, 22]. Cells are able to sense these variances through transmembrane proteins called integrin receptors that help govern cell-

ECM signaling and link the cell to the proteins in the ECM [27, 28, 43-45]. This cell - ECM interaction is crucial to sensing forces through tissue and the surroundings. As early as the 19th century scientists understood physical forces were important to tissue development and were able to show that cultured chick rudiments under static compression following displacement of the periosteum and perichondrium resulted in cartilaginous tissue formation while tensile stresses led to bone formation [51]. More recent studies have uncovered that ECM topography can control cellular organization with the size and geometry of available surface area being able to alter cell shape, traction forces, and cell spreading [19, 52-59]. Single cell studies further show that smaller ECM islands promote rounded cells while cells in larger islands with no restriction flatten and spread similar to 2D cultures [19, 53]. A key study involving adult stem cells showed micropatterned 10,000 μm^2 and 1,024 μm^2 protein areas directed osteogenic differentiation and adipogenic differentiation respectively simply by controlling cell shape and size. Thus, cell shape and size are crucial components in determining stem cell lineage with generally accepted instances of rounded adipocytes [60, 61] and polygonal osteoblasts [62, 63]. Cell shape is also highly influenced by ECM elasticity which has the ability to also impact cell spreading, traction forces, cell motility, and differentiation [18, 20, 46, 64-69]. Researchers have been able to use polyacrylamide gels to mimic tissue elasticity from 1 kPa to 40 kPa and promote differentiation of stem cells into neurogenic, myogenic, and osteogenic lineages through solely altering elasticity [18]. Additionally, matrix elasticity for previously differentiated cells has been shown to alter the cytoskeletal organization as well as the focal adhesion structure [41, 70-72, 198]. Furthermore, three-dimensional experiments have shown cells capable of migrating and

remodeling the ECM in terms of matrix stiffness and topography [35-37] making it vital to understand the significance of physical signaling and cell-ECM interactions.

A significant step towards further decoupling these signals can be achieved through the development of platforms with tunable physical and topographical properties that allow for further exploration of the co-operative involvement directing cell behavior. While both topography and matrix elasticity has been shown to affect cell morphology independently, there lacks sufficient data correlating these signals. Micropost arrays with varying stiffness and topography pioneered by the Chen laboratory have begun to incorporate the concepts of matrix elasticity with patterning proteins and cell alignment [199-204]. This research has laid the groundwork to characterize the interplay between physical signals but lacks the ability to change the elastic modulus of the posts, as opposed to stiffness, as well as the elastic modulus of the background ECM. In this preliminary study on deciphering multiple physical cues, we demonstrate a novel method of micropatterning hydrogels to create a tunable matrix with variable elasticity, topography and ligand density as seen in Table 4.1 and demonstrate how these characteristics affect cell adhesion. A finite element model was also employed to confirm experimental results and utilized as a predictive tool in cell behavior. DPN was employed to micro-pattern islands of poly(ethylene) glycol (PEG) hydrogels onto a polydimethyl siloxane (PDMS) coated surface. DPN is a versatile technique that utilizes a functionalized atomic force microscope tip to transfer molecules of interest to a substrate via a surface meniscus formed between the substrate and tip [145-149, 205]. Hydrogel islands were patterned onto the PDMS substrates [148] to provide a tunable elasticity and

Table 4.1: Table showing the micropatterning characteristics including, background ECM elasticity, island elasticity, island topography, and ligand density values. Also shown are the characteristics analyzed to determine cell behavior and spreading including cell size, focal adhesion distribution, cytoskeleton arrangement, and RhoA signaling pathway knockdowns.

Substrate Design	**Cell Properties Assessed**
Background ECM Elasticity (12 kPa and 2.5 MPa) Island Elasticity (7 kPa and 105 kPa) Island Spacing (3 µm, 7 µm, & 12 µm) Ligand Density (20, 50, & 100 µg ml^{-1})	Cell Area Focal Adhesion Distribution (Vinculin) Cytoskeletal Organization (F-Actin) RhoA Signaling Pathway

pitch. In this study, we report experimental and modeling results on how the interplay between ECM properties controls cell-adhesion characteristics that define hMSC spreading.

4.2 Substrate Preparation

Glass coverslips (22 x 22 mm, Fisher Scientific) were washed with ethanol, dried with nitrogen, and treated for 30 minutes with ozone cleaner (BioforceNano, Ames, IA). PDMS was then spincoated onto cover slips at 500 rotations per minute (RPM) for 10 seconds followed by 2000 RPM for 60 seconds. Cover slips were then sputter coated (Denton Desk II, Moorestown, NJ) with a 5 nm titanium adhesion layer onto PDMS followed by approximately 40 nm of gold.

4.3 Micropatterning of PEG Islands

Islands of PEG hydrogels were patterned using a DPN NSCRIPTOR system with M type pen (Nanoink, Skokie, IL). Pens were ozone treated for 30 minutes prior to inking. PEG precursor was mixed using 700 molecular weight (MW) PEG diacrylate (PEG-DA) (Aldrich, Milwaukee, WI) mixed with 2000 MW 4-arm PEG thiol (PEG-SH)(CreativePEGWorks, Raleigh, NC) in deionized water with 0.5% (v/v) 2-hydroxy-2-methylpropiophenone (Aldrich,Milwaukee, WI). Cover slips were patterned with PEG islands and placed under approximately 4 mW/cm^2 UV light (UVP, Upland, CA) for 2 minutes to gel. Cover slip was then incubated in 50 mM triethylene glycol mono-mercaptoundecyl ether (Aldrich, Allentown, PA) for 20 minutes to render remaining

surface non-adhesive and rinsed with 70% ethanol and subsequently sterile distilled water three times. Fibronectin (FN) from human plasma (Sigma, St Louis, MO) was incubated at 4°C for 2 hours in heterogenous maleimide/N- hydroxysuccinimide bi-functional linker (Thermo Fisher, Rockford, IL) [206] and separated from unreacted linker using a Zeba Spin desalting column (Thermo Fisher, Rockford, IL). Cover slips were then incubated in functionalized FN overnight to allow covalent attachment.

4.4 Hydrogel Characterization

Cylindrical PDMS disks 5 mm in diameter and 5 mm height were fabricated in a 10:1 and 50:1 ratio of base to curing agent and let cure for 48 hours and sputter coated with titanium and gold for differing substrate modulus [207, 208]. PEG hydrogel samples were created 5 mm in diameter and 3 mm height at desired ratio and let soak in deionized water for 48 hours at 37°C. Samples were tested in unconfined compression [209-212], in short, the Young's modulus of each sample was determined using an ElectroForce 3200 (Bose, Eden Prairie, MN) in unconfined compression at 0.05 mm sec^{-1} between parallel nonporous plates while compressive force and displacement were recorded.

4.5 Cell Culture

Human bone marrow-derived mesenchymal stem cells were obtained from Lonza (Walkersville, NC). hMSCs were cultured in basal growth medium (Lonza, Walkersville, NC) in Nunc cell culture treated 75 cm^2 flasks (Fisher Scientific). Growth medium contained 440 mL of hMSC basal medium, 50 mL of mesenchymal cell growth

supplement, 10 mL of 200 mM L-glutamine, and 0.5 mL of a penicillin/streptomycin mixture. Cells were passaged after reaching 90% confluence and collected with 0.05% trypsin/EDTA solution. All cells were plated onto cover slips under passage 6 at 5,000 cells per cm^2. Cells were allowed 4 hours for adhesion onto substrates. For ROCK inhibited cells, 10 μM Y-27632 (Calbiochem, Rockaway, NJ) was applied daily for 1 week prior to seeding.

4.6 Immunofluorescent Staining

After incubation for 4 hours in culture medium, cells were fixed with 4% paraformaldehyde, permeabilized with 0.2% Triton X-100, and blocked with 1% BSA solution. F-Actin, focal adhesions, and nuclei of cells were stained with a rhodamine-phalloidin conjugate (Invitrogen, Grand Island, NY), vinculin (Sigma, St. Louis, MO), and Fluoroshield with DAPI (Sigma, St. Louis, MO) respectively. Fluorescent photographs of hMSCs were captured by a Nikkon Eclipse 80i microscope with CoolSnap HQ camera. Non-fluorescent cells were analyzed using phase contrast microscopy utilizing NIS-Elements-AR 3.2 64 bit software (NIS-Elements, Melville, NY).

4.7 Simulation Model and Analysis

A finite-element model was constructed to quantify the peak deflection of micropatterned substrates in response to cell-derived forces. The model geometry consists of two subdomains, namely a 50 micron thick PDMS substrate and a

hemispherical PEG island with a radius of 5 microns. Both PDMS and PEG were modeled as linear elastic, isotropic, incompressible, and homogeneous materials. Model boundary conditions consisted of a 20 nN lateral body force applied to the PEG island, a fixed constraint on the bottom surface of the PDMS substrate, a rigid contact between the PEG and PDMS, and free deformation for all other surfaces. The Poisson's ratio (υ) and density (ρ) of both materials were assigned fixed values, while the elastic moduli (E) were varied in isolation to delineate the effect of substrate and island stiffness on the mechanical behavior. A commercial finite-element software package with a built-in parametric solver (COMSOL) was used to generate stationary solutions to the defined solid mechanics problem. The peak PEG island deflection was extracted from each simulation result and used as a metric of the micropatterned substrate mechanical response to a cell-derived force. A total of 60,177 tetrahedral mesh elements were used to discretize the model geometry and generate mesh-independent solutions, with mesh-independence defined as the level at which further refinement induced a less than 1% change in the predicted peak deflection.

4.8 Statistics

P-values were calculated using the student t-test function in Excel (Microsoft, Seattle, WA). Linear regression analysis and interaction plot were created using Minitab version 16 software (Minitab Inc., State College, PA). Errors are standard error of the mean.

4.9 Controlling Cell Position and Spreading on Micropatterned ECMs

In this study we fabricated hydrogel islands using a novel process utilizing DPN to deposit micrometer sized PEG islands onto PDMS coated coverslips as shown in Figure 4.1A. PEG was chosen due to the non-toxic properties and the ability of this polymer to resist protein adsorption [213, 214]. DPN is a highly versatile technique able to be used in creating islands at differing spacing using a functionalized atomic force microscope tip to directly transfer molecules of interest to a substrate. PEG-DA and PEG-SH mixture was chosen as hydrogel islands and by varying the concentration of PEG precursor, it was possible to more closely mimic the elasticity of tissue at the subcellular level. PEG islands were patterned onto the gold coated PDMS background backfilled with PEG-SH to render the background non-adhesive to protein adsorption and confine cell adhesion to islands. The PDMS background was able to be altered to achieve differing elasticities of the non-adhesive ECM. Preliminary experiments were performed to confirm the ability of proteins to conjugate exclusively to the hydrogel islands, BSA was used as a demonstration protein as shown in Figure 4.1B. Hydrogel islands were sized at 9.31 ± 0.058 μm in diameter and spaced at 3.15 ± 0.22 μm, 7.09 ± 0.23 μm, and 12.07 ± 0.23 μm pitch to allow cells to spread across multiple islands (50 islands analyzed each case). Hydrogel island elasticities were measured at 7.05 ± 0.72 kPa and 105.07 ± 1.07 kPa respectively. Ligand density was determined by incubating samples in 20 μg ml^{-1}, 50 μg ml^{-1}, and 100 μg ml^{-1} fibronectin concentrations overnight. PDMS was spincoated onto glass coverslips at a 50:1 base:curing ratio and a 10:1 ratio for a differing elasticity of 12 ± 1.0 kPa and 2.5 ± 0.20 MPa respectively [207]. By utilizing a novel

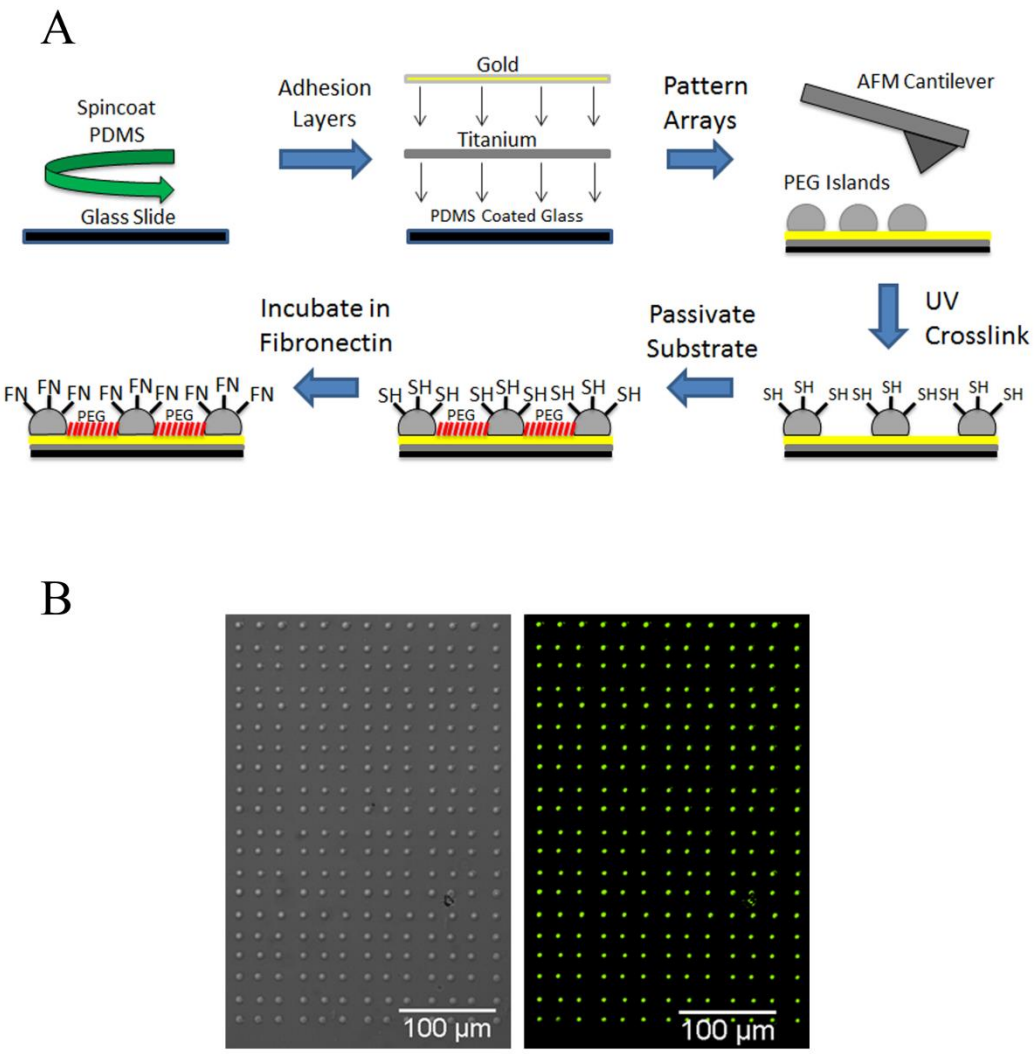

Figure 4.1: DPN enables micropatterning of sub-cellular hydrogel substrates. (A) PDMS was spincoated onto glass slides to form a background of varying elasticity while utilizing DPN to deposit micropatterned hydrogel islands also with varying elasticity. These sub-cellular islands were functionalized with fibronectin at differing ligand densities, which facilitated cell attachment to substrate. (B) Micropatterned PEG hydrogel islands spaced at 12 µm distance between islands showing 100 µg ml^{-1} BSA-FITC conjugated protein covalently bonded.

micropatterning method we were able to create a tunable array of subcellular hydrogels capable of parsing microenvironmental cues presented to a cell. Attaining this allowed us to successfully integrate geometric, mechanical, and biochemical control in understanding cell adhesion and spreading of hMSCs.

4.10 hMSC Cell Shape is Regulated by Matrix Elasticity

To study the behavior of cell spreading on differing physical cues, hMSCs were plated onto micropatterned coverslips. Early passage hMSCs (< passage 6) were plated at a density of 5,000 cells cm^{-2} and given four hours to allow initial cell adhesion. The cells adapted to the patterned islands according to island elasticity, island spacing, ligand density, and background elasticity as shown in Figure 4.2A. Cells were not allowed to interact with the patterns over long periods to minimize cell modification of the ECM due to secretion and synthesis of components by the cells in particular to the PDMS background. Using a statistical software program Minitab, we ran a linear regression analysis on the cell data and it was observed that hydrogel island stiffness was the key factor in regulating cell adhesion as seen in Equation (1). Cell areas from each condition were compiled into Minitab to run regression analysis and normalized prior to analyzing.

Equation 1:

Cell Area = 4061 PEG - 952 Spacing + 824 Ligand Density + 296 PDMS + 1377

By observing the significance shown by PEG (hydrogel islands) in Equation 1 it is clear By observing the significance shown by PEG (hydrogel islands) in Equation 1 it is clear that the island adhesion points are the strongest variable controlling cell adhesion.

Spacing and ligand density both show reduced efficiency with PDMS (background elasticity) showing insignificant effects.

At an island elasticity of 7 kPa, cells preferentially showed a spindle shaped cell orientation similar to myoblasts [28] with smaller cell areas (Figure 4.2B), while 105 kPa islands were larger, well spread cells similar to osteoblasts [18] (Figure 4.2C). Figure 4.3A shows the dependence of cell spreading on island elasticity with stark contrasts in 7 kPa elasticity and 105 kPa elasticity in each condition ($P < 0.002$). Interestingly, when looking at background ECM elasticity for both 7 kPa and 105 kPa islands each case was deemed statistically insignificant to cell area ($P > 0.05$). The interaction plot in Figure 4.3A illustrates the heavy influence of island elasticity, less significant effects of ligand density and island spacing, and insignificant influence of background matrix.

Island spacing was shown to have smaller effects on cell adhesion. Controls were done with non-patterned hydrogel cover slips and compared to patterned cell areas with equal ligand density and elasticity. The results showed cell areas were significantly altered at 12 μm spacing ($P < 0.05$) when compared to unpatterned controls except for a single condition on 7 kPa PEG. 7 μm spacing also proved significant at the two lower ligand densities ($P < 0.05$) when compared to controls except for a single condition of 105 kPa PEG (Figure 4.3B-C). In observing 7 and 12 μm spacing, it is evident that without the aid of increasing ligand density for cell adhesion, this is not optimal for cell spreading when compared to its unpatterned counterpart. 3 μm spacing remains significant at lower densities to controls but was deemed insignificant at 100 μg ml^{-1}. This result was unsurprising due to the increased adhesion area for cells to attach and continue spreading. At both 20 and 50 μg ml^{-1} FN concentration the 3 μm spacing is

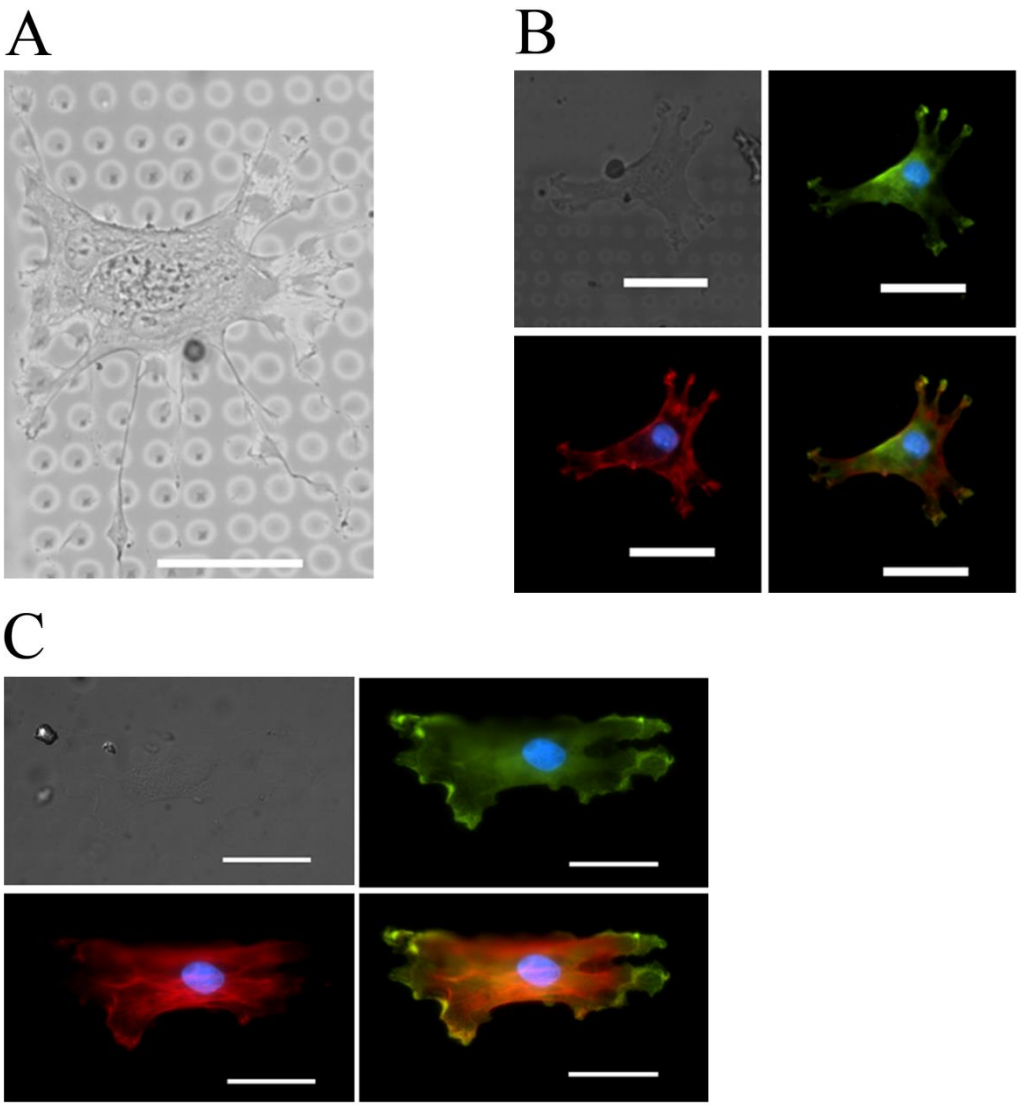

Figure 4.2: Hydrogel island elasticity regulates cell adhesion and spreading size in MSCs. (A) MSC adhered to hydrogel islands showing distinct spreading across individual islands and extensions protruding across PDMS surface (B) MSC adhered to pattern with 7 kPa islands, 12 kPa background elasticity, 3 μm spacing, and 100 μg ml^{-1} FN with a cell area of 2,669 μm^2. Shown as brightfield image (top left), vinculin staining (top right), F-actin staining (bottom left), and merged image (bottom right). Average cell area for data point was 1174.54 $\mu m^2 \pm 113.16 \mu m^2$. (B) MSC adhered to pattern with 105 kPa islands, 12 kPa background elasticity, 3 μm spacing, and 100 μg ml^{-1} FN with a cell area of 6,134 μm^2. Shown as brightfield image (top left), vinculin staining (top right), F-actin staining (bottom left), and merged image (bottom right). Nucleus is shown in blue in all images. Average cell area for these conditions was 5847.13 $\mu m^2 \pm 260.56 \mu m^2$. All scale bars are 50 μm.

significant in 7 kPa PEG on both 12 kPa and 2.5 MPa PDMS backgrounds and 105 kPa on 12 kPa PDMS background ($P < 0.05$) (Figure 4.3B-C). The 105 kPa PEG on 2.5 MPa PDMS background matrix was not significant in the 20 or 50 μg ml^{-1} conditions ($P > 0.05$). As ligand density was increased it proved to negate spacing effects as evidenced in the 100 μg ml^{-1} FN with 3 and 7 μm cases being deemed insignificant ($P > 0.05$) in each elasticity condition for PEG and PDMS (Figure 4.3D). Thus, we observed that higher ligand density per island was able to increase cell adhesion area even when distance between islands was increased.

Ligand density was compared at equal conditions for the 100 μg ml^{-1} and 20 μg ml^{-1} FN to observe affects. Differing ligand densities at 3 μm spacing was shown to be statistically relevant in promoting different cell areas except for a single case with 105 kPa PEG. For example, when comparing 7 kPa islands with 100 μg ml^{-1} FN cell area was 2666.04 ± 284.38 μm^2 to 20 μg ml^{-1} FN and a cell area of 1548.92 ± 203.05 μm2 ($P < 0.003$) (Figure 4.3D). When observing 7 μm spacing the effects of ligand density diminish, but remain noteworthy at two specific 105 kPa and 7 kPa island test cases ($P < 0.05$). The 7 kPa islands proved the most significant with a cell area of 2234.94 ± 187.0 μm^2 at 100 μg ml^{-1} compared with 1110.42 ± 159.26 μm^2 at 20 μg ml^{-1} FN concentration ($P < 0.0001$). As the spacing of the islands increases to 12 μm it was shown to lose statistical relevance. Interestingly, these results show that when only looking at ligand density it has an effect on cell adhesion at smaller spacing and diminishes as spacing is increased. We hypothesize this is due to the amount of adhesive area being greatly

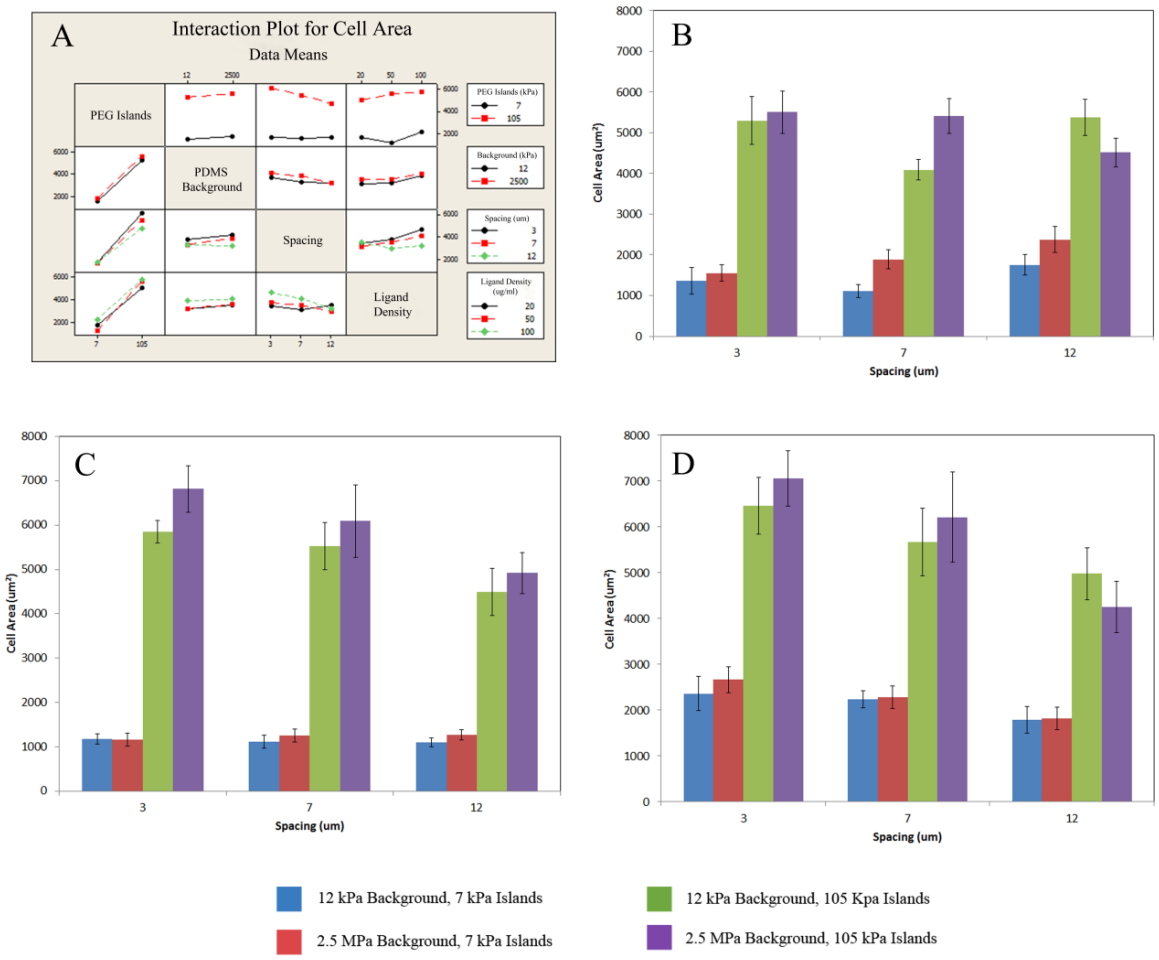

Figure 4.3: (A) The interaction plot illustrates the affects between the non-independent test variables, which include island elasticity, PDMS background ECM elasticity, ligand density, and spacing of islands. Interaction plot uses averages of means to plot interactions. The first column demonstrates the key factor PEG elasticity plays in cell adhesion of MSCs. Spacing and ligand density also are shown to contribute to cell spreading in the interaction plot. PDMS background elasticity was shown to not affect adhesion as shown by PDMS elasticity column showing background elasticity interacting with other variables as nearly parallel lines. Quantification of average cell area for cells with (B) 20 µg/ml, (C) 50 µg/ml, and (D) 100 µg/ml fibronectin concentrations. Error bars are standard error of over 10 cells quantified per condition.

reduced at this large spacing, cells were unable to stretch across the same amount of islands rendering the FN concentration insignificant.

Adhesion-mediated signals are shown to be vital in cell-ECM interactions and guiding cell spreading and size. Other reports have used patterned and unpatterned ECMs to guide cell adhesion on differing gel or PDMS surfaces [18, 203, 215]. These studies generally show a consensus for a plateau of cell spreading over approximately 40 kPa. Our results coincide with these other reports and further show the dependence of cell spreading on matrix elasticity when in the presence of other physical factors affecting hMSC spreading. Furthermore, cell generated forces must act in equilibrium, therefore the soft hydrogel islands provide less resistance to a cell's forces and cell contractility decreases. In contrast, stiff islands are able to provide the necessary counterbalancing forces, intracellular tension is increased leading to well spread cells.

4.11 Island Deflection Simulation Predictions

The mechanical behavior of micropatterned cover slips was characterized with finite-element modeling of the deformation response to cell-derived forces. In all examined cases, PEG islands exhibited significantly greater deflection as compared to the PDMS substrate as seen in Figure 4.4A. As expected, the greatest deflection occurred when both the island and substrate had the lowest elastic moduli in the examined range. Increasing the PEG island stiffness resulted in a nonlinear decrease in the peak deflection, irrespective of the stiffness of the underlying substrate. Increasing the substrate stiffness had a comparatively diminished effect on the peak island deflection, particularly when

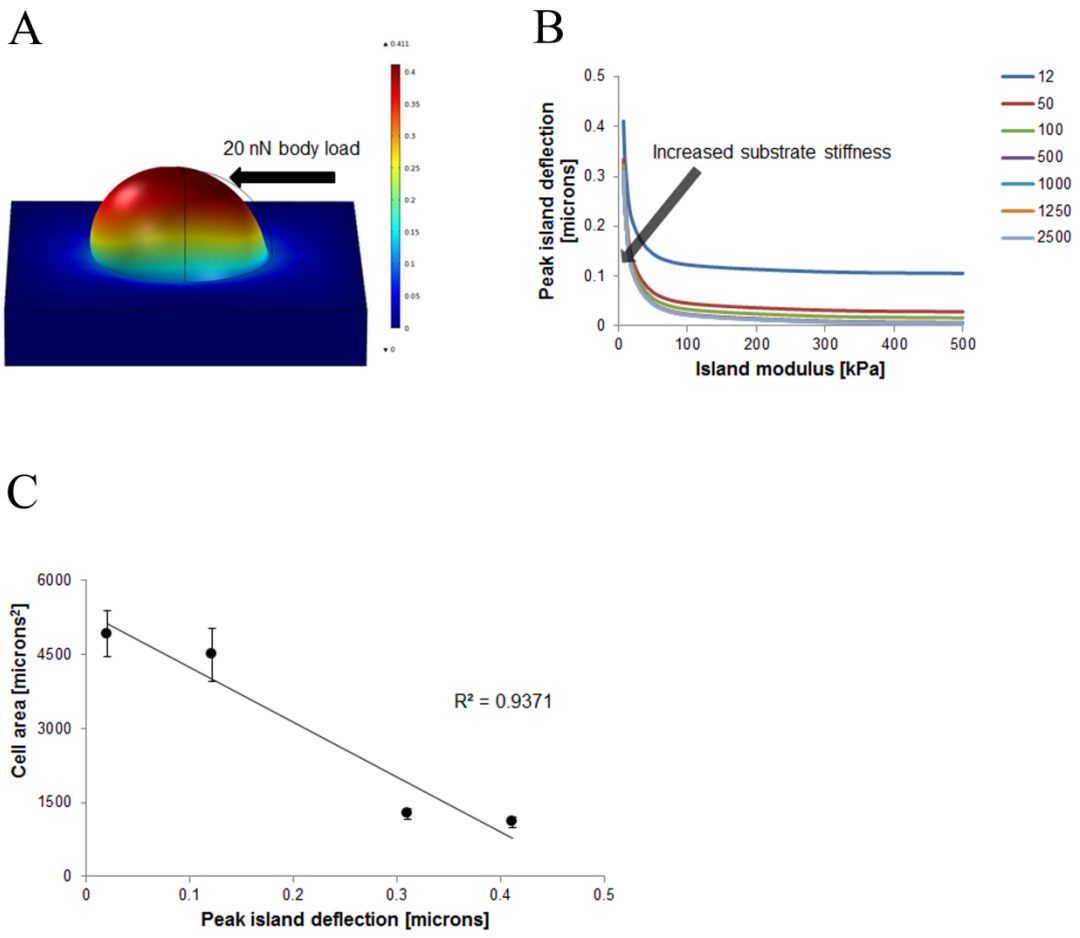

Figure 4.4: Patterned hydrogel islands were analyzed to engineer substrate elasticity (A) Conceptual illustration of horizontal cell traction force of 20 nN on hydrogel island and analysis of deflection of individual island. (B) Hydrogel island deflection is plotted as a function of island modulus with differing background elasticities plotted. (C) Cell area of 12 µm spacing cases plotted versus correlating model peak deflections to show correlation between modeling and experimental components.

the substrate modulus exceeded that of the PEG island shown in Figure 4.4B. The predicted peak island deflection inversely correlated with the cell area following seeding on micropatterned substrates, suggesting that rigid regions-of-contact between the cell and material facilitate cell spreading seen in Figure 4.4C.

4.12 Rho Kinase Inhibition Attenuates Differences in Hydrogel Island Mediated Cell Spreading

RhoA has been shown to affect cell size and shape previously as well as play a significant role in cytoskeletal tension in the cell [55, 57]. To address this factor, myosin-generated cytoskeletal tension was inhibited by culturing hMSCs in the presence of Y-27632, an inhibitor of Rho-associated protein kinase (ROCK) that acts as a downstream Rho protein involved in myosin activation. Cells exhibited elongated neuron-like spindles after treatment with Y-27632 on both 7 kPa islands and 105 kPa islands with no change in regards to patterned island elasticity as shown in Figure 4.5A and Figure 4.5B. 7 kPa island elasticity cell area averages were 1184.37 ± 223.84 μm^2 while 105 kPa island cell areas were 1175.46 μm^2 ± 265.79 μm^2. Integrins and focal adhesions are the binding point of cells to the ECM and our results confirm that this tension sensing occurs through this RhoA signaling pathway [180, 184, 216]. Focal adhesions transmit force to the actin cytoskeleton causing it to remodel according to physical cues and it is able to alter cell size and shape as seen in the schematic in Figure 4.6. Thus, ROCK inhibited cells were confirmed to lose the ability to sense matrix elasticity when myosin contractions were suppressed demonstrating the background elasticity is unimportant and confirms that RhoA plays a prominent role in sensing matrix stiffness.

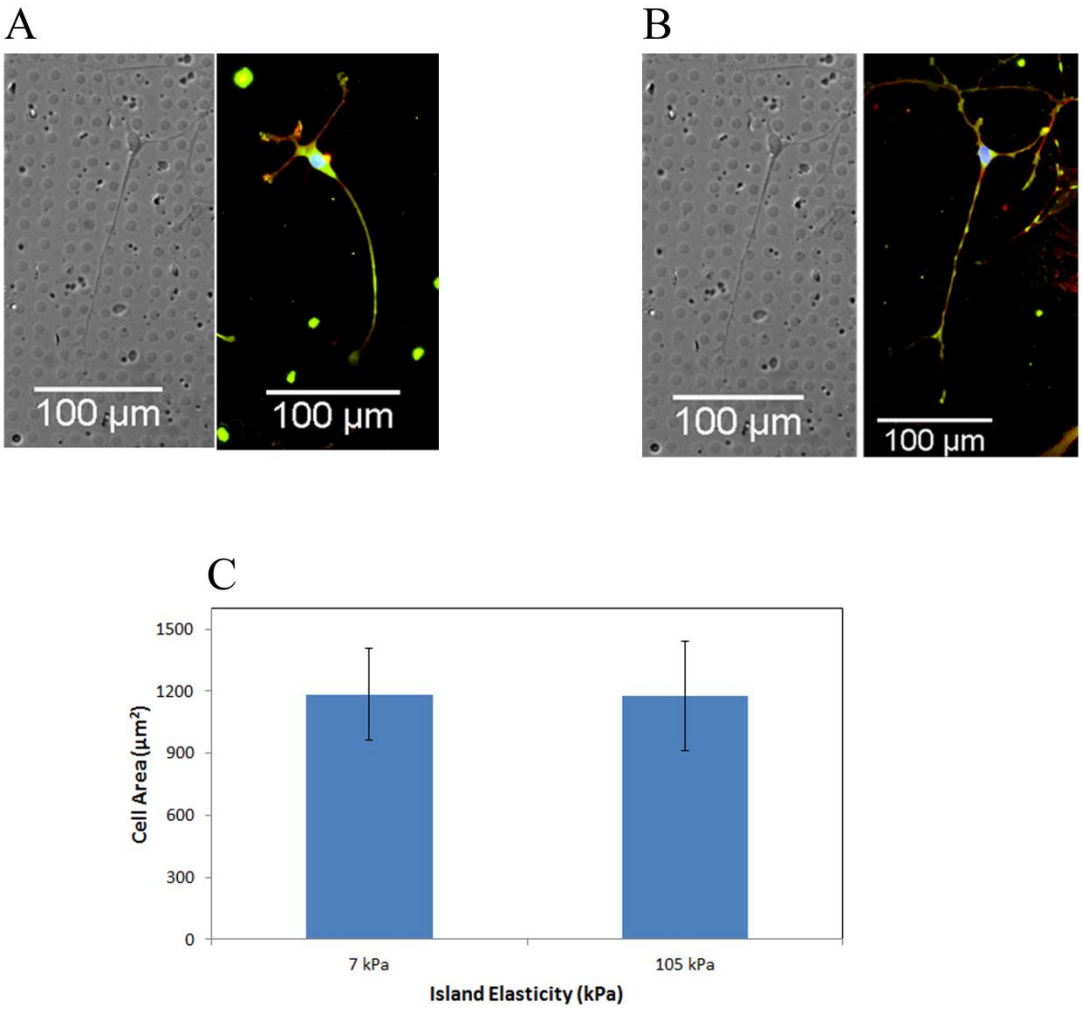

Figure 4.5: ROCK inhibited cells lose ability to sense matrix conditions. Cells were treated for 7 days, which prevented cells from sensing matrix conditions and spreading as was previously found. (A) ROCK inhibited cell on pattern of 7 kPa PEG, 2.5 MPa background elasticity, 7 µm spacing, and 50 µg ml^{-1} ligand density with brightfield image and vinculin, F-actin, and nucleus staining merged image. Average cell area for this ROCK inhibited trial was 1184.37 μm^2 ± 223.84 μm^2. (B) ROCK inhibited cell on pattern of 105 kPa PEG, 2.5 MPa background elasticity, 7 µm spacing, and 50 µg ml^{-1} ligand density with brightfield image and vinculin, F-actin, and nucleus staining merged image. Average cell area for this ROCK inhibited trial was 1175.46 μm^2 ± 265.79 μm^2. Error bars are standard error of over 10 cells quantified per condition.

4.13 Conclusions

In summary, our experimental and modeling findings showed matrix elasticity to be the key regulator of hMSC adhesion on surfaces with independently tunable physical and chemical properties. Cell spreading area was predominantly controlled by matrix elasticity with soft matrices showing smaller cells and stiff matrices showing large cells. Our modeling component was able to show a high degree of correlation between cell spreading and island deflection showing how softer hydrogel islands lead to reduced cell spreading and thus confirming our experimental data. In controlling the ECM characteristics and parsing cooperative signaling pathways, we hope to gain a better understanding of the interactions between cell-ECM interactions and further cell behavior such as lineage commitment. By combining a modeling and experimental component we can gain further understanding and confidently utilize finite element modeling as a predictive tool in analyzing cell function and behavior. This will potentially have great implications in the field of stem cell engineering and regenerative medicine such as optimizing the characteristics of scaffolds and inducing homogenous populations of lineage committed cells.

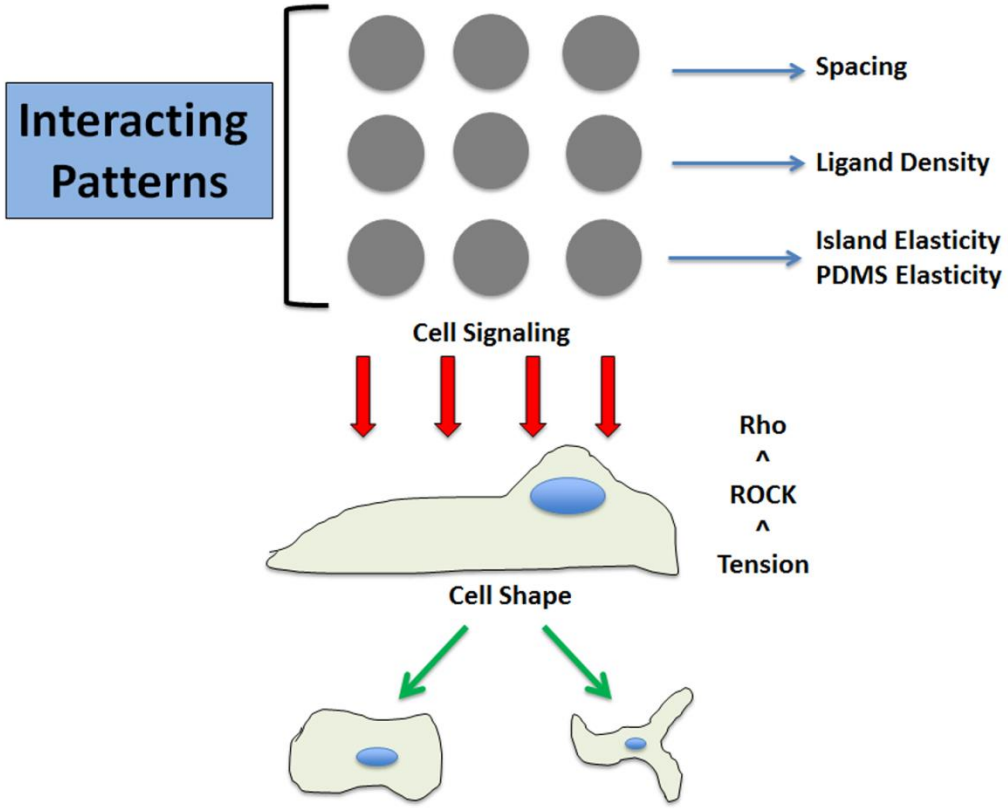

Figure 4.6: Schematic of mechanical decision made in hMSC commitment. Mechanical cues coordinate to drive hMSC cell shape with RhoA signaling. Interference with cytoskeletal tension disrupts this decision showing the RhoA-ROCK pathway appears critical in adhesion properties of hMSCs.

CHAPTER 5: Deconstructing the Effects of Matrix Elasticity and Geometry in Mesenchymal Stem Cell Lineage Commitment

5.1 Introduction

The field of regenerative medicine, stem cells in particular, has become increasingly important with scientists and medical personnel due to their potential to restore or replace injured tissue and organs [1, 3, 5, 77, 217]. The use of MSCs as a therapy option has been progressively more promising in scientific fields by possessing the ability to differentiate into bone cells (osteoblasts), cartilage cells (chondrocytes), and fat cells (adipocytes) among other potential lineages [218, 219]. MSCs may potentially demonstrate to be vital to tissue engineering bone replacements as the need for bone tissue repair in patients suffering from critical bone defects continues to rise [3, 220-223]. Complex combinations of physical, chemical, and biological signals are used to direct stem cell fate and control the natural healing of bone and other tissues *in vivo* [74, 77, 79, 224]. In order to fully elucidate these healing and regeneration principles, we must first understand the complexity of the underlying cellular and biomolecular factors that promote each tissue. To be fully realized as a potential treatment option, numerous cellular responses to microenvironmental cues as well as directed differentiation capacity of these stem cells need to be addressed. A significant challenge facing researchers is the ability to differentiate a stem cell into a certain programmed lineage. In particular, physical and geometric cues have emerged as significant factors in directing stem cell behavior [18, 49, 52, 53, 225].

Physical signals derived from the stem cell microenvironment have been established as increasingly important to the lineage commitment of stem cells [18-20, 41, 52]. These signals were previously recognized as far back as the 1940s with tensile stresses leading to bone formation and compressive stresses leading to cartilage formation in cultured chick rudiments [51]. Further work has been aided with the implementation of microscale technologies to mimic the stem cell microenvironment *in vitro* [226, 227]. These microscale experiments have shown the critical importance of the cell microenvironment to cell behaviors such as apoptosis, migration, and differentiation [52, 225, 228]. In a recent key study, the importance of matrix elasticity has been presented by culturing MSCs on gels of differing elasticity with soft gels (<1 kPa) promoting neurogenic differentiation, intermediate gels (~12 kPa) promoting myocytes, and stiff gels (>25 kPa) promoting osteoblasts [18]. Other studies also showcase the importance of cell geometry on the lineage specification of stem cells with differing densities of cells promoting differing cell lineages as well as micropatterned shapes confirming these findings [19, 225]. These studies both found increasing levels of GTPase RhoA and downstream effectors promoting osteogenesis with lower levels of RhoA signaling being a signal for adipogenesis and neurogenesis. Within these studies it is clear that RhoA and the corresponding actomyosin contractions play a role in the lineage specifications of these stem cells, and thus a correlation between physical signals determining fate. Yet little is known about the cooperative interplay between these types of physical signaling. Therefore, there is a clear need for research determining the interplay between matrix elasticity and cell shape and how this ultimately effects cell lineage specification.

In this work, we present a novel method to decouple multiple physical signals including substrate elasticity, cell shape, and cell size in determining MSC lineage commitment as shown in Figure 5.1. This strategy uses micropatterned PEG hydrogels to vary the elasticity, size, and shape of adhesive area presented to cells cultured in a mixture of adipogenic and osteogenic differentiation medium to direct cell fate. By regulating the physical signals presented, we show that 1,000 μm^2 areas promote adipogenic differentiation regardless of shape and elasticity while 2,500 and 5,000 μm^2 areas are more heavily dependent on shape and elasticity in cell fate commitment. The importance of cytoskeletal tension on patterned areas in MSC differentiation was especially prevalent when cells were treated with Y-27632 and nocodazole and primarily committed to adipocyte and osteoblast lineage respectively. This work is able to further establish the cooperative roles presented through physical signaling due to elasticity and cell shape that are able to promote MSC fate commitment.

5.2 Substrate Preparation

Glass coverslips (22x22 mm, Fisher Scientific) were washed with 70% ethanol and ozone treated (BioforceNano, Ames, IA) for 30 minutes to remove surface contaminants. Cover slips were then sputter coated with a 5 nm titanium adhesion layer (Denton Desk II Turbo, Moorestown, NJ) onto PDMS followed by approximately 40 nm

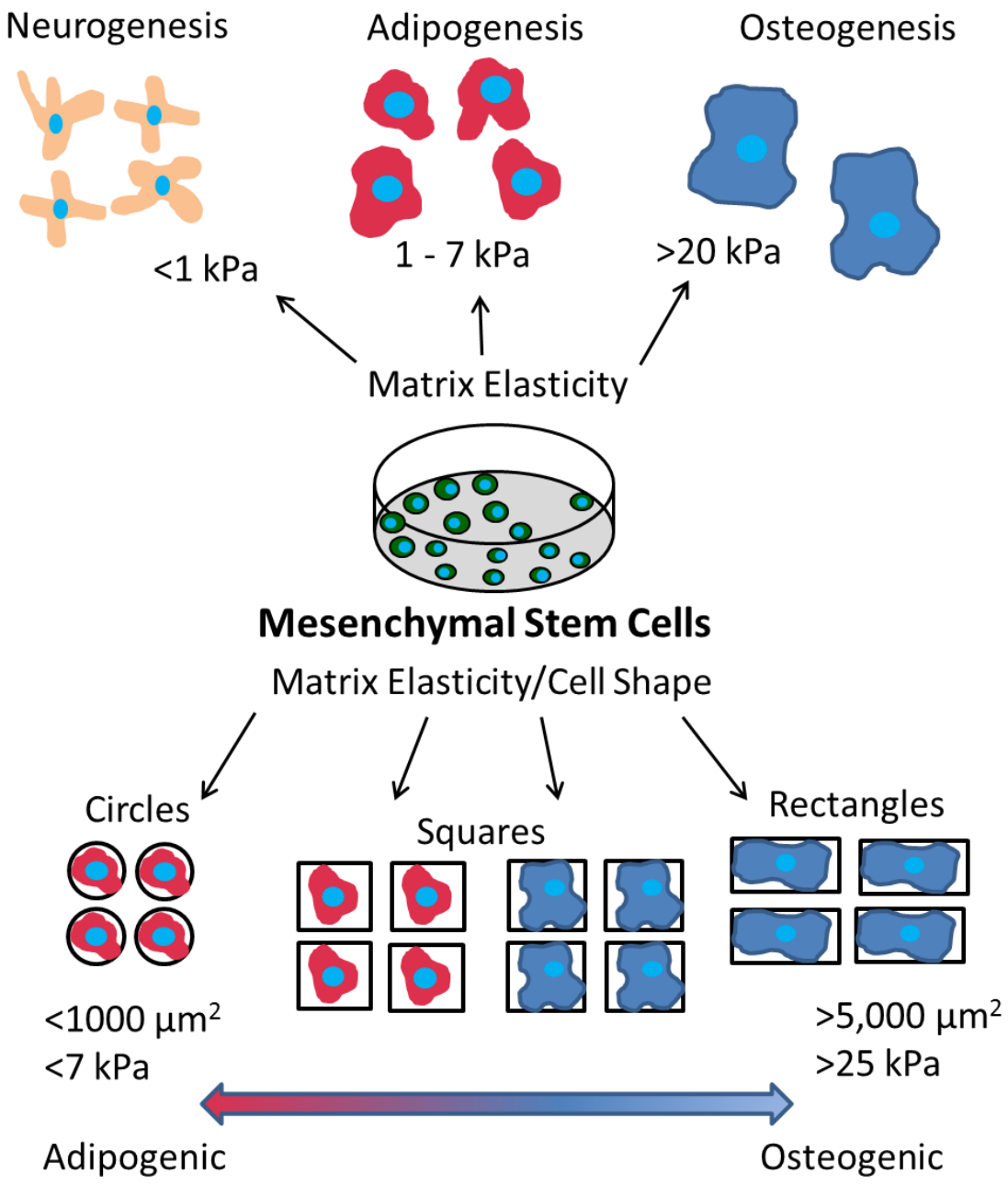

Figure 5.1: Schematic of the methodology to determine the cooperative effects of cell shape, cell size, and matrix elasticity on the lineage commitment of mesenchymal stem cells.

of gold (Denton Desk II, Moorestown, NJ). Coverslips were then stored at room temperature until use.

5.3 Micropatterning Hydrogels

PEG precursor solution was assembled using 700 MW PEG diacrylate (PEG-DA) (Aldrich, Milwaukee, WI) mixed with 2000 MW 4-arm PEG thiol (PEG-SH)(CreativePEGWorks, Raleigh, NC) in H_2O using 0.5% (v/v) 2-hydroxy-2-methylpropiophenone (Aldrich,Milwaukee, WI). Photomasks were produced using AutoCAD software (AutoDesk, San Rafael, CA) and printed on transparencies (CAD/Art Services, Inc, Bandon, OR). PEG precursor was placed onto cover slip, covered with photomask, and placed under approximately 4 mW/cm^2 Blak Ray UV light (UVP, Upland, CA) to polymerize. The patterned cover slip was then incubated in 50 mM triethylene glycol mono-mercaptoundecyl ether (Aldrich, Allentown, PA) for 20 minutes to render unpatterned surfaces non-adhesive to proteins and rinsed with 70% ethanol and subsequently sterile PBS three times. Fibronectin (Sigma, St. Louis, MO) was treated with a heterogenous maleimide/N-hydroxysuccinimide bi-functional linker (Thermo Fisher, Rockford, IL) [206] to allow functionalization of protein in order to attach to PEG patterns. Fibronectin was incubated at room temperature for 1 hour then separated from unreacted crosslinker using a Zeba Spin desalting column (Thermo Fisher, Rockford, IL). PEG patterns were then incubated in functionalized proteins at room temperature for 4 hours and 4°C overnight to allow covalent attachment of proteins to hydrogels. Hydrogel patterns were visualized and characterized by brightfield and fluorescent microscopy to confirm attachment.

5.4 Hydrogel Characterization

PEG hydrogel samples were created 5 mm in diameter and 3 mm height at desired ratio and let soak in deionized water for 48 hours at 37°C. Samples were tested in unconfined compression [209-212], in short, the Young's modulus of each sample was determined using an ElectroForce 3200 (Bose, Eden Prairie, MN) in unconfined compression at 0.05 mm/sec between parallel nonporous plates while compressive force and displacement were recorded.

5.5 Cell Culture

Human bone marrow-derived mesenchymal stem cells were obtained from Lonza (Walkersville, MD). hMSCs were cultured in basal growth media (Lonza, Walkersville, NC) in culture flasks. The growth medium contained 440 mL of hMSC basal medium, 50 mL of mesenchymal cell growth supplement, 10 mL of 200 mM L-glutamine, and 0.5 mL of a penicillin/streptomycin mixture. The cells were passaged after reaching 90% confluence and collected with 0.05% trypsin/EDTA solution. All cells were plated onto substrates under passage 6 and plated at 5,000 cells/cm^2. Cells were allowed 1 day for adhesion onto substrate before being placed in mixed medium which consisted of a 1:1 ratio of adipogenic to osteogenic medium. Adipogenic medium contained 444 mL of DMEM (Invitrogen), 50 mL fetal bovine serum (FBS)(Atlas), 0.5 mL of 1 µM dexamethasone, 0.5 mL of 10 µM insulin (Sigma), 200 µM indomethacin (Sigma), 0.5 mM isobutyl-methylxanthine (Sigma), and 5 mL penicillin/streptomycin. Osteogenic medium consisted of 444 mL DMEM F/12 (Invitrogen), 50 mL FBS, 10 mM β-glycerophosphate, 50 µg/ml ascorbic acid (Sigma), 1 µM dexamethasone (Sigma), and 5

ml penicillin/streptomycin. For ROCK inhibited cells differentiation medium was changed daily and 2 μM Y-27632 (Calbiochem, Rockaway, NJ) was added. For nocodazole treated cells differentiation medium was changed daily and 1 μM nocodazole (Sigma) was added.

5.6 Immunofluorescent Staining and Histology

Cells were fixed with 4% paraformaldehyde, permeabilized with 0.2% Triton X-100, and blocked with 1% BSA solution. The cytoskeleton, focal adhesions, and nuclei of cells were stained with a rhodamine-phalloidin conjugate (Invitrogen, Grand Island, NY), vinculin (Sigma, St. Louis, MO), and Fluoroshield with DAPI (Sigma, St. Louis, MO) respectively. Fluorescent photographs of the stained hMSCs were captured by a Nikkon Eclipse 80i microscope with CoolSnap HQ camera. Non-fluorescent cells were analyzed using phase contrast microscopy utilizing NIS-Elements-AR 3.2 64 bit software (NIS-Elements, Melville, NY). Fate specified cells were analyzed using dual alkaline phosphatase [19, 229] and Oil Red O staining [167, 230] for osteogenesis and adipogenesis using a Nikon Eclipse E600 microscope (Nikon, Melville, NY) with color camera. Cells containing lipid vacuoles stained red were counted as adipocyte specification while cells staining deep blue/purple were counted as osteoblast specification. Rare cells that exhibited both lipid vacuoles and osteoblast staining were not counted. Tiff images were taken of patterned areas and cells were counted individually.

5.7 Statistics

P-value was calculated using the student t-test function in Excel (Microsoft, Seattle, WA). Errors are standard error of the mean.

5.8 Effect of Soluble Factors, Cell Density, and Matrix Elasticity on MSC Differentiation

Trials to assess the differentiation capacity of MSCs to both adipogenic and osteogenic lineage were first run with lineage specific medium and soluble cues for 7 days. In strictly adipogenic medium, we observed 80.3% and 81.9% adipogenic differentiation with 5,000 cells/cm^2 and 25,000 cells/cm^2 compared to 100% and 80.9% osteogenic differentiation in osteogenic medium (Figure 5.2). Further evaluations were done using MSCs in a 1:1 mixture of adipogenic and osteogenic medium for 7 days on unpatterned substrates. As previously shown [19, 76], we confirmed cell density contributed to lineage commitment when looking at the differentiation of MSCs at a density of 5,000 cells/cm^2 and 25,000 cells/cm^2. Our findings show that on glass coverslips, cells continued to show 100% osteogenic differentiation with 5,000 cm^2 density while only 40.6% osteogenic differentiation with 25,000 cells/cm^2. We then coated coverslips with 10% PEG (~7 kPa) and found the softer substrate contributed to 40.4% greater adipogenic differentiation in low plating densities and similar adipogenic differentiation in higher plating densities (Figure 5.2). These results compare similarly

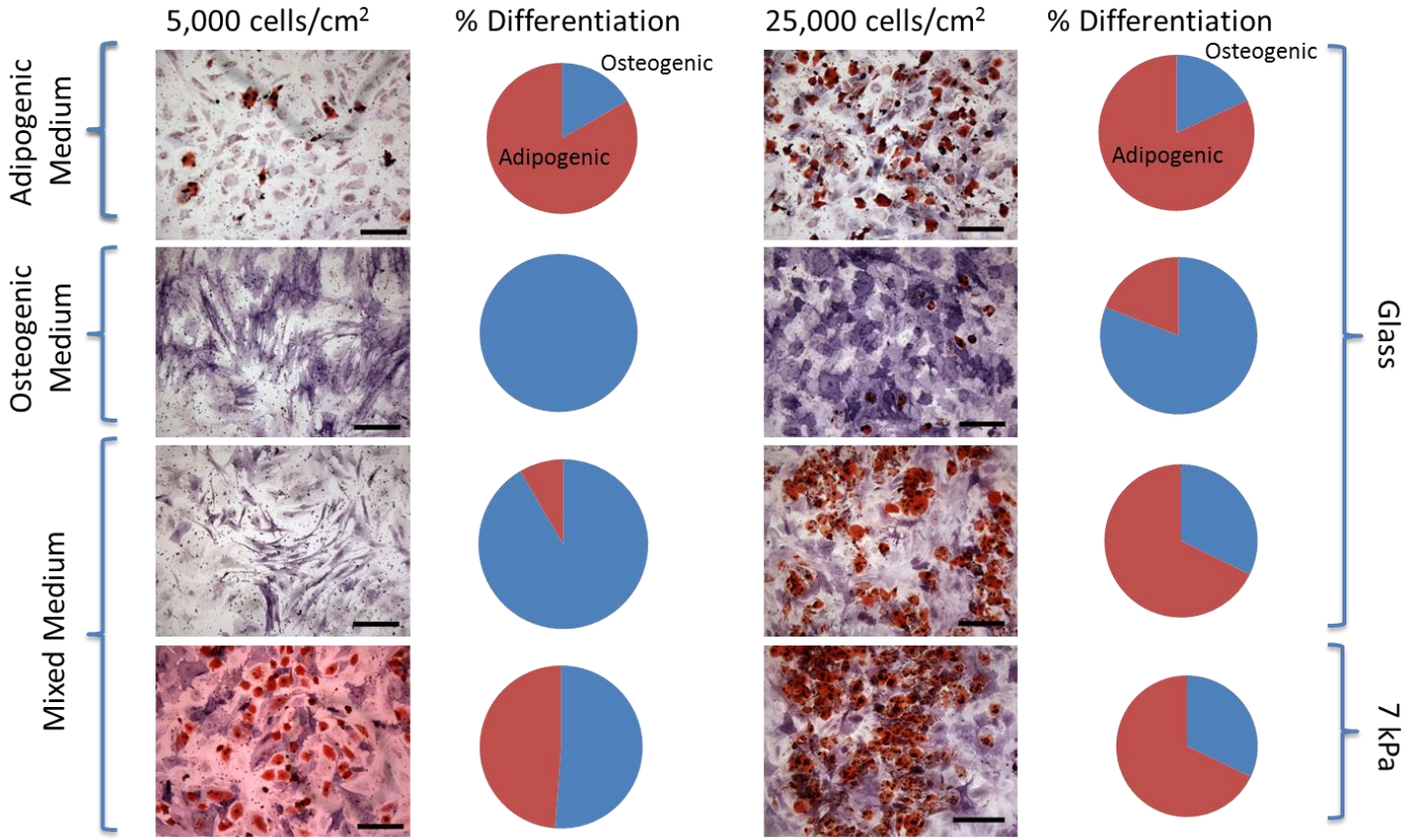

Figure 5.2: MSCs showed multilineage capabilities when cultured in medium containing growth factors promoting osteogenesis and adipogenesis. Dual staining of MSCs after 1 week for osteogenesis (alkaline phosphatase-purple/blue) and adipogenesis (lipids-red). Each line of images and graphs represents a differing culture condition with both 5,000 cells/cm^2 and 25,000 cells/cm^2. Pie charts show the percentage of differentiation to each lineage (red-adipocyte, blue-osteoblast).

to previous studies using differing cell densities and show the effects of cell density and substrate stiffness on the differentiation potential of MSCs in mixed medium. As cell density increases, cell adhesion and spreading are decreased and cell-cell contact is increased which leads to enhanced signaling between cells. This aspect has been confirmed by several studies to control cell behavior [19, 231] and we further show that substrate elasticity along with cell density can control lineage commitment of MSCs. To address the interplay between cell size, shape, and substrate elasticity remaining experiments were conducted using patterned cells cultured in mixed media conditions.

5.9 Micropatterning and Adhesion of Mesenchymal Stem Cells

UV lithography techniques were used to restrict the shape of individual cells into circles, squares, and rectangles onto coverslips (Figure 5.3). A photomask was utilized to control size and shape of the islands with a mixture of PEG-SH and PEG-DA used as the precursor solution for the hydrogels. UV light was employed to selectively crosslink hydrogels into circles, squares, and rectangles on a gold coated glass coverslip through the photomask (Figure 5.4 A-C). The remaining regions of the coverslip were then rendered non-adhesive with a tri(ethylene glycol)-terminated monolayer to prevent non-specific binding of protein or cells. Patterns were incubated in maleimide-modified fibronectin solution to absorb protein exclusively to hydrogel islands to allow cell attachment as seen in Figure 5.4 D and E. MSCs were then able to attach to the hydrogel islands and spread to assume distinct shapes of the underlying islands (Figure 5.4 F-I). Cells were able to attach and spread on patterns while remaining viable and constrained

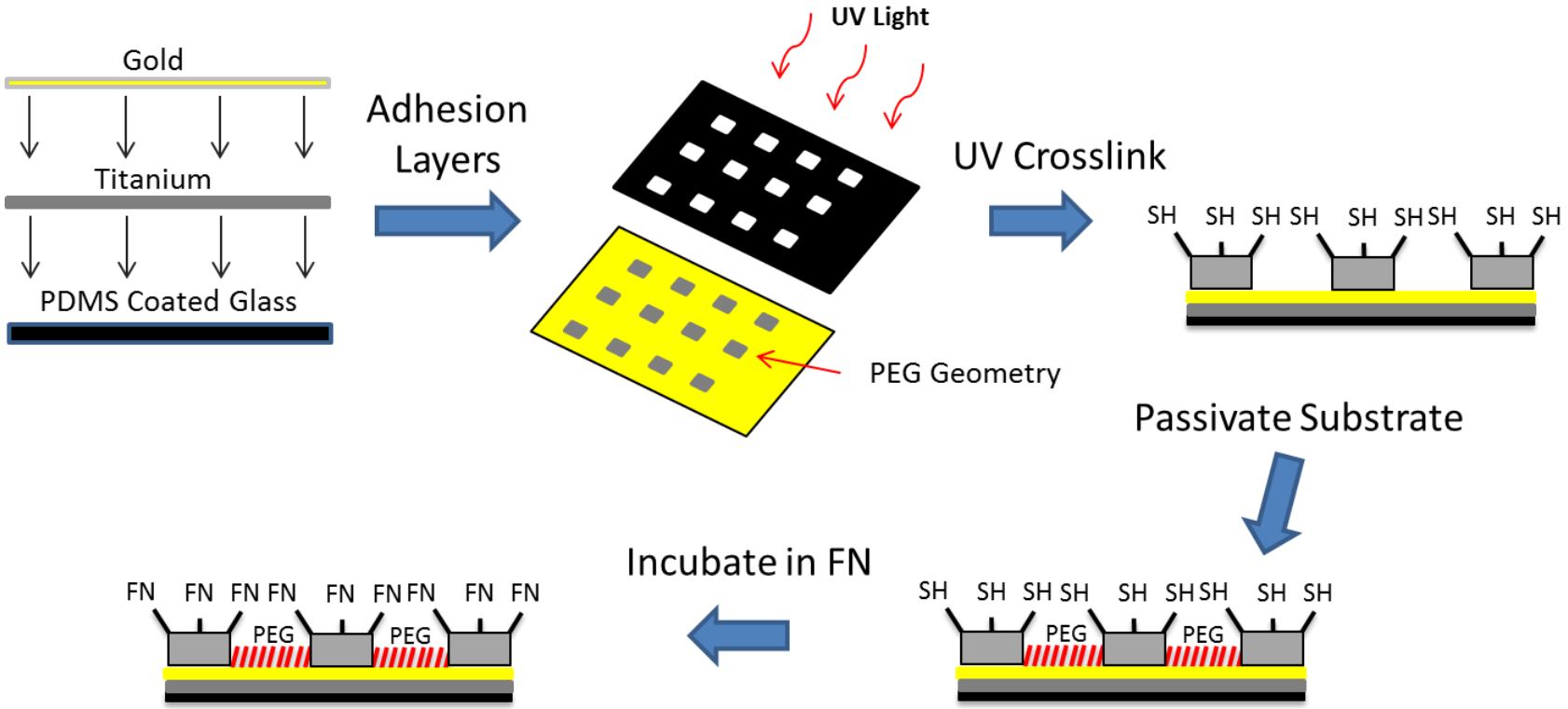

Figure 5.3: Schematic showing UV lithography process used to create hydrogel shapes of varying elasticity. Hydrogel shapes were functionalized with thiol to promote fibronectin binding exclusively to hydrogels.

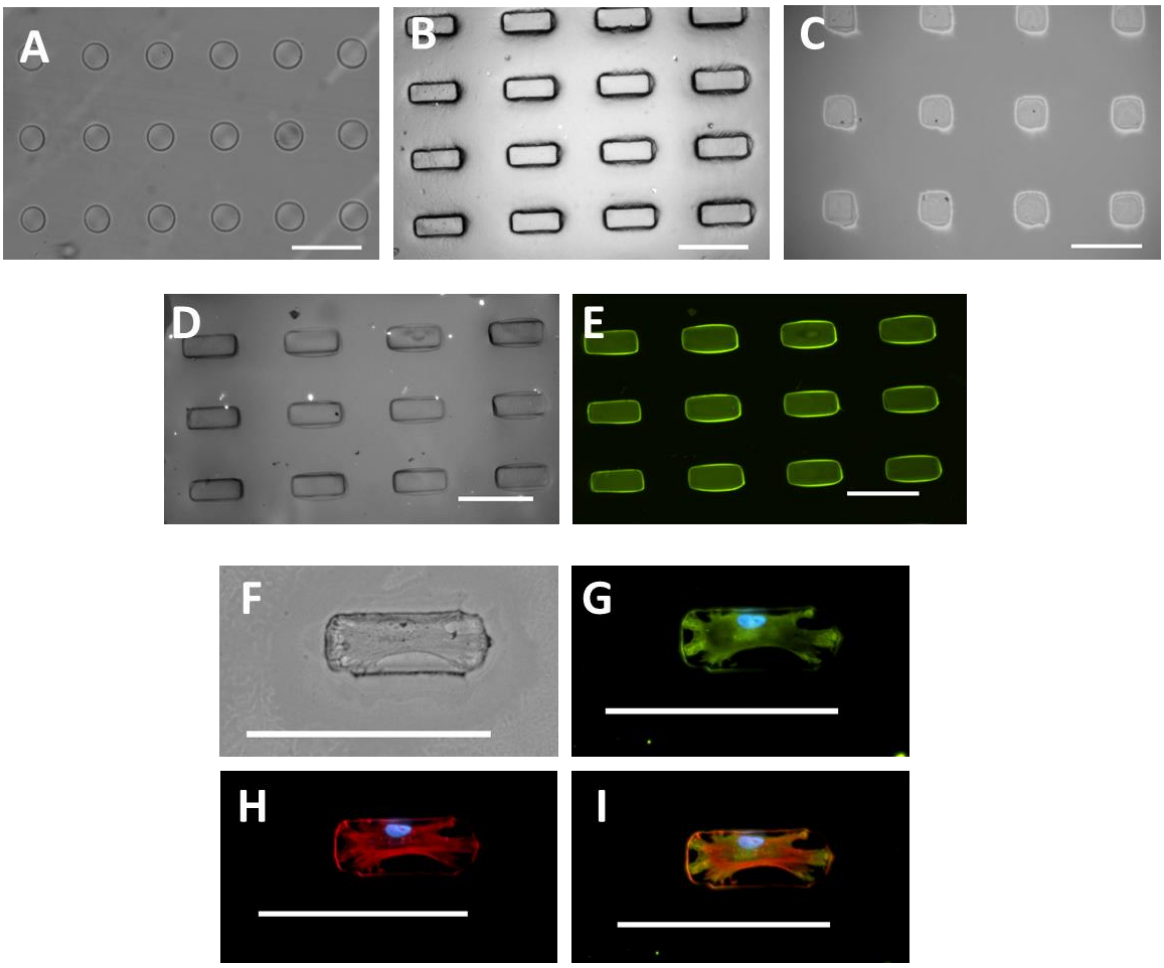

Figure 5.4: Hydrogel islands were fabricated with protein exclusively attached to islands facilitating cell adhesion. Presented are microscopy images with micropatterned shapes showing (A) 5,000 μm^2 circles (B) 5,000 μm^2 rectangles and (C) 5,000 μm^2 squares. Fluorescent bovine serum albumin was used as a model protein to determine protein attachment to micropatterned areas with (D) brightfield microscopy image of 5,000 μm^2 rectangles and (E) bovine serum albumin exclusively attached to hydrogel rectangles. MSC attachment shown with (F) brightfield microscopy and immunofluorescence stained for (G) vinculin to reveal focal adhesions, (H) F-actin, and (I) merged image.

to hydrogel islands for one week in culture to determine the effects of size, shape and elasticity on differentiation. MSCs were plated onto hydrogel islands using MSC growth medium initially, switched to a 50:50 mixture of adipogenic and osteogenic differentiation media, and cultured for 7 days. Cells were then analyzed by staining for lineage specific markers Oil Red O and alkaline phosphatase for adipogenic and osteogenic differentiation respectively.

5.10 MSC Differentiation Directed by Shape, Size, and Matrix Elasticity

MSCs were confined to 1,000, 2,500, and 5,000 μm^2 area circle, square, and rectangular patterns with a substrate elasticity of 7, 47, and 105 kPa. This range of geometric features was considered to promote both adipogenic and osteogenic lineages with circles, squares, and rectangles previously shown capable of directing cell behavior and differentiation (Figure 5.5 and 5.6) [53, 225]. Substrate elasticity was also considered and values were chosen to promote multiple lineages and cell behavior [18, 20] in order to parse differences in physical effects on cell differentiation.

For 1,000 μm^2 islands, we observed primarily adipogenic differentiation in all cases of elasticity and shape. This is consistent with previously reported micropatterning studies as well as matrix elasticity studies observing cell size to be a regulator of lineage commitment [19, 203, 225]. When looking at cells on 2,500 and 5,000 μm^2 patterns with different shape and elasticity we found a more mixed population of adipocytes and osteoblasts (Figure 5.5). With 5,000 μm^2 shapes we found at higher elasticity the cells behaved similar to glass with 74%, 73%, and 52% osteogenic differentiation on rectangles, squares, and circles respectively (Figure 5.5B). When switched to 7 kPa

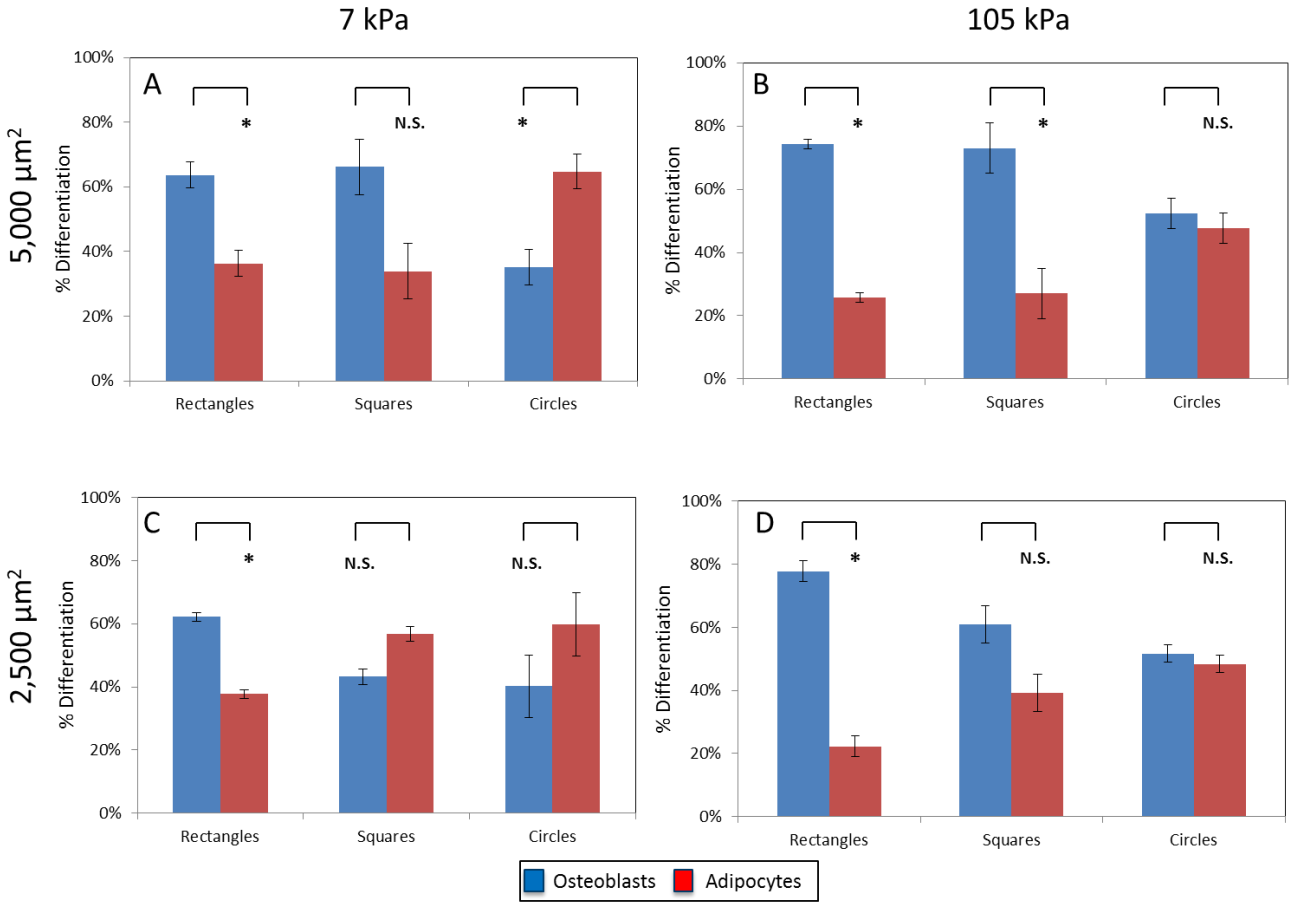

Figure 5.5: By modifying the geometry and matrix elasticity of the underlying patterns, cells were able to choose lineage commitment based on the physical cues presented. (A)-(D) Shown in these graphs are the effect of shape, size, and matrix elasticity on MSC lineage commitment. Error bars are standard error from at minimum 2 separate experiments with over 75 cells per condition.

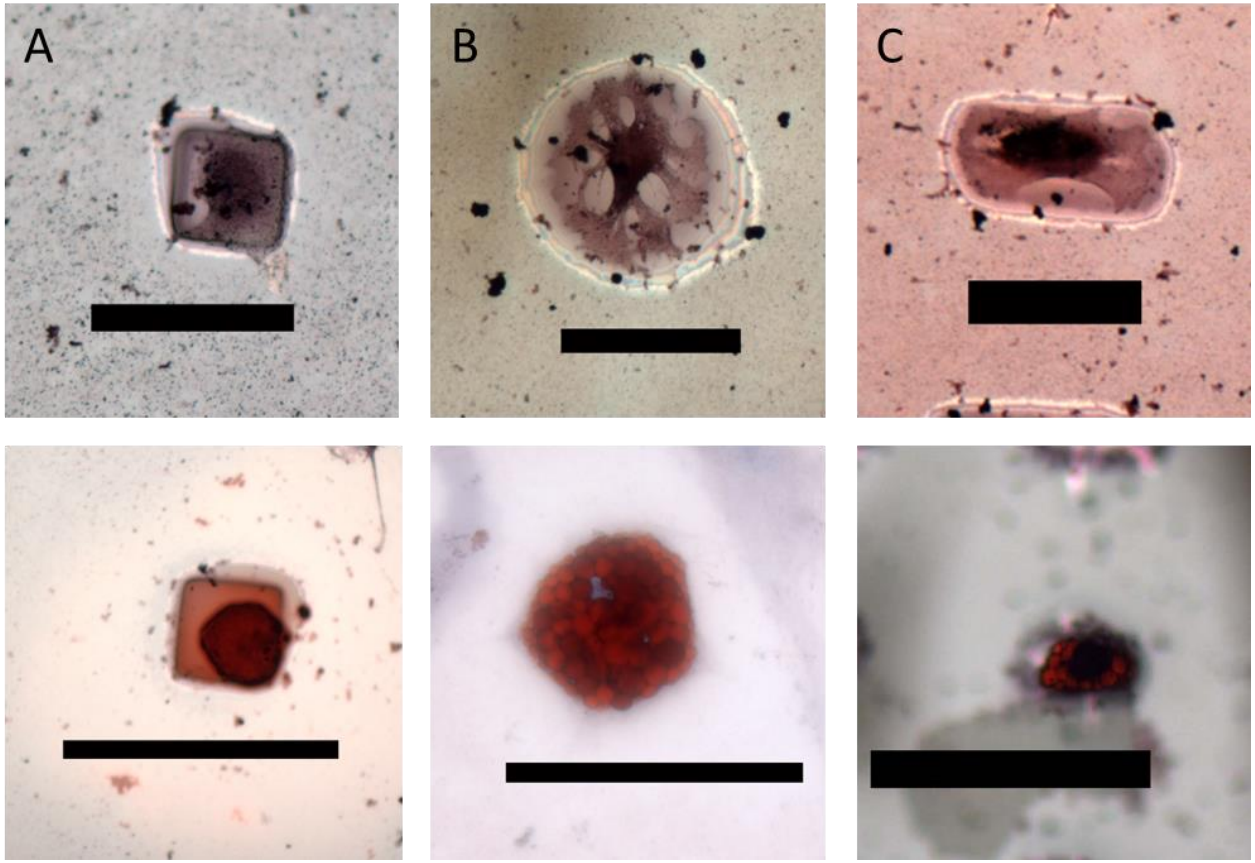

Figure 5.6: MSCs are able to decipher microenvironmental physical signals in order to specify lineage commitment. (A)-(C) Shown are patterns with MSCs commited to osteogenic (top, purple) and adipogenic (bottom, red) fate on squares, circles, and rectangles respectively. Scale bars are 50 μm.

hydrogels, osteogenic differentiation decreased to 61%, 66%, and 35% on these identical shapes (Figure 5A). When switching to 2,500 μm^2 shapes, we saw a much higher variation in lineage commitment with 78%, 61%, and 52% osteogenesis on 105 kPa substrates and 62%, 43%, and 40% osteogenesis on 7 kPa substrates (Figure 5C-D). We also found that our 47 kPa matrix elasticity had similar values to the 105 kPa experiments for each shape excluding the 53% and 52% osteogenic differentiation for rectangles and squares on 2,500 μm^2 patterns (data not shown).

These results remain consistent when looking at patterning studies showing both cell shape and size to be a factor in osteogenic differentiation [19, 167, 225, 232-234] as well as other groups showing the role of matrix elasticity in osteogenic differentiation [18, 41, 235-237]. These studies have further shown that higher levels of RhoA lead to a higher degree of cell spreading and osteogenesis of MSCs [19, 202, 238, 239] on micropatterned surfaces along with similar RhoA pathways being responsible for enhanced cytoskeletal tension and osteogensis on stiffer extracellular matrices [18]. Our studies are able to highlight these cooperative signaling effects from both matrix elasticity and cell shape on the lineage commitment of MSCs. Our interpretation shows that cell size was responsible for lineage commitment choices at 1,000 μm^2 in all cases regardless of matrix elasticity or shape. At larger cell sizes cell shape and matrix elasticity both played a role in the lineage commitment of MSCs with cell shape appearing to play the larger role. As to shape, in all cases rectangles were shown to have higher osteogenesis when compared with circles, showing the immense importance of curvature and cytoskeletal tension in lineage commitment. It is particularly interesting that cell shape seemed to be a more governing physical cue than matrix elasticity, but has

been a theme of recent articles highlighting elasticity and shape as intertwined [18, 41, 240]. This study implies that by controlling cell shape initially and thus RhoA signaling, it is able to lessen the effects of matrix elasticity on lineage commitment

5.11 MSC Differentiation Altered by Cytoskeletal Modifications

The following experiments further proceeded to characterize the differentiation of MSCs on patterns under cytoskeletal manipulation to observe how a contractile cytoskeleton directs cell behavior. The cytoskeleton has previously been shown to strongly guide cell adhesion and behavior on micropatterned geometric shapes [19, 52, 53, 55, 170, 225]. To further confirm our findings that cell spreading and cytoskeletal tension are primarily responsible for osteogenic differentiation in combination with substrate elasticity, we evaluated patterned cells in mixed medium with Y-27632 and nocodazole added, which are pharmacological agents designed to modify the cytoskeleton [172, 241-243]. Cells were plated onto 2,500 μm^2 square patterned surfaces with growth medium and inhibitors and mixed medium was added the following day to ensure cells complete spreading over patterns. Cells patterned on these 2,500 μm^2 squares with 47 kPa matrix elasticity without inhibitors were shown to have 52% osteogenic differentiation. In the presence of nocodazole, a microtubule depolymerizing agent shown to increase cell contractility [244], cells were shown to have 84% osteogenic differentiation. Y-27632, an agent that inhibits ROCK causing a decrease in cell contractility [245], was shown to have 69% adipogenesis on the same patterns (Figure

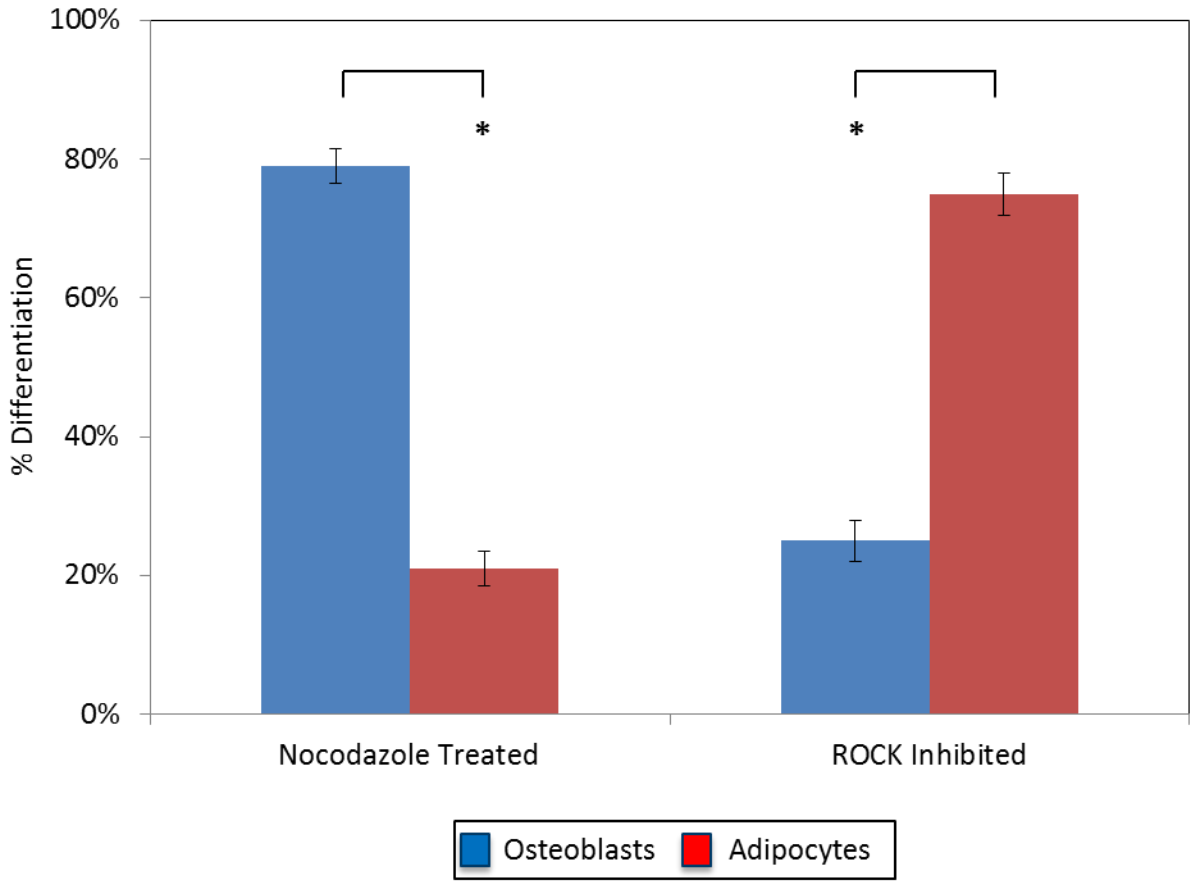

Figure 5.7: Graph showing the percentage of cells committing to adipogenic or osteogenic lineage in the presence of pharmacological agents on 2,500 μm^2 squares with a 47 kPa matrix elasticity.

5.7). These results further confirm that actomyosin contractility is a key regulator in the lineage commitment of MSCs. It is generally accepted that higher degrees of cell spreading promote increased myosin-generated cytoskeletal tension leading to increased levels of RhoA and ROCK [19, 225]. It has also been well noted that as matrix elasticity increases, RhoA and ROCK levels increase as well [18]. Therefore, by inhibiting or promoting ROCK, we observed that with constant matrix stiffness, shape, and size we could promote either osteogenic or adipogenic lineages confirming that ROCK signaling remains vital to lineage commitment when presenting cells with differing physical cues. This work further supports the immense importance of the cytoskeleton in looking at osteogenic differentiation in the presence of physical microenvironmental characteristics, and in our work, the presence of multiple conflicting physical characteristics.

5.12 Conclusions

Through the development of micropatterned hydrogels, we were able to ascertain the relationship between size, shape, and matrix elasticity for the first time in single MSC lineage commitment. UV lithography of PEG hydrogels was employed to provide a platform to study single MSCs in a manner capable of decoupling these physical signaling cues. This work has combined the ability to control cell size and spreading with the ability to adjust matrix elasticity to regulate stem cell lineage commitment and demonstrated that the size, shape, and matrix elasticity possess the ability to use physical characteristics to tune differentiation. The physical signals were critical to lineage commitment with cell size proving to be most significant to lineage commitment at lower adhesive areas and shape being most significant at larger adhesive areas. The use of

single cells to determine lineage commitment parameters of stem cells is has become paramount to engineering homogenous populations of stem cells for use in tissue engineering. Our study is one of the first to be able to present tools and insight into combining these physical characteristics directing stem cell lineage commitment for possible use in designing materials and scaffolds for future regenerative medicine.

CHAPTER 6

Patterning Pluripotent Stem Cells at a Single Cell Level[1]

[1]Pryzhkova, M.V.; Harris, G.M.; Ma, S.; and Jabbarzadeh, E. 2013. Journal of Biomaterials and Tissue Engineering. 3: 461-471.

6.1 Introduction

At present, dip pen nanolithography, microcontact printing, and direct photo-patterning using UV light or laser to deposit adhesive proteins in a desired manner are attractive options for cell biologists to study molecular processes and cell-material interactions at a single cell level [169]. Features designed by these methods can be sized as low as the nanometer scale and generally are produced on glass utilizing self-assembling monolayers as a method for protein adsorption. Random studies of surface functionalization with UV/ozone of polymers such as polyethylene and polyvinyl chloride (PVC) were also reported [246, 247]. Polystyrene (PS) is traditionally used for cell culture applications, where plasma treatment with similar effect is used to make commercially available plastic more hydrophilic to promote cell attachment [248, 249]. A few research groups have applied direct UV/ozone micropatterning of polystyrene for cell studies. These methods are very simple, cost effective and can produce features down to 1 μm.

To date, micropatterning is used to study internal cell organization, cell division, migration, or simply to control cell outgrowth [105, 169]. While cells from established cell lines and adult stem cells, such as human mesenchymal stem cells (hMSCs), are widely used in research, studies of pluripotent stem cells involving micropatterns are under development. This can be partially explained by the properties of pluripotent cells such as growth in colonies, on supporting feeder layers, and the necessary extra-cellular matrix (ECM) [96, 108]. Recent studies have reported the possibility to grow cells in a monolayer culture or in colonies with single cell passaging through the use of ROCK inhibitor to eliminate cell apoptosis during single cell dissociation, which suggests that

human pluripotent stem cells (hPSC) could also be plated on micropatterns for single cell studies. hPSCs are cultured on Matrigel, which is formed by polymerization of a few constitutive proteins and heparan sulphate, thus, making it complicated for micropatterning [104, 250]. However, it has been reported that hPSC express integrins mediating cell binding to vitronectin, which can replace Matrigel and support undifferentiated hPSCs growth in culture [251, 252]. Here we have designed a very simple, affordable, and quick protocol which allows the creation of vitronectin micropatterns with feature resolution down to 1 μm and can be used for single cell studies of different cell types including hPSCs (embryonic stem cells (hESC) and induced pluripotent stem cells (hiPSC)).

6.2 Mask Design and UV/Ozone Micropatterning of Polystyrene

Design and sketching of micropatterns was performed in AutoCAD Design Suite. Super high resolution chrome quartz photomasks (positive and negative), size 10 cm x 10 cm, were ordered from J.D. Photo-Tools, UK. Clear polystyrene sheets 0.3mm thick were from Plastruct (#SSM-101). Polystyrene sheets were cut to approximately 2 cm x 2 cm square coverslips to fit wells of six-well cell culture plates. Before UV/ozone patterning, polystyrene coverslips were disinfected for one hour in 70% ethanol (freshly prepared, Decon Labs) and washed once in sterile distilled water.

A UV/ozone ProCleaner (BioForce Nanosciences) was used for direct UV micropatterning. The UV lamp was preheated for 15-30 minutes before patterning. Quartz photomask was washed with isopropanol, dried under air flow and hydrophylized in UV/ozone ProCleaner with chrome side up for about 10-15 minutes. Polystyrene

coverslips were deposited on desired patterns with a 4μl drop of water to insure close contact with the chrome side of the mask. Polystyrene coverslips/quartz photomask sandwich (photomask up) was exposed for 2.5 minutes to UV light from the distance of about 3 cm from UV lamp. Coverslips were then removed from the mask by adding water around coverslips and allowing them to be lifted from the surface, thus, minimizing photomask damage. Samples were used for protein coating and cell plating immediately or analyzed by XPS within 1-2 hours.

6.3 XPS and Data Analysis

XPS measurements were conducted using a Kratos AXIS Ultra DLD XPS system equipped with a monochromatic Al Ka source. The binding energy is calibrated using an Ag foil with $Ag3d_{5/2}$ set at 368.21 ± 0.025 eV for the monochromatic Al X-ray source. The monochromatic Al Ka source was operated at 15 keV and 120 W. The pass energy was fixed at 80 eV for the detailed scans. A charge neutralizer (CN) was used to compensate for the surface charge. Each case was analyzed and peak fitted using Microsoft Excel. Then, data was normalized and plotted in the same program. The binding energy scale for C1s was set at 285 eV. Elemental surface compositions (atomic %) were calculated based on C1s and O1s detailed scan spectra.

Plastic used in these studies: 1) bacterial grade cell culture polystyrene, 10cm Petri dishes (Greiner, Cat. No. 663 161 or 664 161), tissue culture treated polystyrene, 6-well plates (BD, Cat. No.353046); 2) polyvinyl chloride (PVC) 22x22mm coverslips (Electron Microscopy Sciences, Cat. No.72261-22); 3) clear polystyrene sheets 0.3mm thick Plastruct (#SSM-101).

6.4 Cell Culture

hESC line H9 was purchased from WiCell (Wisconsin) and the two bone marrow derived hiPSC lines BM1M and BM9 were kindly provided by Dr. I. Slukvin (University of Wisconsin-Madison). HES3 line was gratefully provided by Dr. D. Elliott (Monash University). All cell lines were grown on mouse embryonic fibroblast (MEF) (CF-1, Millipore, #PMEF-CFL) feeder layer in DMEM/F12 (Invitrogen, #11330-057) with 20% KnockOut SR (Invitrogen, #10828-028), 0.1mM MEM Non-Essential Amino Acids (Invitrogen, #11140-050), 3.5mM L-Glutamine (final concentration) (Invitrogen, #25030-081), 100µm 2-Mercaptoethanol (Sigma, #M7522) and supplemented with 10ng/ml human recombinant bFGF (PeproTech, #100-18B) (also see WiCell Protocols). Medium was changed daily and cells were passaged on the fifth day of culture with collagenase type IV (Invitrogen, #17104-019).

MEF were grown in DMEM (Invitrogen, #11995-073) with 10% FBS (Invitrogen, #10438-026, or Atlas Biologicals, #F-0500-A) and 100U/100µg/ml of penicillin/streptomycin (Invitrogen, 15140-122).

hPSC monolayer culture with single cell passaging was established mainly as described. Briefly, hPSC were switched from feeder-dependent culture to feeder-free conditions and were grown as colonies for 2-3 passages on growth factor reduced Geltrex (1:400) (Invitrogen, Cat. No.12760-021) coated 6-well plates (BD, Cat. No.353046) in MEF conditioned medium supplemented with 10ng/ml hrbFGF. Cells were passaged mechanically on day five. Conditioned medium was prepared as described: MEF were mitotically inactivated with Mitomycin C (Sigma) at 10µg/ml for 2.5 hours and then plated onto gelatinized flasks (Gelatin, Sigma, #G-1890) at a density of 60,000 cells/cm^2.

The following day cells were washed with PBS (Sigma, #P3813) and medium was changed to hESC medium (without hrbFGF) in a quantity of 0.5 ml/cm^2 and collected every 24 hours for 7 days. Before culture with hPSCs conditioned medium was filtered and supplemented with 10 ng/ml hrbFGF. On the next passaging hPSC colonies were treated with TrypLE Select (Invitrogen, #12563-029) for 1 minute, gently dissociated to single cells and plated to new wells at an approximate density of 80-100,000 cells/cm^2. Cells were grown under the same culture conditions and single cell passaged upon reaching confluence. After stabilization of the cell culture cells were routinely passaged as single cells on each fourth day with seeding density 50,000 cells/cm^2. In second round of experiments after cell passaging with TrypLE Select (Invitrogen, #12563-029) to prevent cell apoptosis and chromosome changes during prolonged culture ROCK inhibitor Y-27632 (Calbiochem, #688000) was added in hPSC culture medium overnight at concentration 10μm. Cells were plated at density 20,000 cells/cm^2.

Bone marrow-derived hMSC were obtained from Lonza (PT-2501) and cultured in hMSC basal growth media (PT-3001 MSCGM BulletKit, Lonza).

6.5 Protein and Cell Deposition on Micropatterned Polystyrene

For hydrophobic surface protein coating UV/ozone patterned coverslips were incubated with 1μg/ml of human recombinant vitronectin (Sigma, #SRP3186) in DMEM/F12 (Invitrogen, #11330-057) for 30 minutes at RT, and further washed three times with DMEM/F12 again. Cells were deposited immediately. For hydrophilic patterns polystyrene coverslips were pretreated with 0.1% solution of BSA (Sigma, #A2153) in PBS (Invitrogen, #14040-141) for 15-20 minutes followed by incubation with

vitronectin as described above. To visualize micropatterns 1.5µg/ml of human fibrinogen Alexa Fluor 488-conjugated (Invitrogen, #F-13191) was added into DMEM/F12 together with 1µg/ml of human recombinant vitronectin, incubated, and washed as described above.

6.6 Karyotyping

Chromosome spreads were prepared by traditional G-banding technique and analyzed by KaryoLogic, Inc.

6.7 Immunocytochemistry

For immunostaining experiments cells were washed with PBS (Sigma, #P3813), fixed with 10% formalin (Sigma, #HT50-1-1) for 20 minutes at room temperature (RT), and permeabilized with 0.1% Triton-X 100 (Sigma, #T8787). To prevent non-specific antibody binding cells were incubated for 30 minutes at RT in 4% goat serum blocking solution (Sigma). Cells were then incubated with primary antibodies in blocking solution for 1 hour at RT, washed with Rinse Buffer (Tris-HCl + 0.05% Tween-20 (Sigma, #T5912, #P9416)), and incubated with secondary fluorochrome-conjugated antibodies, followed by Rhodamine Phalloidin-TRITC staining (Invitrogen, #R415) in PBS for 1 hour at RT and finally washing in Rinse Buffer. Antibodies used are: primary - OCT4 (Santa Cruz, sc-5279), SOX2 (Stemgent, 09-0024), Vinculin (Sigma, V9264), Vimentin (Santa Cruz, #sc-6260), secondary - IgG AF488 (Invitrogen, A31620), IgG AF594 (Invitrogen, A31624). Cells on glass coverslips (Electron Microscopy Sciences, #72230-01), PVC or polystyrene samples were mounted on glass slides (VWR, #16005-106) with

DAPI containing mounting solution (Sigma, #F6057). Samples were analyzed and images taken using either upright Nikon Eclipse 80i or inverted Nikon Eclipse Ti fluorescent microscopes with NIS-Elements imaging software.

6.8 Mask Design and Selection of Micropatterning Method

Mask and pattern design were created using AutoCAD Design Suite. Two identical, but inverted (positive and negative, to produce either hydrophobic or hydrophilic single cell patterns), photomasks were used for studies (Figure 6.1A). Based on our preliminary data on single hPSCs on Cytoo chips (www.cytoo.com), the majority of cells attached to medium (1100 μm^2) and large (1600 μm^2) sized fibronectin patterns (data not shown). Thus, two sizes of patterns (disk, crossbow, T, H, Y) were considered for further applications: #1 1256 μm^2 (disk d = 40 μm) and #2 1962.5 μm^2 (disk d = 50 μm). Pitch between micropatterns was 100 μm with pattern line width 6.6μm for #1 and 8.3 μm for #2. Single cell patterns were organized in six blocks (25x12) within 14 mm diameter circles to fit a well of 24-well plate. Total number of patterns per chip was 1800 (300/block) (Figure 6.1A), which proved sufficient to provide statistically adequate analysis with 50 - 100 cells to be analyzed [168]. Methods such as photolithography and laser/electron beam etching techniques among others require complex equipment and trained personnel to work with it. Thus, for daily-based experiments in a biological laboratory, traditional microcontact printing or UV-based chemistry would be the most facile [170]. Microcontact printing consisting of mold preparation, PDMS stamping, and

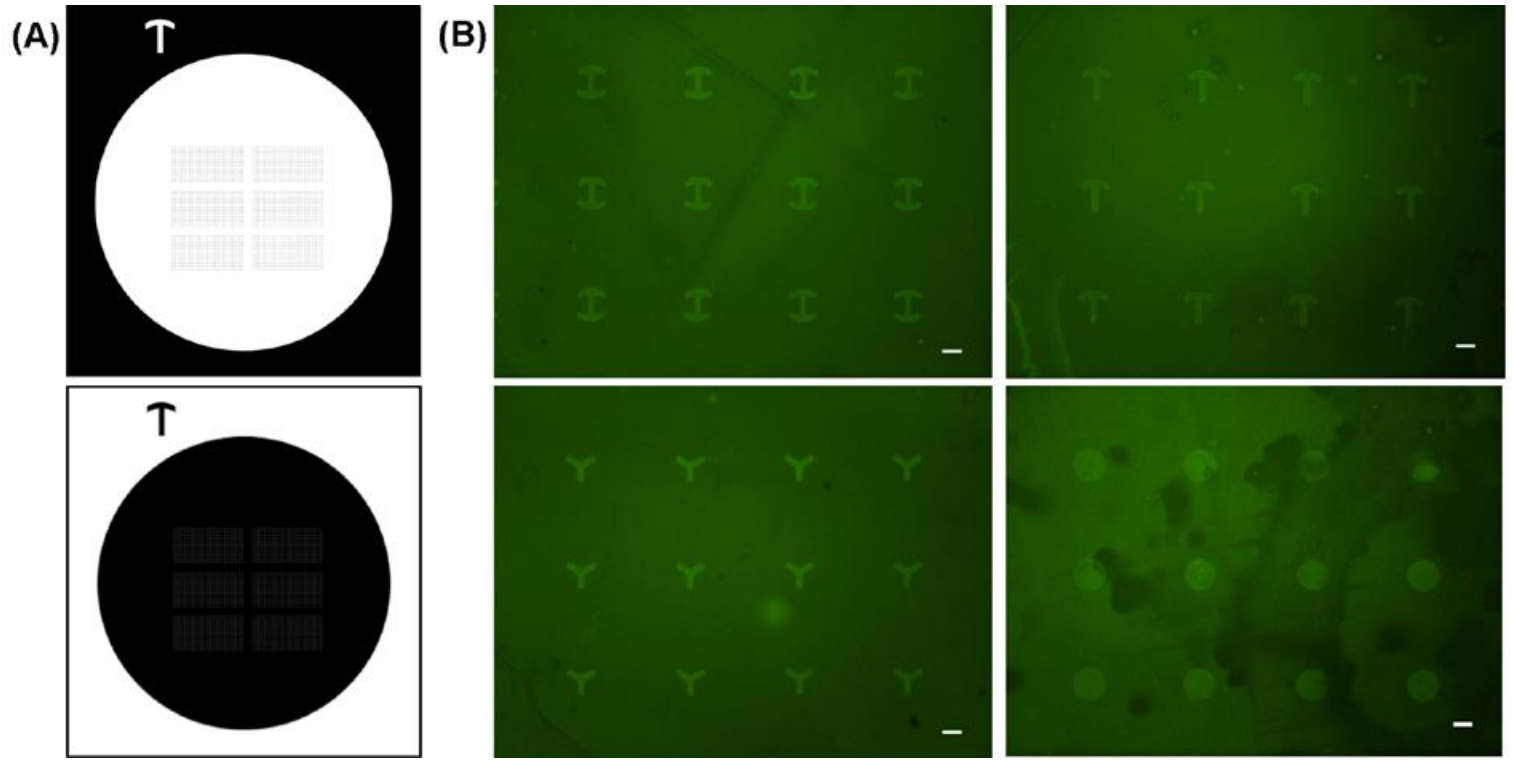

Figure 6.1: (A) Single cell patterns on photomasks. (B) Vitronectin/Fibrinogen-AF488 patterns on polystyrene substrates (scale bar 25 μm).

further protein patterning on self-assembled monolayers (SAM) is still an expensive, time consuming, and complicated approach requiring corresponding skills. Glass is also difficult to resize without the appropriate tools due to its brittle nature. On the other hand, recent advances in substrate surface chemical modification based on direct UV light exposure offer a fast, simple and inexpensive method for ECM micropatterning. A number of publications described UV-based patterning of different polymeric substrates such as polyethylene, polycarbonate, polymethylmethacrylate, and polystyrene (PS) which are very easy to handle and also inexpensive [246, 253]. Moreover, this method was successfully employed for clonal growth of hiPSC on UV-modified polystyrene and polypropylene surfaces [105].

Direct UV patterning methods consist of the treatment of a polymer surface with UV/ozone, which modifies surface chemistry by adding oxygen to its structure, thus, hydrophylizing a substrate and improving cell attachment and ECM proteins deposition. Oxygen can also be added through plasma treatment or ion beam irradiation. For example, successful patterning of cells on polyvinyl chloride (PVC) was achieved through functionalization by ion beam irradiation [247]. Polystyrene is routinely used for cell culture and is usually oxidized by plasma treatment [248, 249].

6.9 Polymer Substrate Characterization

PVC is widely used in clinical settings for a variety of medical applications. Commercially available PVC coverslips (EMS) are not autofluorescent and are used for cell analysis in research applications. However, micropatterning of PVC coverslips appeared unsuccessful. XPS analysis of UV/ozone treated PVC surface revealed that it is

exceedingly difficult to modify in comparison with cell culture polystyrene (Table 6.1), and it demonstrates a high rate of background fluorescence after UV/ozone exposure. In addition, we revealed that PVC initially contains a higher level of bound oxygen (Table 6.1). In a previously reported study it was shown that the washing of oxidized PS with HPLC grade water for one hour resulted in partial removal of bound oxygen from polymer surface (up to 8%) [254]. Interestingly, soaking of PVC and PS samples in 70% ethanol also decreased the oxidation level of plastic (Table 6.1).

Untreated cell culture polystyrene is optimal for chemical modification and has been efficiently used for micropatterning and growth of hPSC from single cells [105]. However, achieved resolution with the custom-made stainless-steel mask was only 30 μm, which is not applicable for single cell patterning. Further, commercially available quartz chrome mask allowing resolution down to 1 μm cannot be used with commercially available cell culture plastic because of technical reasons including flexibility issues and the difficulty to resize thick polystyrene. Thus, we decided to test 0.3mm thin clear Plastruct polystyrene sheets for UV/ozone micropatterning applications. This polymer was analyzed by XPS on surface oxygen binding capacity with different UV/ozone exposure doses and under different conditions (Table 6.1). Similar to PVC, Plastruct PS demonstrated low level of oxygen present (Table 6.1). Based on previous data with ethanol treatment of PVC coverslips, the same procedure minimized surface oxygen of Plastruct PS to the lowest level (Table 6.1). In a previous report 2.5 minutes of UV/ozone exposure on unmodified cell culture plastic was reported as optimal for hPSC culture,

Table 6.1: Surface chemical composition of the control and UV/ozone-treated polymer samples (atomic %).

	UV/ozone treatment time, minutes					
The type of plastic	00	1	1.5	2.5	4	7.5
Polyvinylchloride (PVC)						
PVC *sample washed with EtOH after UV/ozone	C 90.65 O 9.35	C 87.84 O 12.16	-	C 85.92 O 14.08 C 89.18* O 10.82*	C 81.55 O 18.45	-
Cell culture polystyrene (PS)						
Bacterial grade unmodified PS	C 99.63 O 0.37	-	-	C 80.93 O 19.07	-	-
Tissue culture treated PS	C 87.43 O 12.57	-	-	-	-	-
Plastruct polystyrene (PS)						
Unmodified PS *sample washed with EtOH after UV/ozone	C 97.31 O 2.69	C 90.91 O 9.09	-	C 82.51 O 17.49	C 72.16 O 27.84 C 85.87* O 14.13*	-
PS+ EtOH wash before UV/ozone exposure	C 98.89 O 1.11	-	C 88.17 O 11.83	C 81.84 O 18.16	-	-
PS+EtOH wash before UV/ozone exposure through the glass mask	-	-	-	C 96.33 O 3.67	-	C 95.73 O 4.27

while lower doses decreased cell attachment, and higher doses generated ions negatively affecting cell growth [105]. Another study showed optimal oxygen concentration on polystyrene surface for 3T3-L1 and CHO cell growth at between 5% and 25% (<100 seconds of UV/ozone treatment in UV/ozone cleaner (Jelight Company Inc.)) [254], explaining it by changes in ECM proteins and medium components interaction with the chemically modified polystyrene. Thus, we analyzed oxidation levels of cell culture polystyrene (unmodified PS, unmodified PS exposed for 2.5 minutes to UV/ozone and tissue culture treated PS) (Table 6.1). Next, we compared UV/ozone treatment parameters of Plastruct PS to that of cell culture polystyrene optimized for hPSC culture, i.e. 2.5 minutes of UV/ozone treatment [105]. Results for ethanol treated Plastruct PS samples appeared similar to cell culture PS (Table 6.1). However, it is appeared that the clear quartz mask significantly decreases the oxygen level at 2.5 minutes, and 7.5 minutes of UV/ozone exposure gave us slight shift in the level of bound oxygen (Table 6.1).

6.10 ECM Protein and Cell Deposition on UV/Ozone Micropatterned Polystyrene Coverslips

Unlike somatic cells, hPSCs require specific ECM conditions for their undifferentiated growth. Matrigel (BD) or Geltrex (Invitrogen) are routinely used for feeder-free culture of hPSCs. Matrigel consists of a few ECM proteins (laminin, collagen IV, entactin/nidogen) and heparan sulfate proteoglycan, which polymerase above temperature of 10°C and form a gel [104, 250]. A few studies have shown that hPSCs express the laminin+entactin receptor $\alpha 6\beta 1$, the vitronectin receptor $\alpha V\beta 5$ and the fibronectin receptor $\alpha 5\beta 1$, thus, allowing their attachment to Geltrex or Matrigel as well

as to vitronectin and fibronectin [251, 252]. However, only vitronectin was shown as capable of supporting hPSC self-renewal and able to replace Matrigel in cell culture [251, 252]. Based on published results we chose vitronectin as the ECM protein for micropatterns.

To visualize micropatterns, human fluorescently-labeled fibrinogen Alexa Fluor 488 was co-incubated with human recombinant vitronectin (Figure 6.1B). At low UV/ozone exposure dose (2.5 minutes) fibrinogen tended to attach to hydrophobic (unmodified) areas of PS samples (Figure 6.1B). No cell attachment to hydrophobic single cell patterns, however, was observed for hPSCs, mouse embryonic fibroblasts (MEFs), or hMSCs. Some instances of non-specific cell attachment were also observed. We hypothesize that under these conditions protein binding to chemically patterned PS samples might compete between hydrophobic and hydrophilic surfaces in the benefit of hydrophobic surface.

A previously published study showed that immobilization of laminin on high resolution micropatterns, produced by UV modification of PS, can be eliminated on non-treated (hydrophobic) surface and enhanced twice on treated (hydrophilic) surface by pretreatment with BSA/Pluronic F-68 followed by laminin/Pluronic F-68 [255]. Thus, BSA pretreatment of UV patterned Plastruct PS substrates allowed us to decrease non-specific cell attachment to non-treated hydrophobic surface and achieve attachment and characteristic spreading of MEF and hMSC on hydrophilic micropatterns (Figure 6.2). When attached to micropatterns, cells formed typical stress fibers and focal adhesions (Figure 6.2). Interestingly, BSA prevented fluorescently labeled fibrinogen from binding to the patterned surface (data not shown).

To investigate how higher doses of UV/ozone exposure will affect cell attachment to single cell patterns we modified Plastruct PS samples for 2.5 and 7.5 minutes. PS coverslips were pretreated with BSA and vitronectin as described above. MEF cells were seeded on plastic at a density of 100,000 cells/chip. Since 2.5 and 7.5 minutes of UV/ozone treatment did not give significant difference in cell attachment (0.34 and 0.44% correspondingly, or 19% and 24% of patterns were occupied), in the following experiments we applied 2.5 minutes for PS patterning.

6.11 Micropatterning of Single Human Pluripotent Stem Cells

Our previous data with Cytoo chips showed that single hPSCs can be plated on micropatterns directly from enzymatically treated and resuspended colonies grown under feeder-free conditions, or from a monolayer culture, which includes single cell passaging (data not shown). A few recent studies demonstrated that hPSCs can be grown as a monolayer culture for prolonged period of time without acquiring karyotypic abnormalities [105, 256]. Monolayer culture also allows the expansion of hPSCs as a homogeneous population in contrast to cells grown in colonies [105, 256, 257]. Monolayer culture is also more suitable for single cell studies. However, our attempts to grow hESC and hiPSC for a period of over 10 or 20 passages with single cell passaging and in the absence of supportive feeder cells resulted in extra chromosomes 12 and 20 in hESC (H9) and chromosome 12 in hiPSC (BM9) in each cell analyzed (5 metaphases total) (Figure 6.3 and 6.4). Similarly other reports showed that monolayer culture in

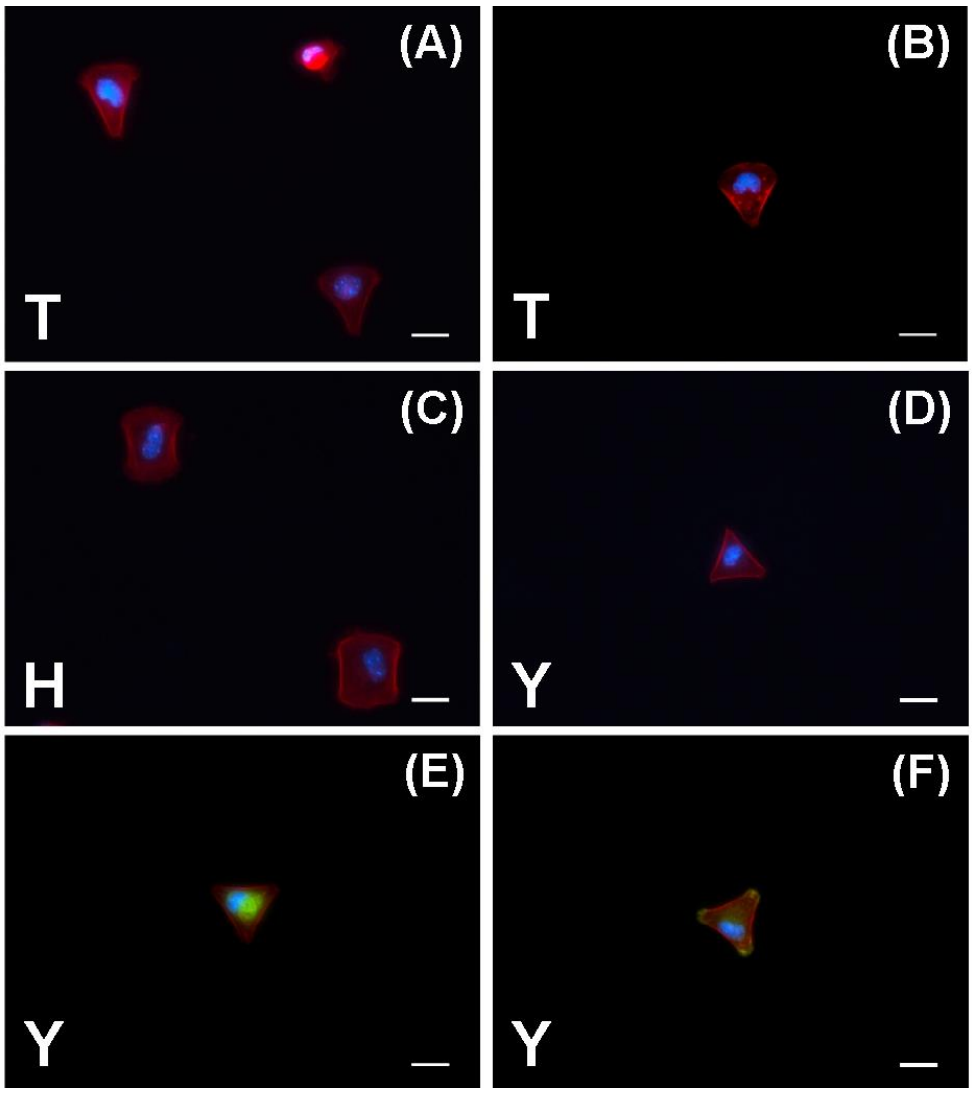

Figure 6.2: (A) – (D) MEFs and (E), (F) hMSCs on single cell patterns (shown in left lower corners). F-actin was stained with Rhodamine Phalloidin-TRITC (red), nuclei were stained with DAPI (blue), additionally, hMSCs were immunostained for vimentin (green, (E)) and vinculin (green, (F)) (scale bar 25 μm).

mTeSR1 media with single cell passaging resulted in chromosomal instability, and the addition of ROCK inhibitor after cell dissociation preserved normal hPSC karyotype [105]. Thus, we reestablished monolayer cell culture from hESCs, and began using ROCK inhibitor postseeding. After 10 passages under these conditions about 50% of cells demonstrated normal karyotype, however, in contrast to the Saha et al. study, other cells revealed various missing and extra chromosomes with aneuploidy of chromosomes 14 and 20 being the most common (8 metaphases analyzed) (Figure 6.4). Thus, cell culture medium (mTeSR1 versus MEF conditioned medium) or genetic background of hPSC lines used might affect chromosomal stability. In addition, our results suggest that the time of ROCK inhibitor treatment (overnight) also may be potentially damaging, leading to even worse outcomes, and further studies are needed to optimize these single cell culture conditions. On the other hand, hPSCs from a monolayer culture could be used for single cell studies at lower passage numbers such as 2-4 [105].

We further studied hPSC attachment and spreading on vitronectin coated single cell micropatterns. Single hPSC from a monolayer culture (BM9 and H9 lines) or colonies (HES3 line) were plated on patterns at a density of 250,000-500,000 cells/chip, allowed to spread and form stress fibers for 2-3 hours and fixed for further immunostaining and analysis. In a few hours after attachment to micropatterns hPSCs formed actin fiber assembly and cell membrane protrusions on adhesive surface and strong stress fibers (acto-myosin contraction) were observed along the non-adhesive cell edges in the manner reported for other cell types (Figure 6.5) [170, 171, 258]. In addition,

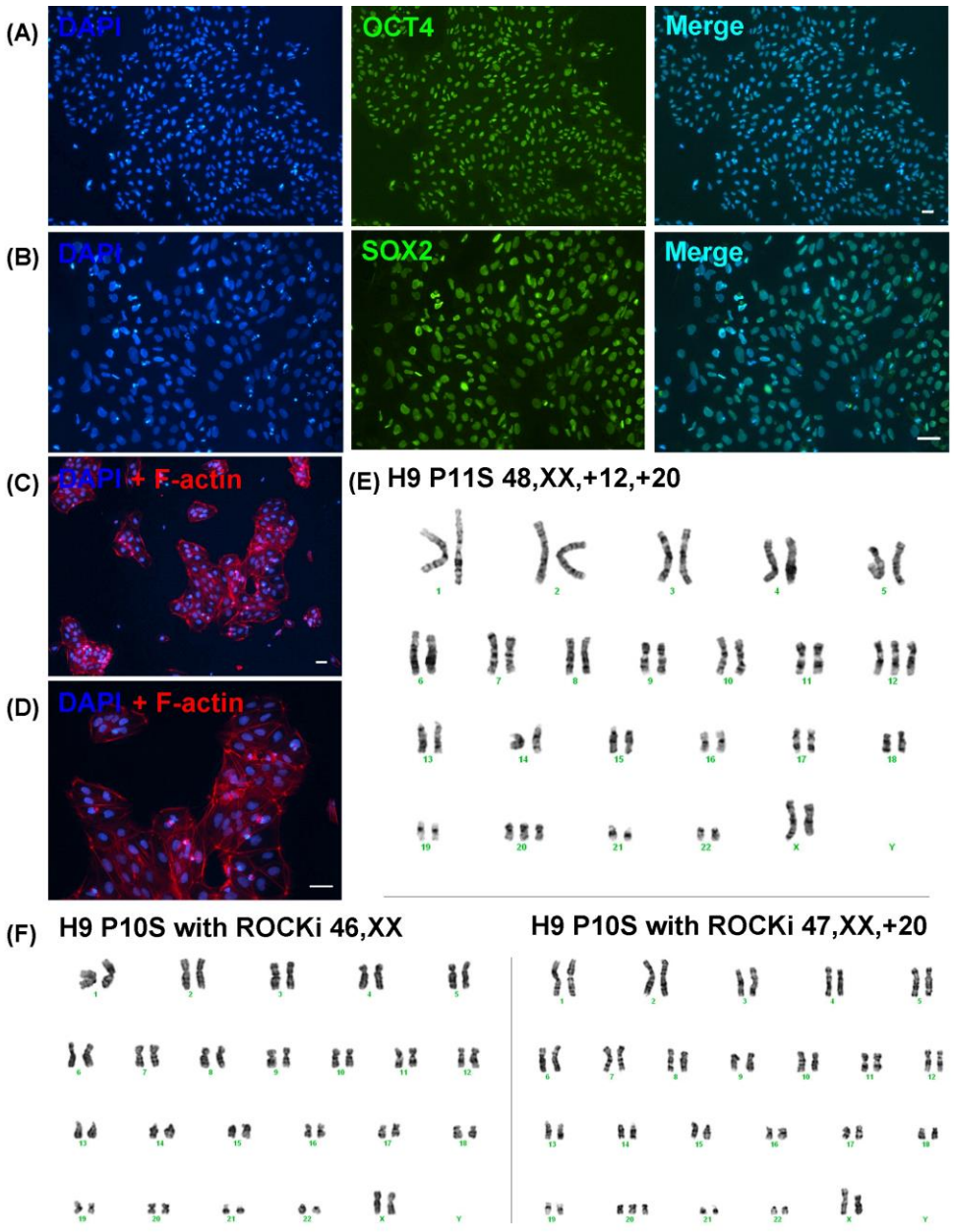

Figure 6.3: hESCs (H9) in a monolayer culture (P11S – passage 11 as single cells) express pluripotency markers OCT4 (A) and SOX2 (B), and demonstrate characteristic cytoskeleton organization (C) and (D) revealed by Rhodamine Phalloidin staining. Nuclei were stained with DAPI (blue). hESCs acquire a trisomy of chromosomes 12 and 20 if passaged without ROCK inhibitor (ROCKi) postseeding (E). The addition of ROCK inhibitor after cell passaging results in cells with normal and abnormal karyotypes (F) (scale bar 50 μm).

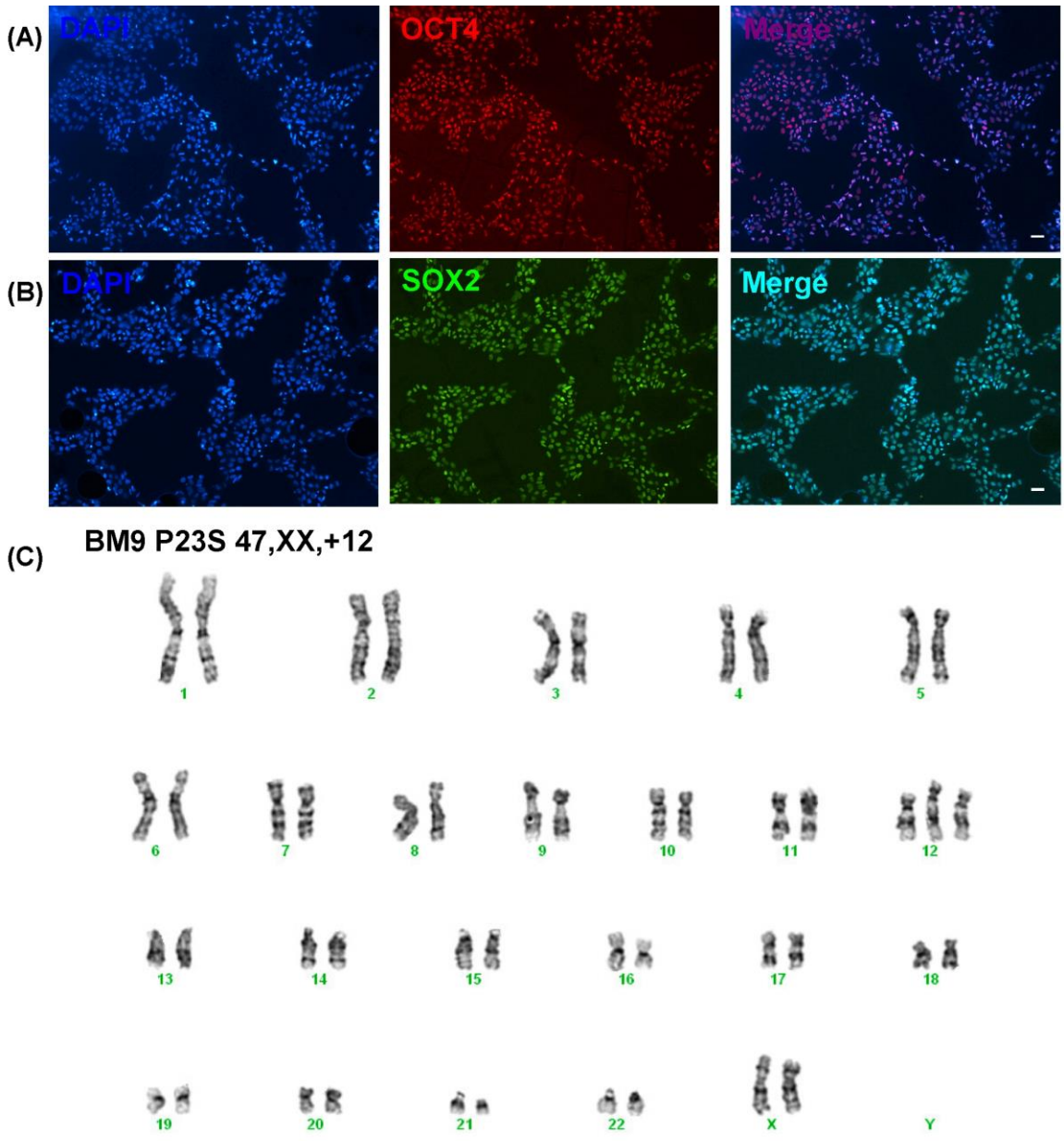

Figure 6.4: hiPSCs (BM9) in a monolayer culture (P19S – passage 19 as single cells) express pluripotency markers OCT4 (A) and SOX2 (B) and demonstrate trisomy of chromosome 12 (C), if passaged without ROCK inhibitor postseeding (scale bar 50 μm).

single hPSCs on vitronectin ECM micropatterns expressed pluripotency marker OCT4. In contrast to hMSC, within 2-3 hours after plating hPSC did not formed vinculin stripes revealing focal adhesion sites on vitronectin patterns, rather, they formed dot-like shaped focal complexes (Figure 6.5). However, cell focal adhesions were clearly seen on micropatterned ECM after overnight culture (Figure 6.5).

To note, cell seeding density on micropatterns needs to be adjusted depending on cell type and size. Larger sizes of patterns resulted in incomplete and non-specific cell spreading. High plating density over 300,000 cells/chip gives up to 76% of patterns filled but can also result in patterns being occupied by multiple cells (data not shown).

Types of micropatterns described in this report are currently applied to investigate mitotic spindle positioning and cell division in somatic cells [170]. Unfortunately, so far our attempts to study single hPSCs entering a metaphase stage on patterns or in a monolayer culture a few hours postseeding were not successful. Synchronization of hPSC in a monolayer culture [259] gave similar amount of cells (~ 30%) at a metaphase stage as in routing culture on Day 3-4 after passaging, but no cells at a metaphase stage were observed after a few hours from cell passaging and spreading, including the day following passaging (data not shown). Surprisingly, single hPSC attached to patterns in the presence of ROCK inhibitor and did not undergo apoptosis during overnight culture while keeping shape and stress fiber formation corresponding to patterns (Figure 6.5). Further studies are required to define optimal conditions to investigate hPSC division on single cell patterns.

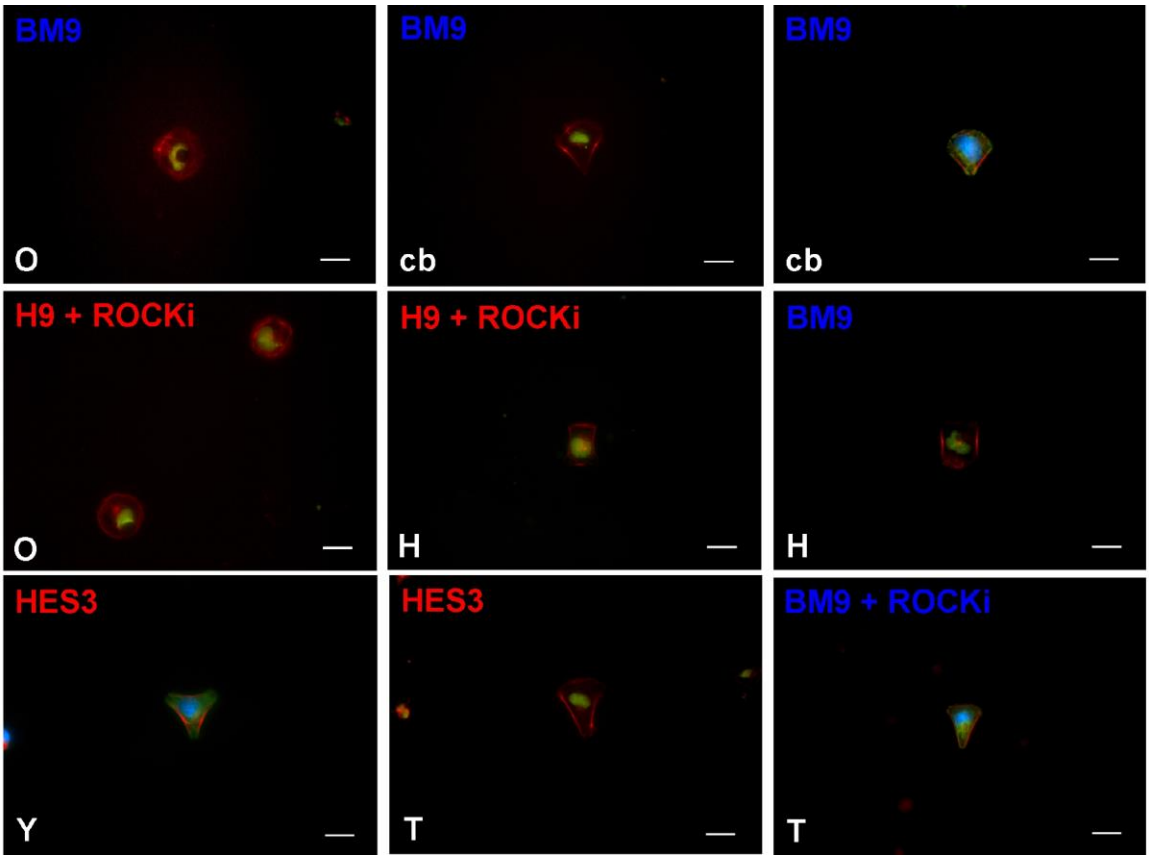

Figure 6.5: Single hPSCs on vitronectin patterns with or without addition of ROCK inhibitor (ROCKi) postseeding. BM9 hiPSCs (A-C, F and I) are shown in blue, H9 hESCs (D, E) and HES3 hESCs (G, H) are shown in red. Corresponding patterns are shown in left lower corners ("cb" – crossbow). BM9 hiPSCs and H9 hESCs were grown in a monolayer culture with single-cell passaging and HES3 hESCs before plating on micropatterns were grown in colonies on Geltrex (to eliminate MEFs) and routinely passaged as clumps. BM9 hiPSC on pattern "O" (A) is shown on D0, BM9 hiPSCs on patterns "crossbow" (B, C) and "T" (I) are shown on D1 after plating and BM9 hiPSC on pattern "H" (F) is shown on D2 (~ 48 hours after plating). For hiPSC on pattern "T" (I), ROCK inhibitor (ROCKi) was added after cell plating and kept overnight. H9 hESCs on patterns "O" (D) and pattern "H" (E) are shown on Day1 (~ 24 hours after plating). ROCK inhibitor was added after cell plating and kept overnight. HES3 hESCs on patterns "Y" (G) and "T" (H) are shown on D0 (~ 4 hours after plating). (F-actin was stained with Rhodamine Phalloidin (red), nuclei were stained with DAPI (blue) or with antibodies specific to OCT4 (green), focal adhesions were immunostained with antibodies specific to vinculin (green) (scale bar 25 μm).

6.12 Conclusions

In this study we described a convenient and simple method for the design of micropatterns for single cell studies. Moreover, we particularly developed conditions for vitronectin binding to chemically modified polystyrene, which makes it possible to conduct research on hPSC at a single cell level. Designed method can find multiple applications for cell studies in traditional biology laboratories without the need for expensive complex equipment.

References

1. Langer, R. and J.P. Vacanti, *Tissue Engineering.* Science, 1993. **260**(5110): p. 920-926.
2. Harris, G.M., et al., *Strategies to Direct Angiogenesis within Scaffolds for Bone Tissue Engineering.* Current Pharmaceutical Design, 2013. **19**(19): p. 3456-3465.
3. Lutolf, M.P. and J.A. Hubbell, *Synthetic biomaterials as instructive extracellular microenvironments for morphogenesis in tissue engineering.* Nature Biotechnology, 2005. **23**(1): p. 47-55.
4. Hubbell, J.A., *Biomaterials in Tissue Engineering.* Bio-Technology, 1995. **13**(6): p. 565-576.
5. Griffith, L.G. and G. Naughton, *Tissue engineering - Current challenges and expanding opportunities.* Science, 2002. **295**(5557): p. 1009-+.
6. Griffith, L.G., *Emerging design principles in Biomaterials and scaffolds for tissue engineering.* Reparative Medicine: Growing Tissues and Organs, 2002. **961**: p. 83-95.
7. Kim, B.S. and D.J. Mooney, *Development of biocompatible synthetic extracellular matrices for tissue engineering.* Trends in Biotechnology, 1998. **16**(5): p. 224-230.

8. Jukes, J.M., C.A. van Blitterswijk, and J. de Boer, *Skeletal tissue engineering using embryonic stem cells.* Journal of Tissue Engineering and Regenerative Medicine, 2010. **4**(3): p. 165-180.

9. Rossi, C.A., M. Pozzobon, and P. De Coppi, *Advances in musculoskeletal tissue engineering Moving towards therapy.* Organogenesis, 2010. **6**(3): p. 167-172.

10. Atala, A., et al., *Tissue-engineered autologous bladders for patients needing cystoplasty.* Lancet, 2006. **367**(9518): p. 1241-6.

11. Borden, M., et al., *Tissue engineered microsphere-based matrices for bone repair: design and evaluation.* Biomaterials, 2002. **23**(2): p. 551-559.

12. Borenstein, J.T., et al., *Microfabrication technology for vascularized tissue engineering.* Biomedical Microdevices, 2002. **4**(3): p. 167-175.

13. Borenstein, J.T., et al., *Microfabrication of three-dimensional engineered scaffolds.* Tissue Engineering, 2007. **13**(8): p. 1837-1844.

14. Grayson, W.L., et al., *Engineering anatomically shaped human bone grafts.* Proceedings of the National Academy of Sciences of the United States of America, 2010. **107**(8): p. 3299-3304.

15. Hollister, S.J., *Porous scaffold design for tissue engineering.* Nature Materials, 2005. **4**(7): p. 518-524.

16. Hutmacher, D.W., *Scaffolds in tissue engineering bone and cartilage.* Biomaterials, 2000. **21**(24): p. 2529-43.

17. Petite, H., et al., *Tissue-engineered bone regeneration.* Nature Biotechnology, 2000. **18**(9): p. 959-963.

18. Engler, A.J., et al., *Matrix elasticity directs stem cell lineage specification.* Cell, 2006. **126**(4): p. 677-689.

19. McBeath, R., et al., *Cell shape, cytoskeletal tension, and RhoA regulate stem cell lineage commitment.* Dev Cell, 2004. **6**(4): p. 483-95.

20. Pelham, R.J., Jr. and Y. Wang, *Cell locomotion and focal adhesions are regulated by substrate flexibility.* Proc Natl Acad Sci U S A, 1997. **94**(25): p. 13661-5.

21. Whittaker, C.A., et al., *The echinoderm adhesome.* Developmental Biology, 2006. **300**(1): p. 252-266.

22. Ozbek, S., et al., *The Evolution of Extracellular Matrix.* Molecular Biology of the Cell, 2010. **21**(24): p. 4300-4305.

23. Aubin, H., et al., *Directed 3D cell alignment and elongation in microengineered hydrogels.* Biomaterials, 2010. **31**(27): p. 6941-6951.

24. Chan, V., et al., *Three-dimensional photopatterning of hydrogels using stereolithography for long-term cell encapsulation.* Lab on a Chip, 2010. **10**(16): p. 2062-2070.

25. Cooke, M.N., et al., *Use of stereolithography to manufacture critical-sized 3D biodegradable scaffolds for bone ingrowth.* Journal of Biomedical Materials Research Part B-Applied Biomaterials, 2003. **64B**(2): p. 65-69.

26. Zhu, J.M., *Bioactive modification of poly(ethylene glycol) hydrogels for tissue engineering.* Biomaterials, 2010. **31**(17): p. 4639-4656.

27. Geiger, B., et al., *Transmembrane crosstalk between the extracellular matrix--cytoskeleton crosstalk.* Nat Rev Mol Cell Biol, 2001. **2**(11): p. 793-805.

28. Palsson, B. and S. Bhatia, *Tissue engineering*. 2004, Upper Saddle River, N.J.: Pearson Prentice Hall. xviii, 407 p.

29. Friedl, P. and K. Wolf, *Tumour-cell invasion and migration: Diversity and escape mechanisms.* Nature Reviews Cancer, 2003. **3**(5): p. 362-374.

30. Sahai, E., *Mechanisms of cancer cell invasion.* Current Opinion in Genetics & Development, 2005. **15**(1): p. 87-96.

31. Muller, W.A., *Leukocyte-endothelial-cell interactions in leukocyte transmigration and the inflammatory response.* Trends in Immunology, 2003. **24**(6): p. 327-334.

32. Rabodzey, A., et al., *Mechanical forces induced by the transendothelial migration of human neutrophils.* Biophysical Journal, 2008. **95**(3): p. 1428-1438.

33. Ghosh, K. and D.E. Ingber, *Micromechanical control of cell and tissue development: Implications for tissue engineering.* Advanced Drug Delivery Reviews, 2007. **59**(13): p. 1306-1318.

34. Martin, P. and S.M. Parkhurst, *Parallels between tissue repair and embryo morphogenesis.* Development, 2004. **131**(13): p. 3021-3034.

35. Paszek, M.J., et al., *Tensional homeostasis and the malignant phenotype.* Cancer Cell, 2005. **8**(3): p. 241-254.

36. Wolf, K. and P. Friedl, *Mapping proteolytic cancer cell-extracellular matrix interfaces.* Clinical & Experimental Metastasis, 2009. **26**(4): p. 289-298.

37. Zaman, M.H., et al., *Migration of tumor cells in 3D matrices is governed by matrix stiffness along with cell-matrix adhesion and proteolysis (vol 103, pg 10889, 2006).* Proceedings of the National Academy of Sciences of the United States of America, 2006. **103**(37): p. 13897-13897.

38. Holle, A.W. and A.J. Engler, *More than a feeling: discovering, understanding, and influencing mechanosensing pathways.* Current Opinion in Biotechnology, 2011. **22**(5): p. 648-654.

39. Flanagan, L.A., et al., *Neurite branching on deformable substrates.* Neuroreport, 2002. **13**(18): p. 2411-2415.

40. Georges, P.C., et al., *Matrices with compliance comparable to that of brain tissue select neuronal over glial growth in mixed cortical cultures.* Biophysical Journal, 2006. **90**(8): p. 3012-8.

41. Engler, A.J., et al., *Myotubes differentiate optimally on substrates with tissue-like stiffness: pathological implications for soft or stiff microenvironments.* Journal of Cell Biology, 2004. **166**(6): p. 877-887.

42. Kondo, T., et al., *Sonic hedgehog and retinoic acid synergistically promote sensory fate specification from bone marrow-derived pluripotent stem cells.* Proceedings of the National Academy of Sciences of the United States of America, 2005. **102**(13): p. 4789-4794.

43. Clark, E.A. and J.S. Brugge, *Integrins and Signal-Transduction Pathways - the Road Taken.* Science, 1995. **268**(5208): p. 233-239.

44. Hynes, R.O., *Integrins - Versatility, Modulation, and Signaling in Cell-Adhesion.* Cell, 1992. **69**(1): p. 11-25.

45. Craig, S.W. and R.P. Johnson, *Assembly of focal adhesions: Progress, paradigms, and portents.* Current Opinion in Cell Biology, 1996. **8**(1): p. 74-85.

46. Almodovar, J., et al., *Gradients of physical and biochemical cues on polyelectrolyte multilayer films generated via microfluidics.* Lab on a Chip, 2013. **13**(8): p. 1562-1570.

47. Discher, D.E., D.J. Mooney, and P.W. Zandstra, *Growth factors, matrices, and forces combine and control stem cells.* Science, 2009. **324**(5935): p. 1673-7.

48. Ghafar-Zadeh, E., J.R. Waldeisen, and L.P. Lee, *Engineered approaches to the stem cell microenvironment for cardiac tissue regeneration.* Lab on a Chip, 2011. **11**(18): p. 3031-3048.

49. Guilak, F., et al., *Control of Stem Cell Fate by Physical Interactions with the Extracellular Matrix.* Cell Stem Cell, 2009. **5**(1): p. 17-26.

50. Kshitiz, et al., *Control of stem cell fate and function by engineering physical microenvironments.* Integrative Biology, 2012. **4**(9): p. 1008-1018.

51. Glucksmann, A., *The role of mechanical stresses in bone formation in vitro.* Journal of Anatomy, 1942. **76**: p. 231-239.

52. Chen, C.S., et al., *Geometric control of cell life and death.* Science, 1997. **276**(5317): p. 1425-1428.

53. Chen, C.S., et al., *Micropatterned surfaces for control of cell shape, position, and function.* Biotechnology Progress, 1998. **14**(3): p. 356-363.

54. Balaban, N.Q., et al., *Force and focal adhesion assembly: a close relationship studied using elastic micropatterned substrates.* Nature Cell Biology, 2001. **3**(5): p. 466-472.

55. Chen, C.S., et al., *Cell shape provides global control of focal adhesion assembly.* Biochemical and Biophysical Research Communications, 2003. **307**(2): p. 355-361.

56. Collins, J.M. and S. Nettikadan, *Subcellular scaled multiplexed protein patterns for single cell cocultures.* Analytical Biochemistry, 2011. **419**(2): p. 339-341.

57. Gray, D.S., et al., *Engineering amount of cell-cell contact demonstrates biphasic proliferative regulation through RhoA and the actin cytoskeleton.* Experimental Cell Research, 2008. **314**(15): p. 2846-2854.

58. Peng, R., X. Yao, and J.D. Ding, *Effect of cell anisotropy on differentiation of stem cells on micropatterned surfaces through the controlled single cell adhesion.* Biomaterials, 2011. **32**(32): p. 8048-8057.

59. Song, W., N. Kawazoe, and G.P. Chen, *Dependence of Spreading and Differentiation of Mesenchymal Stem Cells on Micropatterned Surface Area.* Journal of Nanomaterials, 2011.

60. Green, H. and O. Kehinde, *Sublines of Mouse 3t3 Cells That Accumulate Lipid.* Cell, 1974. **1**(3): p. 113-116.

61. Gregoire, F.M., C.M. Smas, and H.S. Sul, *Understanding adipocyte differentiation.* Physiological Reviews, 1998. **78**(3): p. 783-809.

62. Grigoriadis, A.E., J.N.M. Heersche, and J.E. Aubin, *Differentiation of Muscle, Fat, Cartilage, and Bone from Progenitor Cells Present in a Bone-Derived Clonal Cell-Population - Effect of Dexamethasone.* Journal of Cell Biology, 1988. **106**(6): p. 2139-2151.

63. Sikavitsas, V.I., J.S. Temenoff, and A.G. Mikos, *Biomaterials and bone mechanotransduction.* Biomaterials, 2001. **22**(19): p. 2581-2593.

64. Tse, J.R. and A.J. Engler, *Stiffness Gradients Mimicking In Vivo Tissue Variation Regulate Mesenchymal Stem Cell Fate.* Plos One, 2011. **6**(1).

65. Lo, C.M., et al., *Cell movement is guided by the rigidity of the substrate.* Biophysical Journal, 2000. **79**(1): p. 144-152.

66. Nemir, S. and J.L. West, *Synthetic Materials in the Study of Cell Response to Substrate Rigidity.* Annals of Biomedical Engineering, 2010. **38**(1): p. 2-20.

67. Geiger, B., J.P. Spatz, and A.D. Bershadsky, *Environmental sensing through focal adhesions.* Nature Reviews Molecular Cell Biology, 2009. **10**(1): p. 21-33.

68. Previtera, M.L., et al., *Fibroblast Morphology on Dynamic Softening of Hydrogels.* Annals of Biomedical Engineering, 2011.

69. Evans, N.D., et al., *Substrate stiffness affects early differentiation events in embryonic stem cells.* Eur Cell Mater, 2009. **18**: p. 1-13; discussion 13-4.

70. Bershadsky, A.D., N.Q. Balaban, and B. Geiger, *Adhesion-dependent cell mechanosensitivity.* Annu Rev Cell Dev Biol, 2003. **19**: p. 677-95.

71. Cukierman, E., et al., *Taking cell-matrix adhesions to the third dimension.* Science, 2001. **294**(5547): p. 1708-12.

72. Discher, D.E., P. Janmey, and Y.L. Wang, *Tissue cells feel and respond to the stiffness of their substrate.* Science, 2005. **310**(5751): p. 1139-1143.

73. Davila, J.C., et al., *Use and application of stem cells in toxicology.* Toxicological Sciences, 2004. **79**(2): p. 214-223.

74. Fuchs, E., T. Tumbar, and G. Guasch, *Socializing with the neighbors: Stem cells and their niche.* Cell, 2004. **116**(6): p. 769-778.

75. Liao, S., C.K. Chan, and S. Ramakrishna, *Stem cells and biomimetic materials strategies for tissue engineering.* Materials Science & Engineering C-Biomimetic and Supramolecular Systems, 2008. **28**(8): p. 1189-1202.

76. Pittenger, M.F., et al., *Multilineage potential of adult human mesenchymal stem cells.* Science, 1999. **284**(5411): p. 143-7.

77. Reya, T., et al., *Stem cells, cancer, and cancer stem cells.* Nature, 2001. **414**(6859): p. 105-111.

78. Thomson, M., et al., *Pluripotency Factors in Embryonic Stem Cells Regulate Differentiation into Germ Layers.* Cell, 2011. **145**(6): p. 875-889.

79. Watt, F.M. and B.L.M. Hogan, *Out of Eden: Stem cells and their niches.* Science, 2000. **287**(5457): p. 1427-1430.

80. Griffith, L.G., *Polymeric biomaterials.* Acta Materialia, 2000. **48**(1): p. 263-277.

81. Kim, D., et al., *Multilineage Potential of Porcine Bone Marrow and Adipose-Derived Mesenchymal Stem Cells in 3-D Alginate Hydrogels.* Reproduction Fertility and Development, 2009. **21**(1): p. 237-237.

82. Baksh, D., R. Yao, and R.S. Tuan, *Comparison of proliferative and multilineage differentiation potential of human mesenchymal stem cells derived from umbilical cord and bone marrow.* Stem Cells, 2007. **25**(6): p. 1384-1392.

83. Zahanich, I., et al., *Multilineage potential of human mesenchymal stem cells.* Naunyn-Schmiedebergs Archives of Pharmacology, 2005. **371**: p. R84-R84.

84. Mareschi, K., et al., *Multilineage potential of human mesenchymal stem cells: bone marrow versus cord blood.* Bone Marrow Transplantation, 2001. **27**: p. S322-S323.

85. Smith, A.D., et al., *Mesenchymal stem cells derived from bone marrow and human adipose tissue exhibit multilineage potential.* Journal of Investigative Medicine, 2000. **48**(1): p. 95a-95a.

86. Pittenger, M.F., et al., *Multilineage potential of adult human mesenchymal stem cells.* Science, 1999. **284**(5411): p. 143-147.

87. Dominici, M., et al., *Minimal criteria for defining multipotent mesenchymal stromal cells. The International Society for Cellular Therapy position statement.* Cytotherapy, 2006. **8**(4): p. 315-317.

88. Oswald, J., et al., *Mesenchymal stem cells can be differentiated into endothelial cells in vitro.* Stem Cells, 2004. **22**(3): p. 377-84.

89. Kaigler, D., et al., *Transplanted endothelial cells enhance orthotopic bone regeneration.* Journal of Dental Research, 2006. **85**(7): p. 633-7.

90. Huang, Y.C., et al., *Combined angiogenic and osteogenic factor delivery enhances bone marrow stromal cell-driven bone regeneration.* Journal of Bone and Mineral Research, 2005. **20**(5): p. 848-57.

91. Carpenter, M.K., et al., *Properties of four human embryonic stem cell lines maintained in a feeder-free culture system.* Developmental Dynamics, 2004. **229**(2): p. 243-258.

92. Niwa, H., *How is pluripotency determined and maintained?* Development, 2007. **134**(4): p. 635-646.

93. Pesce, M. and H.R. Scholer, *Oct-4: Gatekeeper in the beginnings of mammalian development.* Stem Cells, 2001. **19**(4): p. 271-278.

94. Rohwedel, J., et al., *Embryonic stem cells as an in vitro model for mutagenicity, cytotoxicity and embryotoxicity studies: present state and future prospects.* Toxicology in Vitro, 2001. **15**(6): p. 741-753.

95. Nishikawa, S.I., L.M. Jakt, and T. Era, *Embryonic stem-cell culture as a tool for developmental cell biology.* Nature Reviews Molecular Cell Biology, 2007. **8**(6): p. 502-507.

96. Thomson, J.A., et al., *Embryonic stem cell lines derived from human blastocysts.* Science, 1998. **282**(5391): p. 1145-1147.

97. Jaenisch, R. and R. Young, *Stem cells, the molecular circuitry of pluripotency and nuclear reprogramming.* Cell, 2008. **132**(4): p. 567-582.

98. Kane, N.M., et al., *Derivation of endothelial cells from human embryonic stem cells by directed differentiation: analysis of microRNA and angiogenesis in vitro and in vivo.* Arterioscler Thromb Vasc Biol, 2010. **30**(7): p. 1389-97.

99. Sone, M., et al., *Pathway for differentiation of human embryonic stem cells to vascular cell components and their potential for vascular regeneration.* Arterioscler Thromb Vasc Biol, 2007. **27**(10): p. 2127-34.

100. Kee, K., et al., *Bone morphogenetic proteins induce germ cell differentiation from human embryonic stem cells.* Stem Cells and Development, 2006. **15**(6): p. 831-837.

101. Lu, M. and R.Y. Lin, *TSH stimulates adipogenesis in mouse embryonic stem cells.* Journal of Endocrinology, 2008. **196**(1): p. 159-169.

102. Mummery, C., et al., *Cardiomyocyte differentiation of mouse and human embryonic stem cells.* Journal of Anatomy, 2002. **200**(3): p. 233-242.

103. Hasegawa, K., et al., *A method for the selection of human embryonic stem cell sublines with high replating efficiency after single-cell dissociation.* Stem Cells, 2006. **24**(12): p. 2649-2660.

104. Kohen, N.T., L.E. Little, and K.E. Healy, *Characterization of Matrigel interfaces during defined human embryonic stem cell culture.* Biointerphases, 2009. **4**(4): p. 69-79.

105. Saha, K., et al., *Surface-engineered substrates for improved human pluripotent stem cell culture under fully defined conditions.* Proceedings of the National Academy of Sciences of the United States of America, 2011. **108**(46): p. 18714-18719.

106. Peerani, R., et al., *Patterning mouse and human embryonic stem cells using micro-contact printing.* Methods Mol Biol, 2009. **482**: p. 21-33.

107. Van Hoof, D., et al., *Differentiation of human embryonic stem cells into pancreatic endoderm in patterned size-controlled clusters.* Stem Cell Research, 2011. **6**(3): p. 276-285.

108. Hu, K.J., et al., *Efficient generation of transgene-free induced pluripotent stem cells from normal and neoplastic bone marrow and cord blood mononuclear cells.* Blood, 2011. **117**(14): p. E109-E119.

109. Lowry, W.E., et al., *Generation of human induced pluripotent stem cells from dermal fibroblasts.* Proceedings of the National Academy of Sciences of the United States of America, 2008. **105**(8): p. 2883-2888.

110. Yu, J.Y., et al., *Induced pluripotent stem cell lines derived from human somatic cells.* Science, 2007. **318**(5858): p. 1917-1920.

111. Cahan, P. and G.Q. Daley, *Origins and implications of pluripotent stem cell variability and heterogeneity.* Nature Reviews Molecular Cell Biology, 2013. **14**(6): p. 357-368.

112. Volz, K.S., et al., *Development of pluripotent stem cells for vascular therapy.* Vascul Pharmacol, 2012. **56**(5-6): p. 288-96.

113. Rufaihah, A.J., et al., *Endothelial cells derived from human iPSCS increase capillary density and improve perfusion in a mouse model of peripheral arterial disease.* Arterioscler Thromb Vasc Biol, 2011. **31**(11): p. e72-9.

114. Suzuki, H., et al., *Therapeutic angiogenesis by transplantation of induced pluripotent stem cell-derived Flk-1 positive cells.* BMC Cell Biol, 2010. **11**: p. 72.

115. Nelson, T.J., et al., *Repair of acute myocardial infarction by human stemness factors induced pluripotent stem cells.* Circulation, 2009. **120**(5): p. 408-16.

116. Paik, I., et al., *Rapid micropatterning of cell lines and human pluripotent stem cells on elastomeric membranes.* Biotechnology and Bioengineering, 2012.

117. van Kooten, T.G. and A.F. von Recum, *Cell adhesion to textured silicone surfaces: The influence of time of adhesion and texture on focal contact and fibronectin fibril formation.* Tissue Engineering, 1999. **5**(3): p. 223-240.

118. Jiang, X.Y., et al., *Controlling mammalian cell spreading and cytoskeletal arrangement with conveniently fabricated continuous wavy features on poly(dimethylsiloxane).* Langmuir, 2002. **18**(8): p. 3273-3280.

119. Curtis, A. and C. Wilkinson, *New depths in cell behaviour: reactions of cells to nanotopography.* Cell Behaviour: Control and Mechanism of Motility, 1999(65): p. 15-26.

120. Lampin, M., et al., *Correlation between substratum roughness and wettability, cell adhesion, and cell migration.* Journal of Biomedical Materials Research, 1997. **36**(1): p. 99-108.

121. D'Angelo, F., et al., *Micropatterned Hydrogenated Amorphous Carbon Guides Mesenchymal Stem Cells Towards Neuronal Differentiation.* European Cells & Materials, 2010. **20**: p. 231-244.

122. Raghavan, S., et al., *Geometrically Controlled Endothelial Tubulogenesis in Micropatterned Gels.* Tissue Engineering Part A, 2010. **16**(7): p. 2255-2263.

123. Moon, J.J., et al., *Micropatterning of Poly(Ethylene Glycol) Diacrylate Hydrogels with Biomolecules to Regulate and Guide Endothelial Morphogenesis.* Tissue Engineering Part A, 2009. **15**(3): p. 579-585.

124. Jiang, X.Y., et al., *Directing cell migration with asymmetric micropatterns.* Proceedings of the National Academy of Sciences of the United States of America, 2005. **102**(4): p. 975-978.

125. Hsu, S., et al., *Effects of shear stress on endothelial cell haptotaxis on micropatterned surfaces.* Biochemical and Biophysical Research Communications, 2005. **337**(1): p. 401-409.

126. Sieminski, A.L., R.P. Hebbel, and K.J. Gooch, *The relative magnitudes of endothelial force generation and matrix stiffness modulate capillary morphogenesis in vitro.* Experimental Cell Research, 2004. **297**(2): p. 574-584.

127. Vailhe, B., et al., *In vitro angiogenesis is modulated by the mechanical properties of fibrin gels and is related to alpha(v)beta(3) integrin localization.* In Vitro Cellular & Developmental Biology-Animal, 1997. **33**(10): p. 763-773.

128. Stephanou, A., et al., *The rigidity in fibrin gels as a contributing factor to the dynamics of in vitro vascular cord formation.* Microvascular Research, 2007. **73**(3): p. 182-190.

129. Lo, C.M. and Y.L. Wang, *Guidance of cell movement by substrate rigidity.* Molecular Biology of the Cell, 1999. **10**: p. 259a-259a.

130. Yeung, T., et al., *Effects of substrate stiffness on cell morphology, cytoskeletal structure, and adhesion.* Cell Motility and the Cytoskeleton, 2005. **60**(1): p. 24-34.

131. Tranqui, L. and P. Tracqui, *Mechanical signalling and angiogenesis. The integration of cell-extracellular matrix couplings.* Comptes Rendus De L Academie Des Sciences Serie Iii-Sciences De La Vie-Life Sciences, 2000. **323**(1): p. 31-47.

132. Califano, J.P. and C.A. Reinhart-King, *The effects of substrate elasticity on endothelial cell network formation and traction force generation.* Conf Proc IEEE Eng Med Biol Soc, 2009. **2009**: p. 3343-5.

133. Fidkowski, C., et al., *Endothelialized microvasculature based on a biodegradable elastomer.* Tissue Engineering, 2005. **11**(1-2): p. 302-309.

134. Shin, M., et al., *Endothelialized networks with a vascular geometry in microfabricated poly(dimethyl siloxane).* Biomedical Microdevices, 2004. **6**(4): p. 269-278.

135. Du, Y.A., et al., *Sequential Assembly of Cell-Laden Hydrogel Constructs to Engineer Vascular-Like Microchannels.* Biotechnology and Bioengineering, 2011. **108**(7): p. 1693-1703.

136. Khademhosseini, A. and R. Langer, *Microengineered hydrogels for tissue engineering.* Biomaterials, 2007. **28**(34): p. 5087-5092.

137. Mironov, V., et al., *Organ printing: computer-aided jet-based 3D tissue engineering.* Trends in Biotechnology, 2003. **21**(4): p. 157-161.

138. Yang, H.Y., et al., *Fine ceramic lattices prepared by extrusion freeforming.* Journal of Biomedical Materials Research Part B-Applied Biomaterials, 2006. **79B**(1): p. 116-121.

139. Tan, W. and T.A. Desai, *Layer-by-layer microfluidics for biomimetic three-dimensional structures.* Biomaterials, 2004. **25**(7-8): p. 1355-1364.

140. Rivron, N.C., et al., *Tissue deformation spatially modulates VEGF signaling and angiogenesis.* Proceedings of the National Academy of Sciences of the United States of America, 2012. **109**(18): p. 6886-6891.

141. Madaboosi, N., et al., *Microfluidics meets soft layer-by-layer films: selective cell growth in 3D polymer architectures.* Lab on a Chip, 2012. **12**(8): p. 1434-1436.

142. Tan, W. and T.A. Desai, *Microscale multilayer cocultures for biomimetic blood vessels.* Journal of Biomedical Materials Research Part A, 2005. **72A**(2): p. 146-160.

143. King, K.R., et al., *Biodegradable microfluidics.* Advanced Materials, 2004. **16**(22): p. 2007-+.

144. Choi, N.W., et al., *Microfluidic scaffolds for tissue engineering.* Nature Materials, 2007. **6**(11): p. 908-915.

145. Sistiabudi, R. and A. Ivanisevic, *Dip-Pen Nanolithography of Bioactive Peptides on Collagen-Terminated Retinal Membrane.* Advanced Materials, 2008. **20**(19): p. 3678-+.

146. Lim, J.H., et al., *Direct-write dip-pen nanolithography of proteins on modified silicon oxide surfaces.* Angewandte Chemie-International Edition, 2003. **42**(20): p. 2309-2312.

147. Tinazli, A., et al., *Native protein nanolithography that can write, read and erase.* Nature Nanotechnology, 2007. **2**(4): p. 220-225.

148. Zheng, Z., et al., *Topographically Flat, Chemically Patterned PDMS Stamps Made by Dip-Pen Nanolithography.* Angewandte Chemie-International Edition, 2008. **47**(51): p. 9951-9954.

149. Curran, J.M., et al., *Introducing dip pen nanolithography as a tool for controlling stem cell behaviour: unlocking the potential of the next generation of smart materials in regenerative medicine.* Lab on a Chip, 2010. **10**(13): p. 1662-1670.

150. Sekula, S., et al., *Multiplexed Lipid Dip-Pen Nanolithography on Subcellular Scales for the Templating of Functional Proteins and Cell Culture.* Small, 2008. **4**(10): p. 1785-1793.

151. Newton, L., et al., *Self assembled monolayers (SAMs) on metallic surfaces (gold and graphene) for electronic applications.* Journal of Materials Chemistry C, 2013. **1**(3): p. 376-393.

152. Mrksich, M., et al., *Controlling cell attachment on contoured surfaces with self-assembled monolayers of alkanethiolates on gold.* Proceedings of the National Academy of Sciences of the United States of America, 1996. **93**(20): p. 10775-10778.

153. Du, Y.A., et al., *Directed assembly of cell-laden microgels for fabrication of 3D tissue constructs.* Proceedings of the National Academy of Sciences of the United States of America, 2008. **105**(28): p. 9522-9527.

154. Tsang, V.L., et al., *Fabrication of 3D hepatic tissues by additive photopatterning of cellular hydrogels.* Faseb Journal, 2007. **21**(3): p. 790-801.

155. Du, Y.N., et al., *Convection-driven generation of long-range material gradients.* Biomaterials, 2010. **31**(9): p. 2686-2694.

156. Revzin, A., et al., *Fabrication of poly(ethylene glycol) hydrogel microstructures using photolithography.* Langmuir, 2001. **17**(18): p. 5440-5447.

157. Revzin, A., R.G. Tompkins, and M. Toner, *Surface engineering with poly(ethylene glycol) photolithography to create high-density cell arrays on glass.* Langmuir, 2003. **19**(23): p. 9855-9862.

158. Burdick, J.A. and K.S. Anseth, *Photoencapsulation of osteoblasts in injectable RGD-modified PEG hydrogels for bone tissue engineering.* Biomaterials, 2002. **23**(22): p. 4315-4323.

159. Dikovsky, D., H. Bianco-Peled, and D. Seliktar, *The effect of structural alterations of PEG-fibrinogen hydrogel scaffolds on 3-D cellular morphology and cellular migration.* Biomaterials, 2006. **27**(8): p. 1496-1506.

160. Raeber, G.P., M.P. Lutolf, and J.A. Hubbell, *Molecularly engineered PEG hydrogels: A novel model system for proteolytically mediated cell migration.* Biophysical Journal, 2005. **89**(2): p. 1374-1388.

161. Brigham, M.D., et al., *Mechanically Robust and Bioadhesive Collagen and Photocrosslinkable Hyaluronic Acid Semi-Interpenetrating Networks.* Tissue Engineering Part A, 2009. **15**(7): p. 1645-1653.

162. Camci-Unal, G., et al., *Surface-modified hyaluronic acid hydrogels to capture endothelial progenitor cells.* Soft Matter, 2010. **6**(20): p. 5120-5126.

163. Gerecht, S., et al., *Hyaluronic acid hydrogen for controlled self-renewal and differentiation of human embryonic stem cells.* Proceedings of the National Academy of Sciences of the United States of America, 2007. **104**(27): p. 11298-11303.

164. Fukuda, J., et al., *Micropatterned cell co-cultures using layer-by-layer deposition of extracellular matrix components.* Biomaterials, 2006. **27**(8): p. 1479-1486.

165. Benton, J.A., et al., *Photocrosslinking of Gelatin Macromers to Synthesize Porous Hydrogels That Promote Valvular Interstitial Cell Function.* Tissue Engineering Part A, 2009. **15**(11): p. 3221-3230.

166. Hutson, C.B., et al., *Synthesis and Characterization of Tunable Poly(Ethylene Glycol): Gelatin Methacrylate Composite Hydrogels.* Tissue Engineering Part A, 2011. **17**(13-14): p. 1713-1723.

167. Song, W., et al., *Adipogenic Differentiation of Individual Mesenchymal Stem Cell on Different Geometric Micropatterns.* Langmuir, 2011. **27**(10): p. 6155-6162.

168. Azioune, A., et al., *Protein Micropatterns: A Direct Printing Protocol Using Deep UVs.* Microtubules: In Vivo, 2010. **97**: p. 133-146.

169. Thery, M., *Micropatterning as a tool to decipher cell morphogenesis and functions.* Journal of Cell Science, 2010. **123**(24): p. 4201-4213.

170. Thery, M., et al., *Cell distribution of stress fibres in response to the geometry of the adhesive environment.* Cell Motility and the Cytoskeleton, 2006. **63**(6): p. 341-355.

171. Thery, M., et al., *Anisotropy of cell adhesive microenvironment governs cell internal organization and orientation of polarity.* Proceedings of the National Academy of Sciences of the United States of America, 2006. **103**(52): p. 19771-19776.

172. Apodaca, G., *Endocytic traffic in polarized epithelial cells: role of the actin and microtubule cytoskeleton.* Traffic, 2001. **2**(3): p. 149-59.

173. Aspenstrom, P., *The Rho GTPases have multiple effects on the actin cytoskeleton.* Experimental Cell Research, 1999. **246**(1): p. 20-25.

174. Begum, R., M.S.A. Nur-E-Kamal, and M.A. Zaman, *The role of Rho GTPases in the regulation of the rearrangement of actin cytoskeleton and cell movement.* Experimental and Molecular Medicine, 2004. **36**(4): p. 358-366.

175. Sit, S.T. and E. Manser, *Rho GTPases and their role in organizing the actin cytoskeleton.* Journal of Cell Science, 2011. **124**(5): p. 679-683.

176. Knoblich, J.A., *Mechanisms of asymmetric stem cell division.* Cell, 2008. **132**(4): p. 583-597.

177. Neumuller, R.A. and J.A. Knoblich, *Dividing cellular asymmetry: asymmetric cell division and its implications for stem cells and cancer.* Genes & Development, 2009. **23**(23): p. 2675-2699.

178. Schaefer, M., et al., *Heterotrimeric G proteins direct two modes of asymmetric cell division in the Drosophila nervous system.* Cell, 2001. **107**(2): p. 183-194.

179. Schaefer, M., et al., *A protein complex containing inscuteable and the G alpha-binding protein Pins orients asymmetric cell divisions in Drosophila.* Current Biology, 2000. **10**(7): p. 353-362.

180. Zamir, E. and B. Geiger, *Molecular complexity and dynamics of cell-matrix adhesions.* Journal of Cell Science, 2001. **114**(20): p. 3583-3590.

181. Zheng, Z., et al., *LGN regulates mitotic spindle orientation during epithelial morphogenesis.* Journal of Cell Biology, 2010. **189**(2): p. 275-288.

182. Du, Q.S. and I.G. Macara, *Mammalian pins is a conformational switch that links NuMA to heterotrimeric G proteins.* Cell, 2004. **119**(4): p. 503-516.

183. Du, Q.S., P.T. Stukenberg, and I.G. Macara, *A mammalian Partner of inscuteable binds NuMA and regulates mitotic spindle organization.* Nature Cell Biology, 2001. **3**(12): p. 1069-1075.

184. Nobes, C.D. and A. Hall, *Rho, Rac, and Cdc42 Gtpases Regulate the Assembly of Multimolecular Focal Complexes Associated with Actin Stress Fibers, Lamellipodia, and Filopodia.* Cell, 1995. **81**(1): p. 53-62.

185. Weisberg, E., et al., *Role of focal adhesion proteins in signal transduction and oncogenesis.* Critical Reviews in Oncogenesis, 1997. **8**(4): p. 343-358.

186. Park, J.Y., et al., *Simultaneous generation of chemical concentration and mechanical shear stress gradients using microfluidic osmotic flow comparable to interstitial flow.* Lab on a Chip, 2009. **9**(15): p. 2194-2202.

187. Park, I.H., et al., *Reprogramming of human somatic cells to pluripotency with defined factors.* Nature, 2008. **451**(7175): p. 141-6.

188. Zhang, J.H., et al., *Functional Cardiomyocytes Derived From Human Induced Pluripotent Stem Cells.* Circulation Research, 2009. **104**(4): p. E30-E41.

189. Kamp, T.J. and G.E. Lyons, *On the road to iPS cell cardiovascular applications.* Circulation Research, 2009. **105**(7): p. 617-9.

190. Murtuza, B., J.W. Nichol, and A. Khademhosseini, *Micro- and nanoscale control of the cardiac stem cell niche for tissue fabrication.* Tissue Eng Part B Rev, 2009. **15**(4): p. 443-54.

191. Underhill, G.H. and S.N. Bhatia, *High-throughput analysis of signals regulating stem cell fate and function.* Current Opinion in Chemical Biology, 2007. **11**(4): p. 357-366.

192. Eckfeldt, C.E., E.M. Mendenhall, and C.M. Verfaillie, *The molecular repertoire of the 'almighty' stem cell.* Nature Reviews Molecular Cell Biology, 2005. **6**(9): p. 726-737.

193. Van Hoof, D., et al., *A quest for human and mouse embryonic stem cell-specific proteins.* Molecular & Cellular Proteomics, 2006. **5**(7): p. 1261-1273.

194. Voldman, J., M.L. Gray, and M.A. Schmidt, *Microfabrication in biology and medicine.* Annual Review of Biomedical Engineering, 1999. **1**: p. 401-425.

195. Khademhosseini, A., et al., *Microfluidic patterning for fabrication of contractile cardiac organoids.* Biomedical Microdevices, 2007. **9**(2): p. 149-157.

196. Lutolf, M.P., P.M. Gilbert, and H.M. Blau, *Designing materials to direct stem-cell fate.* Nature, 2009. **462**(7272): p. 433-441.

197. Sudo, R., et al., *Transport-mediated angiogenesis in 3D epithelial coculture.* Faseb Journal, 2009. **23**(7): p. 2155-2164.

198. Grevesse, T., et al., *A simple route to functionalize polyacrylamide hydrogels for the independent tuning of mechanotransduction cues.* Lab on a Chip, 2013. **13**(5): p. 777-780.

199. Sochol, R.D., et al., *Unidirectional mechanical cellular stimuli via micropost array gradients.* Soft Matter, 2011. **7**(10): p. 4606-4609.

200. Xia, N., et al., *Directional control of cell motility through focal adhesion positioning and spatial control of Rac activation.* Faseb Journal, 2008. **22**(6): p. 1649-1659.

201. Zhao, Y., et al., *Simultaneous orientation and cellular force measurements in adult cardiac myocytes using three-dimensional polymeric microstructures.* Cell Motility and the Cytoskeleton, 2007. **64**(9): p. 718-725.

202. Tan, J.L., et al., *Cells lying on a bed of microneedles: An approach to isolate mechanical force.* Proceedings of the National Academy of Sciences of the United States of America, 2003. **100**(4): p. 1484-1489.

203. Fu, J.P., et al., *Mechanical regulation of cell function with geometrically modulated elastomeric substrates.* Nature Methods, 2010. **7**(9): p. 733-U95.

204. Sochol, R.D., et al., *Effects of micropost spacing and stiffness on cell motility.* Micro & Nano Letters, 2011. **6**(5): p. 323-326.

205. Jegadesan, S., S. Sindhu, and S. Valiyaveettil, *Fabrication of nanostructure on a polymer film using atomic force microscope.* Journal of Nanoscience and Nanotechnology, 2007. **7**(6): p. 2172-2175.

206. Yoshitake, S., et al., *Mild and Efficient Conjugation of Rabbit Fab' and Horseradish-Peroxidase Using a Maleimide Compound and Its Use for Enzyme-Immunoassay.* Journal of Biochemistry, 1982. **92**(5): p. 1413-1424.

207. Gray, D.S., J. Tien, and C.S. Chen, *Repositioning of cells by mechanotaxis on surfaces with micropatterned Young's modulus.* Journal of Biomedical Materials Research Part A, 2003. **66A**(3): p. 605-614.

208. Ochsner, M., et al., *Micro-well arrays for 3D shape control and high resolution analysis of single cells.* Lab on a Chip, 2007. **7**(8): p. 1074-1077.

209. Bryant, S.J., et al., *Crosslinking density influences chondrocyte metabolism in dynamically loaded photocrosslinked poly(ethylene glycol) hydrogels.* Annals of Biomedical Engineering, 2004. **32**(3): p. 407-417.

210. Huang, T., et al., *A novel hydrogel with high mechanical strength: A macromolecular microsphere composite hydrogel.* Advanced Materials, 2007. **19**(12): p. 1622-+.

211. Stammen, J.A., et al., *Mechanical properties of a novel PVA hydrogel in shear and unconfined compression.* Biomaterials, 2001. **22**(8): p. 799-806.

212. Weinand, C., et al., *Hydrogel-beta-TCP scaffolds and stem cells for tissue engineering bone.* Bone, 2006. **38**(4): p. 555-63.

213. Harris, J.M., *Poly(ethylene glycol) chemistry : biotechnical and biomedical applications*. Topics in applied chemistry. 1992, New York: Plenum Press. xxi, 385 p.

214. Hern, D.L. and J.A. Hubbell, *Incorporation of adhesion peptides into nonadhesive hydrogels useful for tissue resurfacing.* Journal of Biomedical Materials Research, 1998. **39**(2): p. 266-276.

215. Lanniel, M., et al., *Substrate induced differentiation of human mesenchymal stem cells on hydrogels with modified surface chemistry and controlled modulus.* Soft Matter, 2011. **7**(14): p. 6501-6514.

216. Wang, N., J.P. Butler, and D.E. Ingber, *Mechanotransduction across the Cell-Surface and through the Cytoskeleton.* Science, 1993. **260**(5111): p. 1124-1127.

217. Hutmacher, D.W., *Scaffolds in tissue engineering bone and cartilage.* Biomaterials, 2000. **21**(24): p. 2529-2543.

218. Bosnakovski, D., et al., *Isolation and multilineage differentiation of bovine bone marrow mesenchymal stem cells.* Cell and Tissue Research, 2005. **319**(2): p. 243-253.

219. Jiang, Y., et al., *Pluripotency of mesenchymal stem cells derived from adult marrow.* Nature, 2002. **418**(6893): p. 41-9.

220. Park, J., et al., *Bone regeneration in critical size defects by cell-mediated BMP-2 gene transfer: a comparison of adenoviral vectors and liposomes.* Gene Therapy, 2003. **10**(13): p. 1089-1098.

221. Dupont, K.M., et al., *Human stem cell delivery for treatment of large segmental bone defects.* Proceedings of the National Academy of Sciences of the United States of America, 2010. **107**(8): p. 3305-10.

222. Winnier, G., et al., *Bone Morphogenetic Protein-4 Is Required for Mesoderm Formation and Patterning in the Mouse.* Genes & Development, 1995. **9**(17): p. 2105-2116.

223. Charge, S.B.P. and M.A. Rudnicki, *Cellular and molecular regulation of muscle regeneration.* Physiological Reviews, 2004. **84**(1): p. 209-238.

224. Ohlstein, B., et al., *The stem cell niche: theme and variations.* Current Opinion in Cell Biology, 2004. **16**(6): p. 693-699.

225. Kilian, K.A., et al., *Geometric cues for directing the differentiation of mesenchymal stem cells.* Proceedings of the National Academy of Sciences of the United States of America, 2010. **107**(11): p. 4872-4877.

226. Khademhosseini, A., et al., *Microscale technologies for tissue engineering and biology.* Proceedings of the National Academy of Sciences of the United States of America, 2006. **103**(8): p. 2480-2487.

227. Nikkhah, M., et al., *Engineering microscale topographies to control the cell-substrate interface.* Biomaterials, 2012. **33**(21): p. 5230-5246.

228. Gunawan, R.C., et al., *Cell migration and polarity on microfabricated gradients of extracellular matrix proteins.* Langmuir, 2006. **22**(9): p. 4250-4258.

229. Sila-Asna, M., et al., *Osteoblast differentiation and bone formation gene expression in strontium-inducing bone marrow mesenchymal stem cell.* The Kobe journal of medical sciences, 2007. **53**(1-2): p. 25-35.

230. Koopman, R., G. Schaart, and M.K. Hesselink, *Optimisation of oil red O staining permits combination with immunofluorescence and automated quantification of lipids.* Histochemistry and cell biology, 2001. **116**(1): p. 63-8.

231. Nelson, C.M. and C.S. Chen, *Cell-cell signaling by direct contact increases cell proliferation via a PI3K-dependent signal.* Febs Letters, 2002. **514**(2-3): p. 238-242.

232. Cheng, S.L., et al., *Differentiation of Human Bone-Marrow Osteogenic Stromal Cells in Vitro - Induction of the Osteoblast Phenotype by Dexamethasone.* Endocrinology, 1994. **134**(1): p. 277-286.

233. Ruiz, S.A. and C.S. Chen, *Emergence of Patterned Stem Cell Differentiation Within Multicellular Structures.* Stem Cells, 2008. **26**(11): p. 2921-2927.

234. Oh, S., et al., *Stem cell fate dictated solely by altered nanotube dimension.* Proc Natl Acad Sci U S A, 2009. **106**(7): p. 2130-5.

235. Rowlands, A.S., P.A. George, and J.J. Cooper-White, *Directing osteogenic and myogenic differentiation of MSCs: interplay of stiffness and adhesive ligand presentation.* American Journal of Physiology-Cell Physiology, 2008. **295**(4): p. C1037-C1044.

236. Evans, N.D., et al., *Substrate Stiffness Affects Early Differentiation Events in Embryonic Stem Cells.* Eur Cell Mater, 2009. **18**: p. 1-14.

237. Shih, Y.R.V., et al., *Matrix Stiffness Regulation of Integrin-Mediated Mechanotransduction During Osteogenic Differentiation of Human Mesenchymal Stem Cells.* Journal of Bone and Mineral Research, 2011. **26**(4): p. 730-738.

238. Arthur, W.T. and K. Burridge, *RhoA inactivation by p190RhoGAP regulates cell spreading and migration by promoting membrane protrusion and polarity.* Molecular Biology of the Cell, 2001. **12**(9): p. 2711-2720.

239. Wang, Y.K., et al., *Bone Morphogenetic Protein-2-Induced Signaling and Osteogenesis Is Regulated by Cell Shape, RhoA/ROCK, and Cytoskeletal Tension.* Stem Cells and Development, 2012. **21**(7): p. 1176-1186.

240. Docheva, D., et al., *Researching into the cellular shape, volume and elasticity of mesenchymal stem cells, osteoblasts and osteosarcoma cells by atomic force microscopy.* Journal of Cellular and Molecular Medicine, 2008. **12**(2): p. 537-552.

241. Maekawa, M., et al., *Signaling from rho to the actin cytoskeleton through protein kinases ROCK and LIM-kinase.* Science, 1999. **285**(5429): p. 895-898.

242. Wojciak-Stothard, B., et al., *Rho and Rac but not Cdc42 regulate endothelial cell permeability.* Journal of Cell Science, 2001. **114**(Pt 7): p. 1343-55.

243. Malek, A.M. and S. Izumo, *Mechanism of endothelial cell shape change and cytoskeletal remodeling in response to fluid shear stress.* Journal of Cell Science, 1996. **109**: p. 713-726.

244. Chang, Y.C., et al., *GEF-H1 couples nocodazole-induced microtubule disassembly to cell contractility via RhoA.* Molecular Biology of the Cell, 2008. **19**(5): p. 2147-2153.

245. Bourgier, C., et al., *Inhibition of Rho kinase modulates radiation induced fibrogenic phenotype in intestinal smooth muscle cells through alteration of the cytoskeleton and connective tissue growth factor expression.* Gut, 2005. **54**(3): p. 336-343.

246. Poulsson, A.H.C., et al., *Attachment of Human Primary Osteoblast Cells to Modified Polyethylene Surfaces.* Langmuir, 2009. **25**(6): p. 3718-3727.

247. Jung, C.H., et al., *Patterning of cells on a PVC film surface functionalized by ion irradiation.* Polymers for Advanced Technologies, 2010. **21**(2): p. 135-138.

248. Dupont-Gillain, C.C., et al., *Plasma-oxidized polystyrene: Wetting properties and surface reconstruction.* Langmuir, 2000. **16**(21): p. 8194-8200.

249. van Kooten, T.G., H.T. Spijker, and H.J. Busscher, *Plasma-treated polystyrene surfaces: model surfaces for studying cell-biomaterial interactions.* Biomaterials, 2004. **25**(10): p. 1735-1747.

250. Emonard, H., et al., *Reconstituted Basement-Membrane Matrix Modulates Fibroblast Activities Invitro.* Journal of Cellular Physiology, 1987. **133**(1): p. 95-102.

251. Braam, S.R., et al., *Recombinant vitronectin is a functionally defined substrate that supports human embryonic stem cell self-renewal via alpha V beta 5 integrin.* Stem Cells, 2008. **26**(9): p. 2257-2265.

252. Rowland, T.J., et al., *Roles of Integrins in Human Induced Pluripotent Stem Cell Growth on Matrigel and Vitronectin.* Stem Cells and Development, 2010. **19**(8): p. 1231-1240.

253. Welle, A. and E. Gottwald, *UV-based patterning of polymeric substrates for cell culture applications.* Biomedical Microdevices, 2002. **4**(1): p. 33-41.

254. Mitchell, S.A., et al., *Cellular attachment and spatial control of cells using micro-patterned ultra-violet/ozone treatment in serum enriched media.* Biomaterials, 2004. **25**(18): p. 4079-4086.

255. Welle, A., et al., *Photo-chemically patterned polymer surfaces for controlled PC-12 adhesion and neurite guidance.* Journal of Neuroscience Methods, 2005. **142**(2): p. 243-250.

256. Hudson, J., et al., *Primitive Cardiac Cells from Human Embryonic Stem Cells.* Stem Cells and Development, 2012. **21**(9): p. 1513-1523.

257. Burridge, P.W., et al., *A Universal System for Highly Efficient Cardiac Differentiation of Human Induced Pluripotent Stem Cells That Eliminates Interline Variability.* Plos One, 2011. **6**(4).

258. Kwon, M., et al., *Mechanisms to suppress multipolar divisions in cancer cells with extra centrosomes.* Genes & Development, 2008. **22**(16): p. 2189-2203.

259. Ballabeni, A., et al., *Cell cycle adaptations of embryonic stem cells.* Proceedings of the National Academy of Sciences of the United States of America, 2011. **108**(48): p. 19252-19257.

Appendix A: Copyright Permissions

RE: Permission for use of manuscript in dissertation

Dr. H. S. Nalwa [nalwa@mindspring.com]
Sent: Tuesday, October 22, 2013 11:03 PM
To: HARRIS, GREG
Cc: editorjbt@gmail.com

Dear Greg:

American Scientific Publishers grants permission to re-use whole article or parts of the follow research article in your forthcoming PhD thesis to be submitted to the University of South Carolina.

Patterning Pluripotent Stem Cells at a Single Cell Level
Marina V. Pryzhkova, Greg M. Harris, Shuguo Ma, and Ehsan Jabbarzadeh, J. Biomater. Tissue Eng. 3, 461-471 (2013)

H. S. Nalwa, PhD
American Scientific Publishers
www.aspbs.com

From: Editor-in-Chief, JBT [mailto:editorjbt@gmail.com]
Sent: Tuesday, October 22, 2013 7:46 PM
To: Dr. H. S. Nalwa
Subject: Fwd: Permission for use of manuscript in dissertation

RE: C-Query: Permission Requests

AMBREEN IRSHAD - BSP [ambreenirshad@benthamscience.org]
Sent: Tuesday, October 15, 2013 12:48 PM
To: HARRIS, GREG
Cc: m.ahmed@benthamscience.org

Grant of Permission

Dear Dr. Harris
:

Thank you for your interest in our copyrighted material, and for requesting permission for its use.

Permission is granted for the following subject to the conditions outlined below:

Strategies to Direct Angiogenesis within Scaffolds for Bone Tissue Engineering" published in Current Pharmaceutical Design, 2013, Volume 19.

To be used in the following manner:

1. Bentham Science Publishers grants you the right to reproduce the material indicated above on a one-time, non-exclusive basis, solely for the purpose described. Permission must be requested separately for any future or additional use.

2. For an article, the copyright notice must be printed on the first page of article or book chapter. For figures, photographs, covers, or tables, the notice may appear with the material, in a footnote, or in the reference list.

Thank you for your patience while your request was being processed. If you wish to contact us further, please use the address below.

Sincerely,

AMBREEN IRSHAD

***Permissions & Rights* Manager**
Bentham Science Publishers
Email: ambreenirshad@benthamscience.org
URL: www.benthamscience.com